Award Number: W81XWH-10-1-0933

TITLE: Ready to Use Tissue Construct for Military Bone & Cartilage Trauma

PRINCIPAL INVESTIGATOR: Francis Y. Lee, MD, PhD

CONTRACTING ORGANIZATION: Columbia University in the City of New York
New York, NY 10032

REPORT DATE: December 2015

TYPE OF REPORT: Final

PREPARED FOR: U.S. Army Medical Research and Materiel Command
Fort Detrick, Maryland 21702-5012

REPORT DOCUMENTATION PAGE

Form Approved
OMB No. 0704-0188

1. REPORT DATE :	2. REPORT TYPE:	3. DATES COVERED
December 2015	Final	30Sep2010 - 29Sep2015

4. TITLE AND SUBTITLE
Ready to Use Tissue Construct for Military Bone & Cartilage Trauma

5a. CONTRACT NUMBER
W81XWH-10-1-0933

5b. GRANT NUMBER
OR090175 - Orthopaedic

5c. PROGRAM ELEMENT NUMBER

6. AUTHOR(S)
Francis Y. Lee, MD, PhD

E-Mail: fl127@columbia.edu

5d. PROJECT NUMBER

5e. TASK NUMBER

5f. WORK UNIT NUMBER

7. PERFORMING ORGANIZATION NAME(S) AND ADDRESS(ES)
Trustees of Columbia University in the City of New York
Columbia University Medical Center
650 West 168th Street
New York, NY 10032

8. PERFORMING ORGANIZATION REPORT NUMBER

9. SPONSORING / MONITORING AGENCY NAME(S) AND ADDRESS(ES)
U.S. Army Medical Research and Materiel Command
Fort Detrick, Maryland 21702-5012

10. SPONSOR/MONITOR'S ACRONYM(S)

11. SPONSOR/MONITOR'S REPORT NUMBER(S)

12. DISTRIBUTION / AVAILABILITY STATEMENT
Approved for Public Release; Distribution Unlimited

13. SUPPLEMENTARY NOTES

14. ABSTRACT

Our study "Ready-to-Use Tissue Construct for Military Bone and Cartilage Trauma" addresses the current limitations in treating complex, high-energy musculoskeletal wounds incurred in active combat. High-energy blast-injuries produce immediate, short-term and long-term consequences such as acute limb loss, bone loss, cartilage loss, stiffness, limping, pain, arthritis, and permanent disability, often requiring multiple reconstructive surgeries and prolonged rehabilitation. These 'osteochondral health' issues ultimately affect a soldier's quality of life both during active service and after retirement. Tissue engineering technology is a rapidly evolving field and utilizes mesenchymal cells, tissue scaffolds and growth factors. However, there are no currently available tissue-engineering constructs exhibiting 'Ready-to-Use' functionality. The most significant barrier to the practical application of tissue engineering for combat-related bone and cartilage defects is the *time- and labor-intensive process of mesenchymal stem cell expansion*. The **goal** of this study was to introduce a new tissue engineering paradigm to the Defense Health Program (**DHP**) by utilizing a biomechanically competent and anatomically matched tissue construct without resorting to the cumbersome process of mesenchymal stem cell expansion.

15. SUBJECT TERMS
Ready to use tissue construct, biomechanically competent anatomically matched tissue construct

16. SECURITY CLASSIFICATION OF:			17. LIMITATION OF ABSTRACT	18. NUMBER OF PAGES	19a. NAME OF Responsible Person USAMRMC
a. REPORT	b. ABSTRACT	c. THIS PAGE			19b. TELEPHONE NUMBER
U	U	U	UU	64	

Table of Contents

1. **Introduction……** **3**
2. **Body……** **4**
   - **2.0 Overview…….** **4**
   - **2.1 Aim 1……** **4**
   - **2.2 Aim 2……** **15**
   - **2.3 Aim 3……** **60**
3. **Key Research Accomplishments……..** **65**
4. **Reportable Outcomes……** **66**
5. **Conclusions…….** **66**
6. **References……** **67**
7. **Appendices……..** **64**

1. INTRODUCTION

Our study "Ready-to-Use Tissue Construct for Military Bone and Cartilage Trauma" addresses current limitations in treating complex, high-energy musculoskeletal wounds incurred in active combat. High-energy blast-injuries produce immediate, short-term and long-term consequences such as acute limb loss, bone loss, cartilage loss, stiffness, limping, pain, arthritis, and permanent disability, often requiring multiple reconstructive surgeries and prolonged rehabilitation. These 'osteochondral health' issues ultimately affect a soldier's quality of life both during active service and after retirement. Tissue engineering technology is a rapidly evolving field and utilizes mesenchymal cells, tissue scaffolds and growth factors. However, there are no currently available tissue-engineering constructs exhibiting 'Ready-to-Use' functionality. The most significant barrier to the practical application of tissue engineering for combat-related bone and cartilage defects is the *time- and labor-intensive process of mesenchymal stem cell expansion*. The goal of the current study was to introduce a new tissue engineering paradigm to the Defense Health Program (DHP) by utilizing a biomechanically competent and anatomically matched tissue construct without resorting to the cumbersome process of mesenchymal stem cell expansion. Our project utilized a series of *in vivo* large animal translational experiments that will hopefully lead to the development of new military technology products and utilities for the definitive and preventive orthopaedic care of military personnel and retirees. The project had 3 major aims, excerpted and updated from the Statement of Work and listed below:

Aim 1. To examine whether our prefabricated constructs can reconstitute osteochondral defects of critical-size in a canine distal femoral condyle defect model simulating high-energy blast-injury. Osteochondral injuries of any size require anatomically perfect reconstruction to prevent pain and post-traumatic arthritis. We hypothesized that anatomically-conforming osteochondral constructs with controlled release of TGF-β3 can reconstitute physiologic *hyaline cartilage*-osseous transition in massive osteochondral defects in large animals. We conducted functional outcome analysis, X-ray/MRI examination and histologic analysis.

Aim 2. To examine whether our prefabricated construct can reconstitute critical size segmental defects in canine tibiae. Critical-size segmental defects in long bone diaphyses require extensive reconstructive procedures and prolonged rehabilitation times. We hypothesized that our *Ready-to-Use* constructs can successfully restore 3 cm critical size segmental defects in dog tibiae. We examined the incorporation and regeneration of the biogenic implant with host bone by conducting functional outcome assessments, radiography, biomechanical torsional testing and histologic examination.

Aim 3. To examine biomechanical suitability of ready-to-use constructs in massive osteochondral defects and segmental bone defects in human cadaveric femora. We have successfully developed anatomically conforming bone and cartilage constructs for rats and rabbits. Early joint motion and ambulation are important in human patients. We hypothesized that our *ready-to-use* construct can maintain the biomechanical and functional properties in human cadaveric bones under simulated physiologic load. We verified the biomechanical competence in a critical size defect in human tibiae by simulating loads seen during ambulation.

Our central hypothesis is that an anatomically and biomechanically compatible scaffold with BMP-2 can reconstitute massive cartilage/bone defects without exogenous MSCs. The goal of this Technology Development Project was to simplify the current paradigm of tissue engineering by 1) eliminating the need for time- and labor-intensive stem cell harvesting and expansion and 2) adopting anatomically conforming constructs which promote incorporation, remodeling, early joint motion, partial weight bearing, and ambulation. Our hypothesis was based on our compelling preliminary data in small animal models, such as mice, rats and rabbits. The current protocol took another step towards military application by verifying successful implantation of the osteochondral implant (**Aim 1)** and segmental defect scaffold (**Aim 2**) in massive canine bone defects and by confirming biomechanical and functional suitability in human cadaveric tibia defect models (**Aim 3**). **Aim 1** and **Aim 2** are significant in that they introduce a simpler, more cost-effective approach to tissue engineering that obviates the need for extensive cell culturing and laboratory support. **Aim 3** is significant in that the injured soldiers can start early rehabilitation and ambulation following reconstructive surgeries using Ready-to-Use anatomically and biomechanically conforming biogenic scaffolds.

2. BODY

2.0 Overview

We followed our Columbia and USAMRMC Animal Care and Use Review Office (ACURO) approved IACUC protocol and performed surgeries on 3 Aim 1 (osteochondral defect) dogs and 28 Aim 2 (segmental defect) dogs for the period September 2010 through September 2015. All dogs received scaffolds composed of 90% poly-caprolactone (PCL) and 10% hydroxyapatite (HA) by weight (PCL+HA). The 3 osteochondral defect dogs received unseeded scaffolds. 10 segmental defect dogs received unseeded scaffolds, 6 segmental defect dogs received canine allografts, 6 segmental defect dogs received scaffolds seeded with BMP-2 and 6 segmental defect dogs received scaffolds seeded with cMSC. 29 of the dogs (3 osteochondral defect dogs and 26 segmental defect dogs) were taken to the full 16 week duration of the experiment and then humanely sacrificed. Two of early segmental defect dogs experienced premature plate failure and were sacrificed early. Switching from a standard size plate to a broad locking plate resolved the problem with plate failure. The purpose of these surgeries was threefold, a) to demonstrate that the surgery did not result in excessive pain and discomfort to the animal; b) to demonstrate that there was no immune response to the implanted scaffolds; and c) to demonstrate the stable performance and outcome of this technique. None of the dogs experienced excessive pain and discomfort, there was no immune response to the implanted scaffolds in any of the dogs and the stable performance and outcome of this technique was demonstrated for both osteochondral and segmental defect dogs.

Immediately after euthanizing, both hind tibias were dissected and harvested with soft tissue, and were stored at -80°C for subsequent mechanical testing. Three of the unseeded scaffold segmental defect dogs, 2 of the BMP-2 seeded scaffold segmental defect dogs and 2 of the allograft dogs underwent mechanical testing.

As per protocol, radiographs were taken on a bi-weekly basis for all dogs to document the progression of bony healing. Outcome measures were recorded throughout the 16 week experimental period for all dogs. Hard section histology was selectively performed following mechanical testing.

The subsections to follow elaborate on the above accomplishments and experimental results.

2.1 Aim 1 - Osteochondral Defects

The design of the osteochondral defect was developed and surgical procedures were performed on 3 osteochondral dogs and radiological and MR images were obtained as well as outcome measures.

2.1.1 Osteochondral Defect Scaffold Design

The objective of the osteochondral defect scaffold is to promote both bony ingrowth into the subchondral bone as well as to promote the development of articular cartilage at the articular surface of the implant. The scaffold architecture is based on the previous work of Lee et al (1), one of the co-investigators on this grant. The efficacy of the design was first demonstrated in rabbit femurs by removing most of the rabbit condyle and replacing it with an implant made from Poly-caprolactone (PCL). A unique feature of this scaffold was that it was constructed with two layers, a top layer of 500μm with a pore size of 400μm to promote articular cartilage growth and a second layer with a pore size of 200μm to support bone ingrowth from the surrounding subchondral bone. This design philosophy was replicated for the dog osteochondral scaffold with some modifications. First, the effective size of the scaffold was reduced to be more representative of a large defect in the medial condyle rather than to replace the entire condyle. Second, because the entire scaffold was not being replaced, it was decided to design the scaffold to be held in place as a press-fit as performed in the previous rabbit model. Accordingly, the scaffold was designed with a "hat" the curvature of which approximately matched that of the canine medial condyle from the region shown in Figure 1, with a size of approximately 13 x 6 x 9 mm^3 and a tapered keel (9 mm by 4 mm by 4 mm) to provide stability to the implant and prevent any rotation of the implant. The location, and hence curvature of the implant, was selected to place the implant in the load bearing region of the canine knee joint (2) while still allowing access to the joint without disrupting the main ligaments of the knee. Both the implant design and surgical approach were determined and refined by trialing on several cadaveric canine knees of approximately the same size as the experimental dogs were anticipated to be.

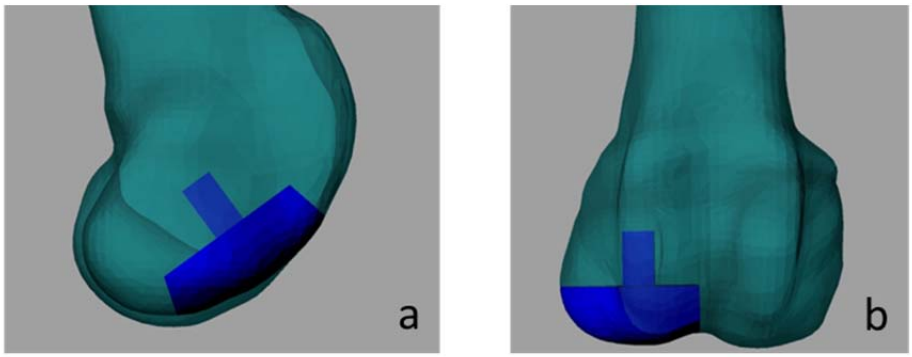

Figure 1: computer model of osteochondral scaffold virtually implanted in a 3-D computer model of the medial condyle of left canine knee, a) medial to lateral direction, b) anterior to posterior direction

The scaffolds were manufactured by first obtaining CTs of several of the cadaveric canine knees. The digital files from the CTs were then imported in a program (Mimics, Materialise) that combines the individual slices to create accurate three-dimensional models of the knee. This 3-D model was then exported as an STL file, which was then converted into a DXF file to create the internal architecture of the scaffold, which in turn was used to create the commands to drive a 3D printer (Bioplotter™, EnvisionTec, Germany,) which created the scaffold by laying down microstrands of scaffold material using a 27 G stainless steel needle for the articular layer pores and the subchondral bone pores. The resulting scaffold (Figure 2) had a pore size of 400 μm in the articular layer, which was approximately 5 mm deep. The underlying layer for subchondral bone growth had a pore size of 200 μm.

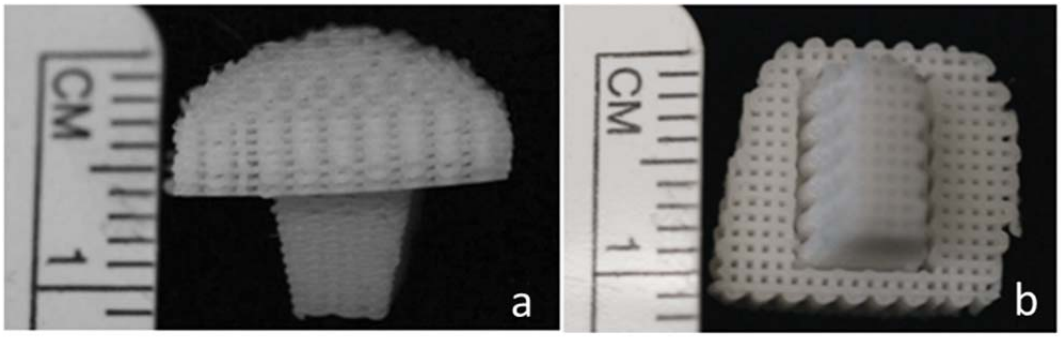

Figure 2: Osteochondral scaffold showing a) side view in superior-inferior direction, b) keel of scaffold

2.1.2 Osteochondral Defect Surgeries

After adequate anesthesia in accordance with the IACUC protocol, the dog was placed in a supine position. The leg was shaved and painted with Betadine® solution and the draping of the left leg to the groin was performed in a sterile fashion. The leg was flexed 90˚ and supported with a sterile cushion. A longitudinal midline incision (5 cm) was made on the left knee. Subcutaneous tissue and myofascial sheath were separated. A medial parapatellar approach was used by making an incision through the medial retinaculum and continued to the tendinous part of the vastus medialis muscle through which the joint capsule was entered and the medial femoral condyle identified. The medial condyle was cut en bloc, 1.4x 1.2 x 0.5 cm, the same size as the scaffold using an electric mini saw. A trough of 1.0 x 0.8 x 0.5 cm was created in the medial condyle manually using osteotomes to accommodate to the keel of the scaffold. The scaffold was firmly placed in the space. Minimal adjustment was made to achieve pressed-fit settlement in the positions of full flexion, neutral flexion and full extension. The normal gliding of patella was checked prior to closure. Hemostasis was reassured and the joint capsule was closed. The medial retinaculum and quadriceps were reattached using 2-0 Vicryl (Ethicon, Inc., Somerville, NJ) sutures. The subcutaneous tissue was closed using 4-0 Vicryl sutures. The skin was closed using skin staples and a compression dressing was applied. Post-op radiographs were taken immediately following closure. Intraoperative photographs of the placed unseeded scaffold for all three osteochondral segmental defect dogs just prior to closure are provided in Figure 3.

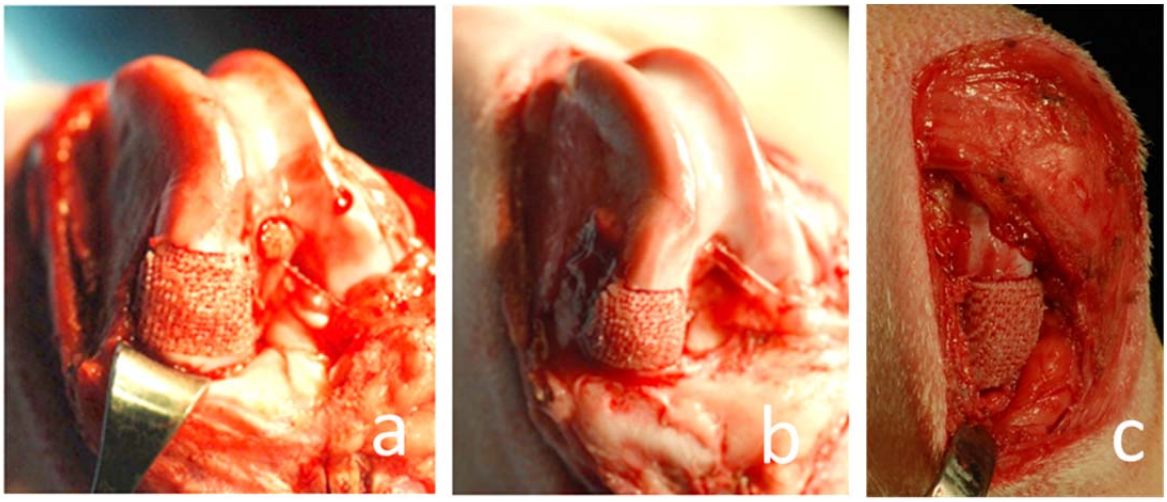

Figure 3: Osteochondral defect (Aim 1) surgeries showing scaffold implanted in medial condyle of left femur for a) Dog 1, b) Dog 2 and c) Dog 3. Note the minimally invasive surgical approach used for Dog 3.

2.1.2 Outcome Measures for Osteochondral Defect Dogs

Outcome measures of gait, lameness, pain, knee motion and an aggregate of these measures were recorded for Osteochondral Defect Dogs 1, 2 and 3 every weekday, excluding Saturdays and Sundays and reported below in Figures 3, 4, and 5, respectively. The criteria used to determine the outcome measures are provided in Table 1. However, because sling walking was prescribed immediately following surgery, no outcome measures were obtained until Day 10 for all three dogs. Figure 4 shows that Dog 1 had a steady improvement in its aggregate outcome score until approximately 40 days post-surgery. After that point, the aggregate outcome score leveled off and remained somewhat constant until sacrifice. Figure 5 shows that Dog 2 started out with a relatively high total outcome score, but then the score degraded at about day 30 post-op and remained low until sacrifice. Figure 6 shows that Dog 3 had a steady improvement in its total outcome score until approximately day 30 post-op, after which the score plateaued and remained relatively high until sacrifice.

Clinical observation of the dogs was consistent with the outcome measures. Dogs 1 and 2 were observed to have lateral patella subluxation, with Dog 2 consistently dislocating its patella. Dog 3 exhibited no obvious patella subluxation. Post-mortem observations, reported in Section 2.1.6 below further support these findings. The surgeries for Dogs 1 and 2 were performed by one surgeon whereas the surgery for Dog 3 was performed by a different surgeon. The first surgeon performed a wide incision and exposure to place the scaffold for Dogs 1 and 2 whereas the second surgeon used a minimally invasive surgical approach with a much smaller incision and far less disruption to the patella ligaments and surrounding soft tissues. It is speculated that the reattachment of the medial patella femoral ligaments for Dogs 1 and 2 was inadequate, resulting in the lateral subluxation of their patellae. With much less soft tissue disruption, Dog 3 appeared not to experience any patella subluxation.

Outcome	Criteria	Range
Gait	Non weight-bearing	0
	Partial weight-bearing	1
	Full weight-bearing	2
Lameness	Does not use limb during walking	0
	Partial use of affected limb, walks with noticeable limb	1
	No lameness when walking	2
Pain	Severe reaction to touch, withdraws upon the slightest touch with guarding behavior and/or vocalization	0
	Mild reaction to touch, withdraws limb upon touch	1
	No reaction to touch of affected limb	2
Knee	Significant reduction in range of motion (0-30%)	0

Motion	Moderate reduction in range of motion (30-60%)	1
	Slightly reduced range of motion (60-80 %)	2
	Normal range of motion (90-100%, preoperative range)	3
Total		0-9

Table 1: Criteria used to grade Outcome Measures for both Osteochondral Defect and Segmental Defect Dogs.

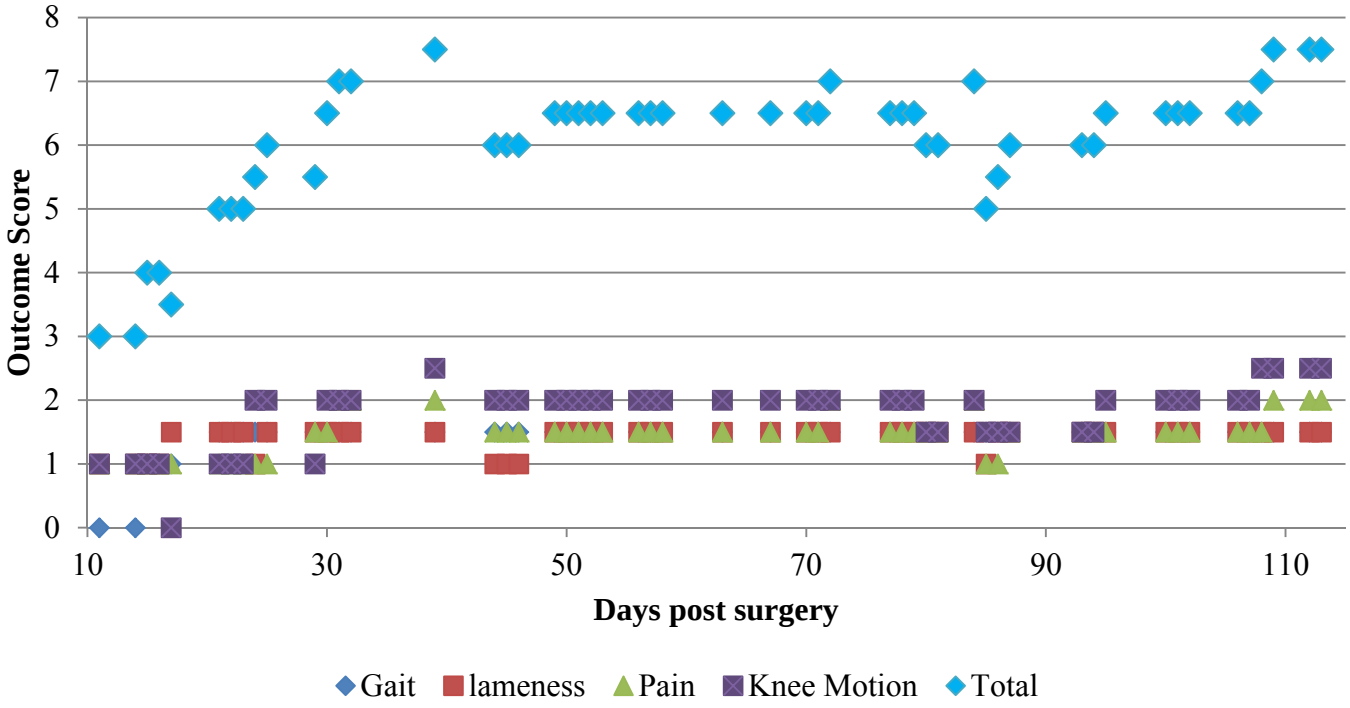

Figure 4: Outcome measurement for Osteochondral Defect Dog 1.

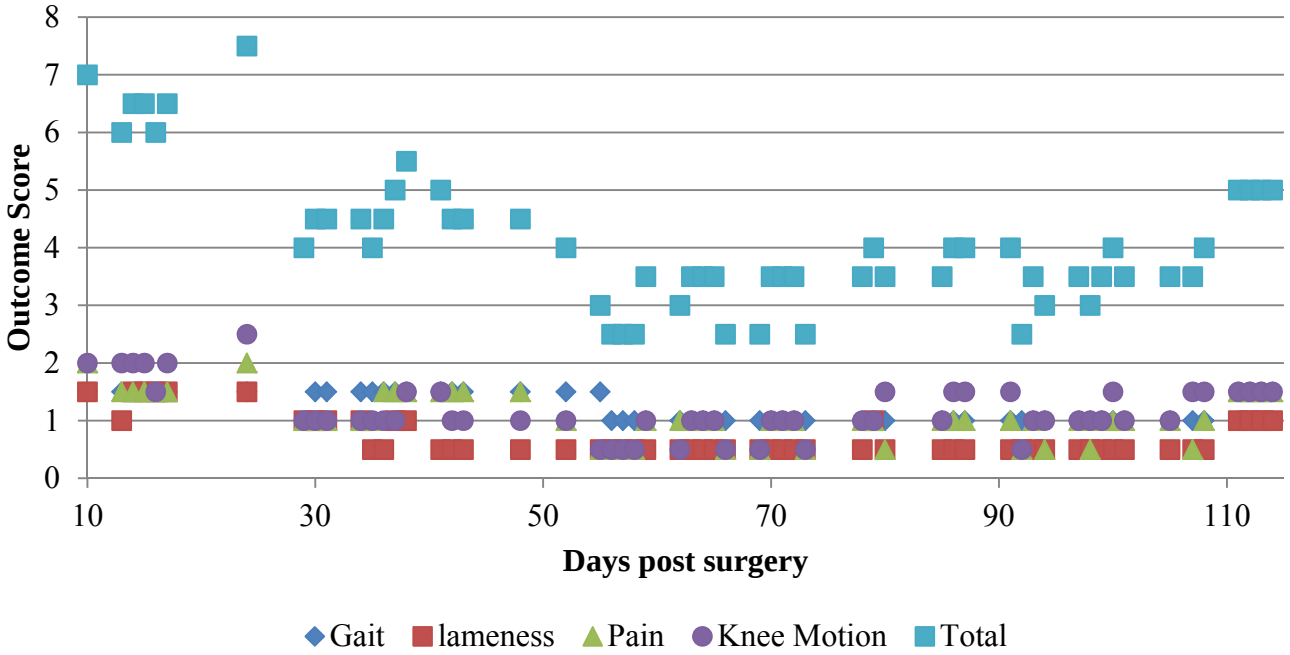

Figure 5: Outcome measurement for Osteochondral Defect Dog 2.

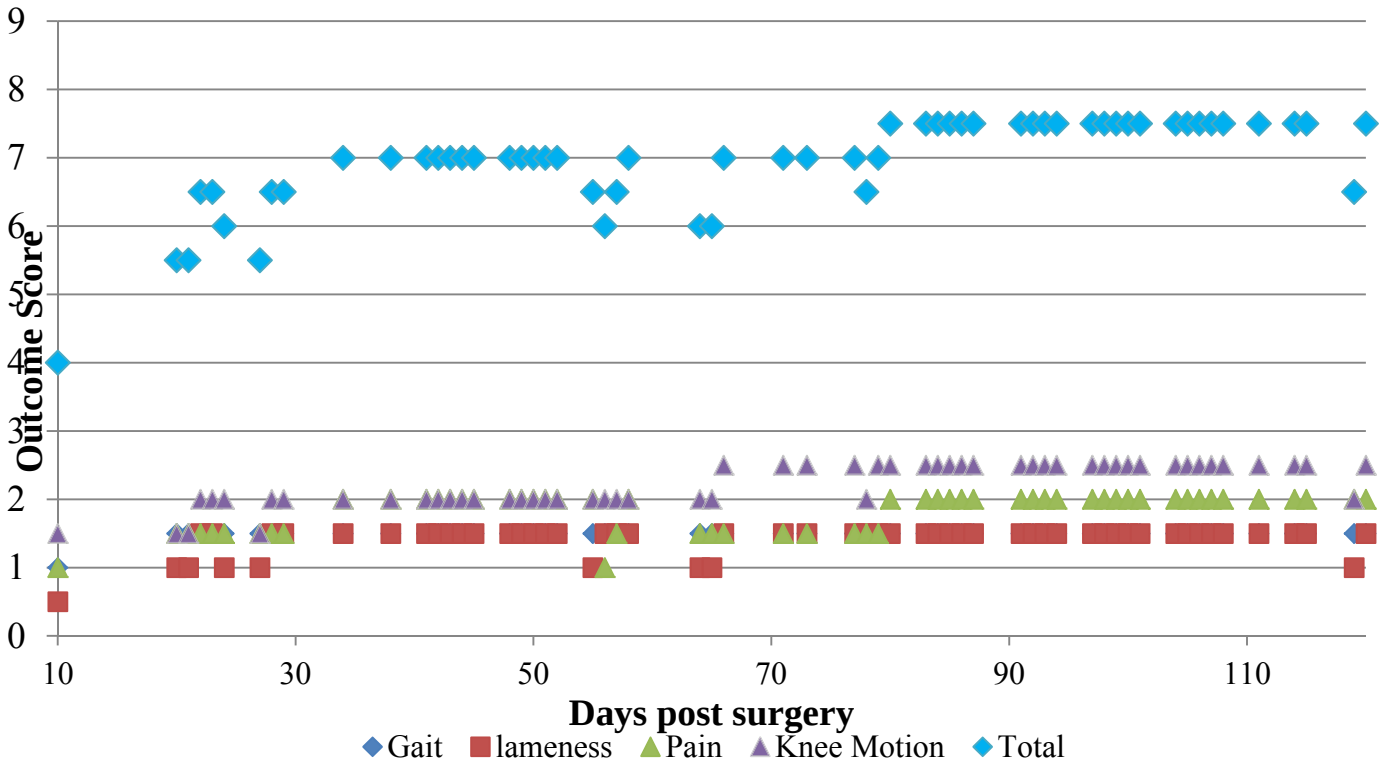

Figure 6: Outcome measurement for Osteochondral Defect Dog 3.

2.1.3 Osteochondral Defect Radiographs

Radiographs of Osteochondral Defect Dogs 1, 2 and 3 as a function of time are provided in Figures 7, 8 and 9, respectively. The outline of the scaffold trough can be seen in the radiographs and is highlighted by red circles in the posterior-anterior views. For all three dogs, the radiographs demonstrate the large surgically created bony defect at time 0 in the area of the unseeded scaffold. By week 4, there is some blunting at the scaffold-bone interface indicative of bony ingrowth. This progresses through week 16 indicating continued osseous integration. In these unloaded scaffolds, the articular surface remains radiolucent indicating little tissue formation.

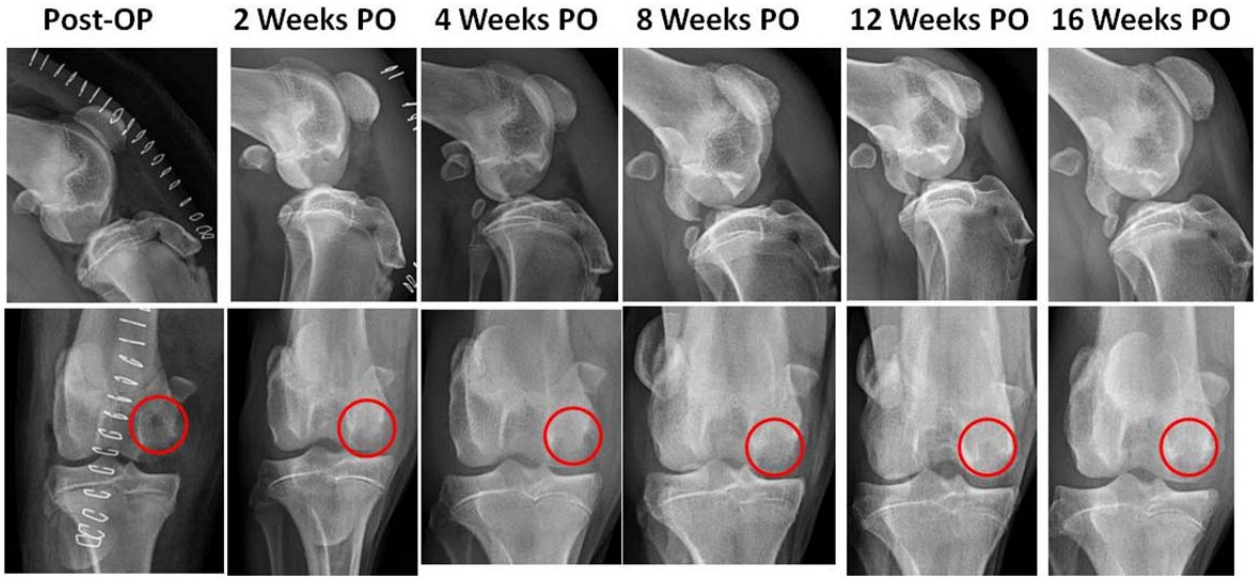

Figure 7: Radiographs for Osteochondral Dog 1 as a function of time; top row: medial-lateral view; bottom row: posterior-anterior view.

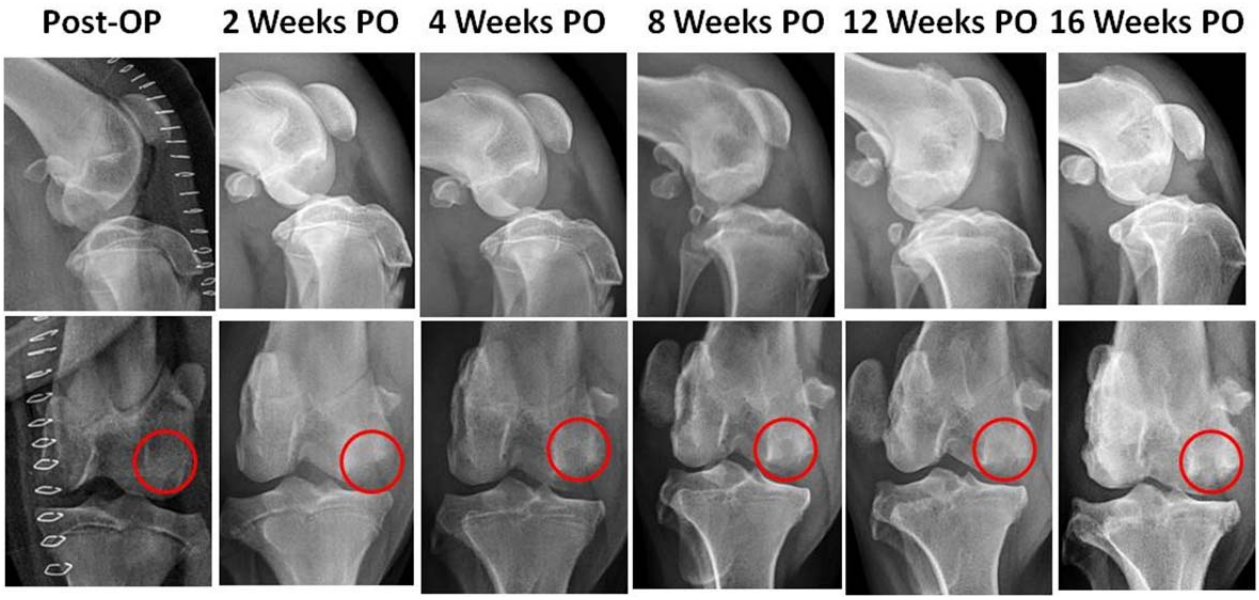

Figure 8: Radiographs for Osteochondral Dog 2 as a function of time; Top row: medial-lateral view, Bottom row: posterior-anterior view.

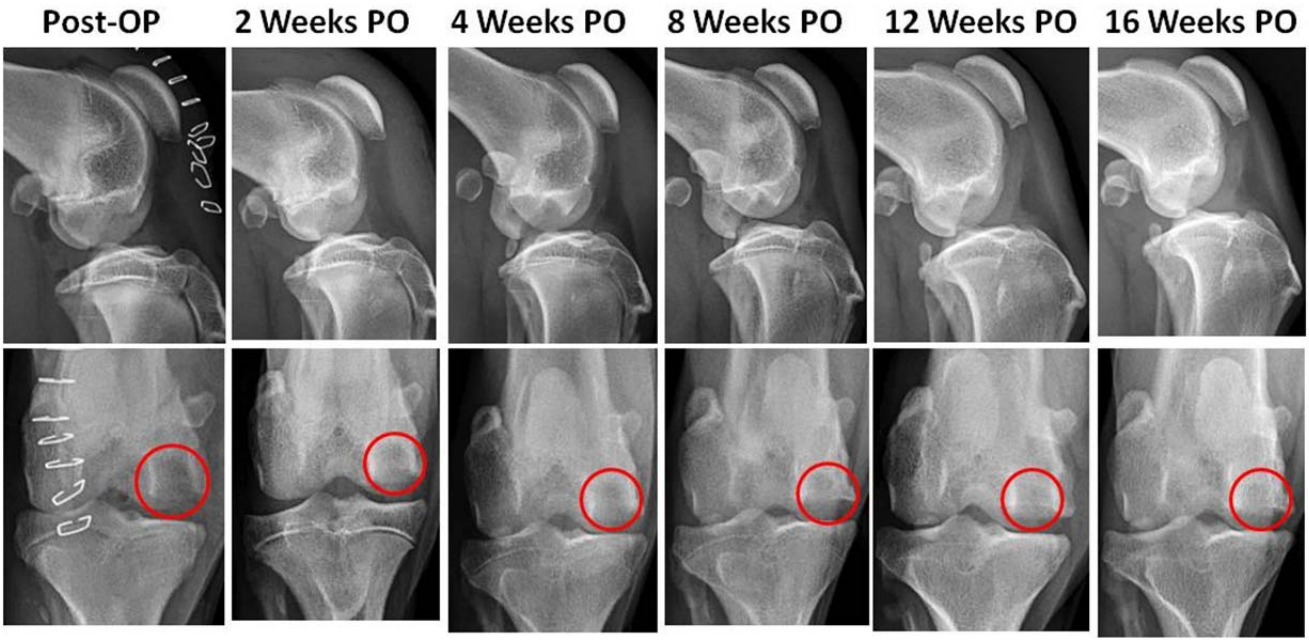

Figure 9: Radiographs for Osteochondral Dog 3 as a function of time: top row: medial-lateral view, bottom row: posterior-anterior view.

2.1.4 Osteochondral Defect MR Imaging

T1 and T2 MR images of Osteochondral Defect Dogs 1, 2 and 3 as a function of time are provided in Figures 10, 11 and 12, respectively. There was no apparent cartilage growth on the surface of unseeded scaffolds even at week 16. There were no apparent changes in the MR images as post-op time progressed. The red circles clearly outline the trough created in the condyle to receive the scaffold keel, which appear black in the MR image. A three-dimensional model of the distal femur of Osteochondral Dog 1 at post-op week 4 is shown in Figure 13. The sectioned condyle and trough created in the bone is apparent. The PCL-HA scaffold does not appear in the MR images and hence a model of it cannot be created from the MR images. The T1 MR images demonstrates low signal of the scaffold and sharp edges at the initial post-op 4 week. In agreement with the radiographic findings there is progressive blunting of the implant bone interface indicating some bony ingrowth.

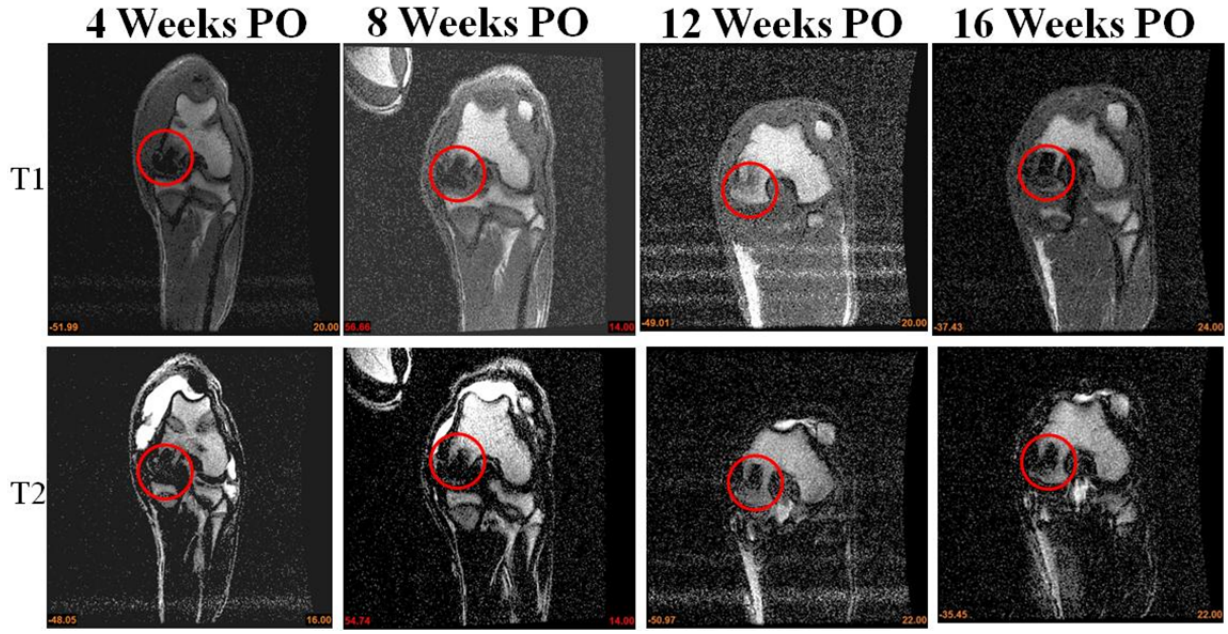

Figure 10: MR images of Osteochondral Dog 1 as a function of time: top row: T1 signal, bottom: T2 signal

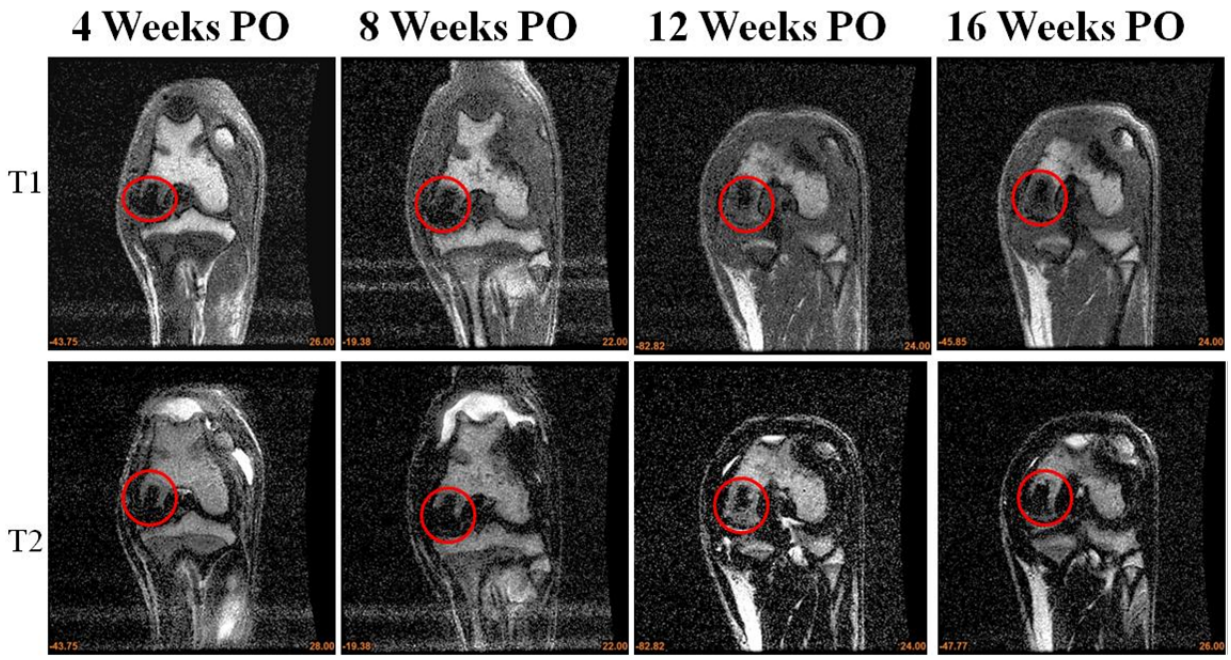

Figure 11: MR images of Osteochondral Dog 2 as a function of time: top row: T1 signal, bottom: T2 signal

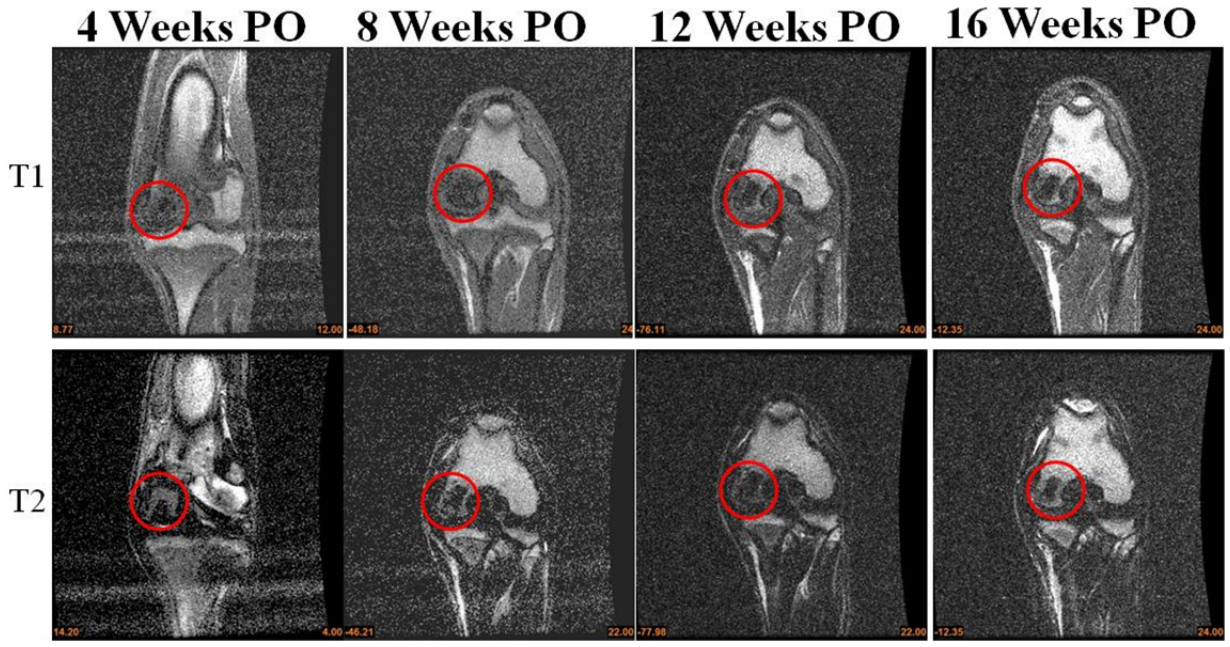

Figure 12: MR images of Osteochondral Dog 3 as a function of time: top row: T1 signal, bottom: T2 signal

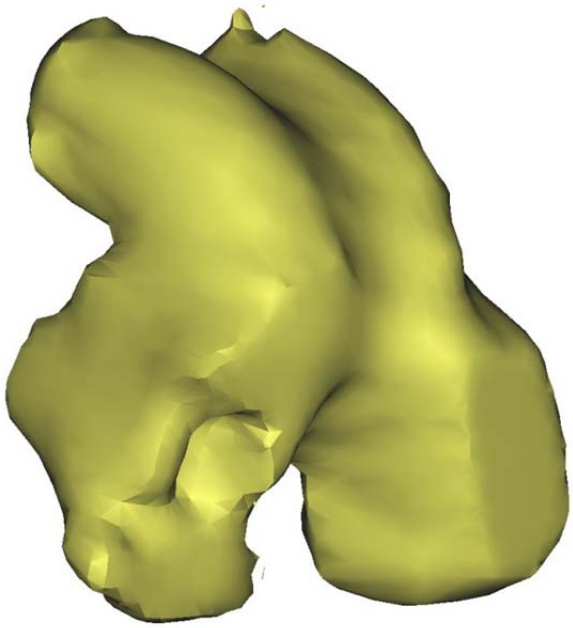

Figure 13: 3-D computer model of experimental left knee of Osteochondral Defect Dog 1 on Post-op week 4.

2.1.5 Post-mortem Observations for Osteochondral Defect Dogs

Following the prescribed 16 week post-op recovery period, all three osteochondral defect dogs were sacrificed and the intact joint capsules of both the experimental and contralateral control legs were carefully dissected out. The maximum flexion angle of each dog was measured. All three dogs had a maximum flexion angle of approximately 120˚ for the contralateral (control limb). The maximum flexion angle of the experimental limb for all three dogs was slightly less than that of their control limb, as shown in Figure 14.

Following the flexion angle measurement, the joints were disarticulated. The intra-operative photographs of the medial condyles with the scaffold implants are repeated from last year's report in Figure 15 (top row). The bottom row of Figure 15 shows the post dissection images. As mentioned above, Osteochondral Dogs 1 and 2 experience significant patella subluxation, and there is frequent patella dislocation for Dog 2. The repeated trauma caused by the patella dislocations resulted in the generation of a synovial pannus on the surfaces of the lateral condyles of the knees shown in dissection Figure 15 (a) and (b), bottom row, as well as malformations of the patella grooves and assorted osteophytes. The apparent damage to these knees is consistent with the lower outcome scores for these dogs and the clinically observed limp that these dogs occasionally exhibited. However, the articular surfaces of Osteochondral Dog 3, which was not observed to have any noticeable patella subluxation, appear relatively normal. Osteochondral Dog 2 was also somewhat heavier (>55 lbs) than Dogs 1 and 3 which may have exacerbated this effect, leading to the very poor condition of this knee. As mentioned above, it is suspected that the much larger surgical exposures for Dogs 1 and 2 than for Dog 3 are the main cause for the patella subluxations/dislocations and the resulting damage to the knees.

The prominence of the osteochondral scaffold above the native articular surface can be seen in Figure 14, top row for all three dogs. It is suspected that this prominence led to the breakdown of some of the top regions of the scaffold, as can be seen from the fine strands of PCL+HA extending from the scaffolds. This is most obvious for Dog 1, but was present for all three dogs. Scratches to the opposing medial tibial plateau were observed that further supports the potential abrasive effect of having the scaffolds seated proud. It is thought that this surface shearing effect may have prevented any soft tissue from forming on the articular surface of the scaffold. However, it is also possible that the plain scaffold may not lend itself to soft tissue formation on the articular surface. Of note is that care should be taken in osteochondral defect surgeries to ensure that the articular surface of the implant is at least 1-2 mm below that of the native articular cartilage to avoid any surface shear to allow soft tissue to form on the articular surface of the plain scaffold.

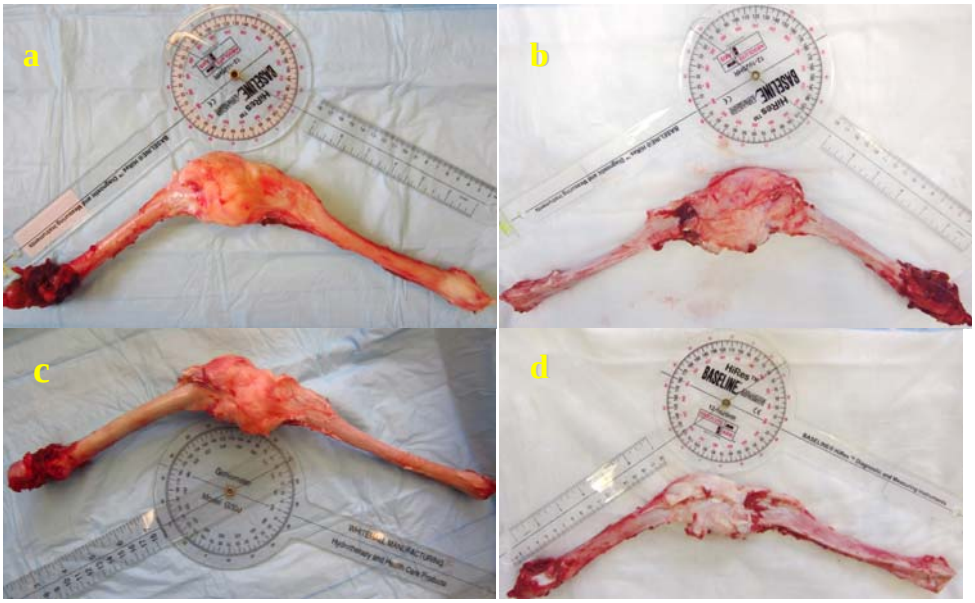

Figure 14: Maximum knee flexion angle of Osteochondral Defect dogs with capsule, tendon and patella, (a) Dog 1: 113°, (b) Dog 2: 114°, (c) Dog 3: 132°, (d) Dog 2 contralateral control: 120°.

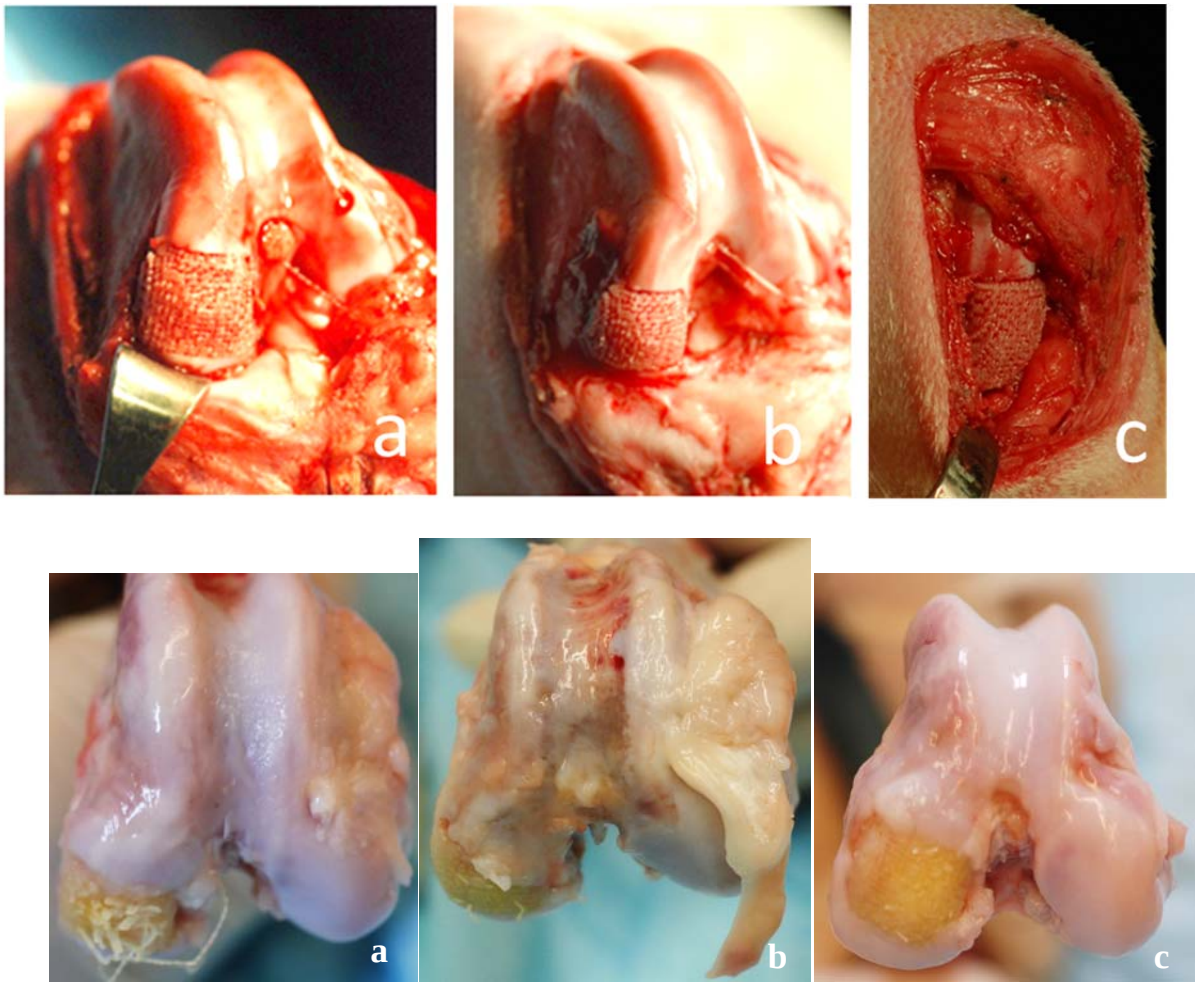

Figure 15: Inferior view of Osteochondral Defect dogs: (a) Dog 1, (b) Dog 2, (c) Dog 3. Top row: intraoperative view. Bottom row – view following dissection.

2.1.6 Osteochondral Defect Hard Sectioning Histology Study

Preparation

After dissection and photographing, the entire knee condyles of the three osteochondral dogs were sectioned and immediately immersed in 10% formalin solution for two months for fixation. Following fixation, the condyles underwent automatic dehydration and plastic infiltration (Leika TP 1020, Germany). The samples were put in a mold and covered with Technovit 7200 media (EXAKT, Germany). The submersed samples were than exposed to yellow and blue wavelength through the Light Polymerization Utility (EXAKT, Germany) for a period of two days to create a hard specimen block. The specimen block was then trimmed with a band saw (EXAKT, Germany), and the cut surface was ground smooth with 800 or 1000 grit sandpaper. The smoothed side was then glued to a 4"× 2" plastic template slide by Technovit 7210 and the glue was hardened on a Light-Polymerization-Block-Sandwich machine (EXAKT, Germany) with blue light for 5 min. The process was repeated for the other side to create a specimen block sandwich. The block was then cut on a band saw with a 1 cm-wide diamond blade (EXAKT, Germany). The cut direction was parallel to the surface to be stained resulting in 800 to 1000 μm thick slide specimen. To prepare the specimen for staining, the surface underwent a series of progressively finer polishing using 800 grit paper, 1000 grit paper and 1200 grit paper until only a 50~80 μm specimen layer was left. To eliminate scratches from cutting and grinding, and to improve transparency of the slide surface, the specimen surface was polished with 4000 polish paper for more than one hour on the same grinding machine. The entire protocol followed the method provided by the EXAKT company (1).

The slides were then stained with the standard Haematoxylin & Eosin (H&E) Stain or Masson's Trichrome Stain to distinguish connective tissues.

Microscopic Imaging

The hard tissue histology images were viewed with a Leica Microscope under 2X magnification. A montage was created from a number of 2X images using the Leica software and is shown in Figure 16a. Figure 16b shows a zoom-in view of the scaffold and the surrounding native bone chopped from the original large montage image generated by Leica software. Figure 17 shows the same region stained with Masson's Trichrome. From Figures 15 there appears to be tissue ingrown (darker pink) at the scaffold / native bone interface, with very light pink being the PCL+HA scaffold material. From Figure 17, there also appears to be some tissue ingrowth. However, there is no cartilage formation on the articular surface of the unseeded scaffold. This may be due to either an inability of the plain scaffold to incorporate chondrocytes, or it may be because, as is apparent in Figure 16(a), the scaffold was placed proud, and therefore there was a continuous shear of the scaffold surface against the tibia, possibly preventing any soft tissue from forming on this surface. Similar histological results were obtained for Osteochondral Dogs 2 and 3.

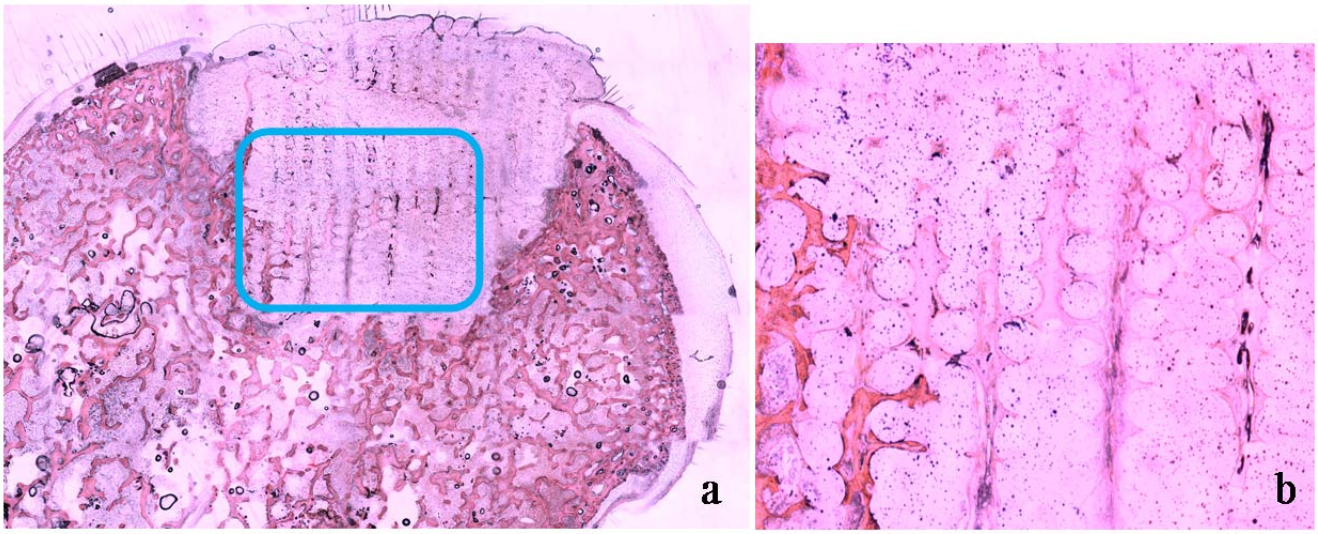

Figure 16: Hard sectioning histology image of Osteochondral Dog 1, stained by H&E method. (a) Montage of entire knee condyle. (b) Close-up of enclosed area showing the scaffold and adjacent native bone.

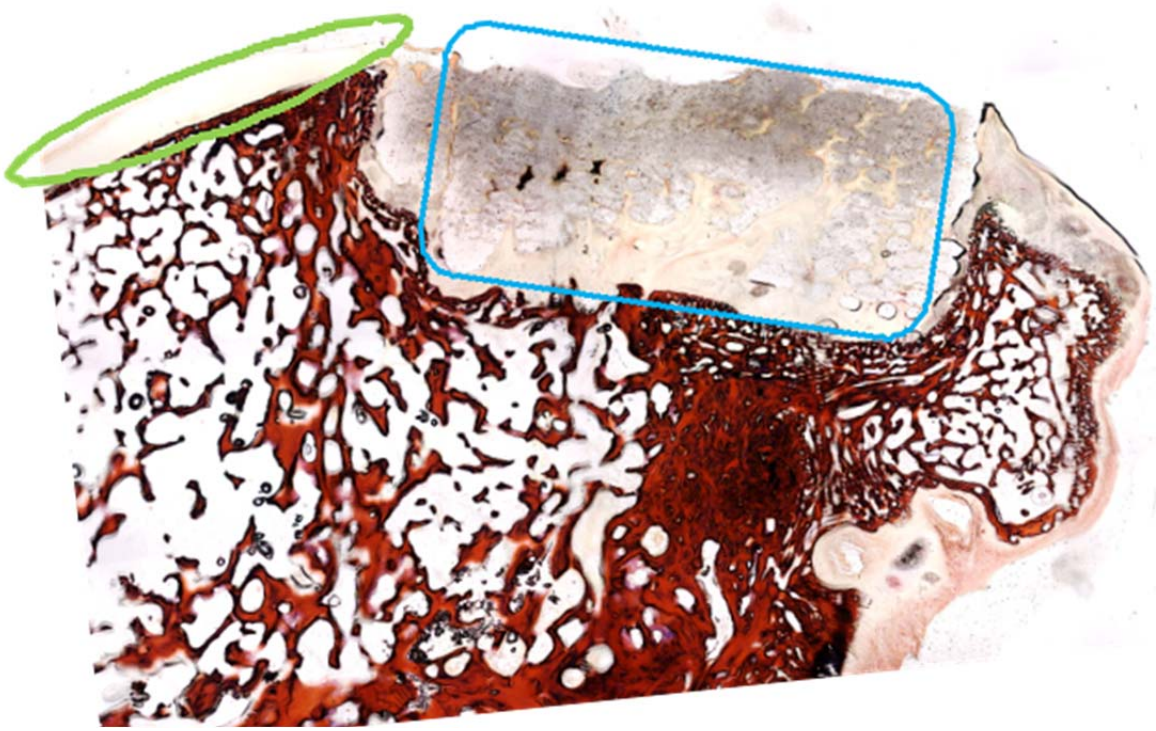

Figure 17: Hard sectioning histology image of Osteochondral Dog 2, stained with Masson's Trichrome. The region enclosed by the green oval is native articular cartilage, the region enclosed by blue represents the PCL+HA scaffold.

2.2. Aim 2 - Segmental Defects

A total of 28 segmental defect dogs underwent surgery. Six dogs received canine allografts, 10 segmental defect dogs received unseeded scaffolds, 6 segmental defect dogs received scaffolds seeded with BMP-2 and 6 segmental defect dogs received scaffolds seeded with cMSC. Twenty-six of the segmental defect dogs were taken to the full 16 week duration of the experiment and then humanely sacrificed. Two of early segmental defect dogs experienced premature plate failure and were sacrificed early. Switching from a standard size plate to a broad locking plate resolved the problem with plate failure. Radiologic images of the hind limbs following surgery were obtained for all dogs. Outcome measures were also recorded on nominally daily basis throughout the 16 week recovery period. Following sacrifice, mechanical testing was performed on the experimental (surgery) and control (contralateral) limbs. Details are provided below.

2.2.1 Segmental Defect Scaffold Design

The objective of the segmental defect scaffold is to promote both bony ingrowth into the subchondral bone. As for the osteochondral defect scaffold design, the scaffold architecture is based on the previous work of Lee et al, (Lancet 2010) (1) one of the co-investigators on this grant. As compared to the osteochondral defect, the segmental defect scaffold has the same pore size throughout. It was decided to not have an outer cortex layer (effectively a closed surface with no pores) which might be considered to be representative of cortical bone to facilitate infiltration from the tissue surrounding the scaffold. In addition, the scaffold was constructed as an annulus, with an inner lumen of 8 mm and an outer diameter of 16 mm. The surface of the scaffold adjacent to the lumen also did not have a closed surface, rather it had pores that permitted the infusion of bone marrow material through the lumen and into the scaffold through the pores (Figure 18.) The scaffolds were made 20 mm long to represent a critical size defect in the dog (1).

The scaffolds were manufactured in the same manner as the osteochondral defect by first obtaining CTs of several of the cadaveric canine tibiae. The digital files from the CTs were then imported in a program (Mimics, Materialise, Plymouth, MI) that combines the individual slices to create accurate three-dimensional models of the tibia. This 3-D model was then exported as an STL file, which was then imported into a DXF file to create the internal architecture of the scaffold, which in turn was used to devise the commands to drive a 3-printer (Bioplotter™, EnvisionTec, Germany,) which manufactured the scaffold by laying down small droplets of the liquid 90% poly-caprolactone (PCL) and 10% hydroxyapatite (HA) by weight using a 25 G needle. The resulting scaffold (Figure 8) had a pore size of 400 μm. Manufacturing time was approximately 4 hours.

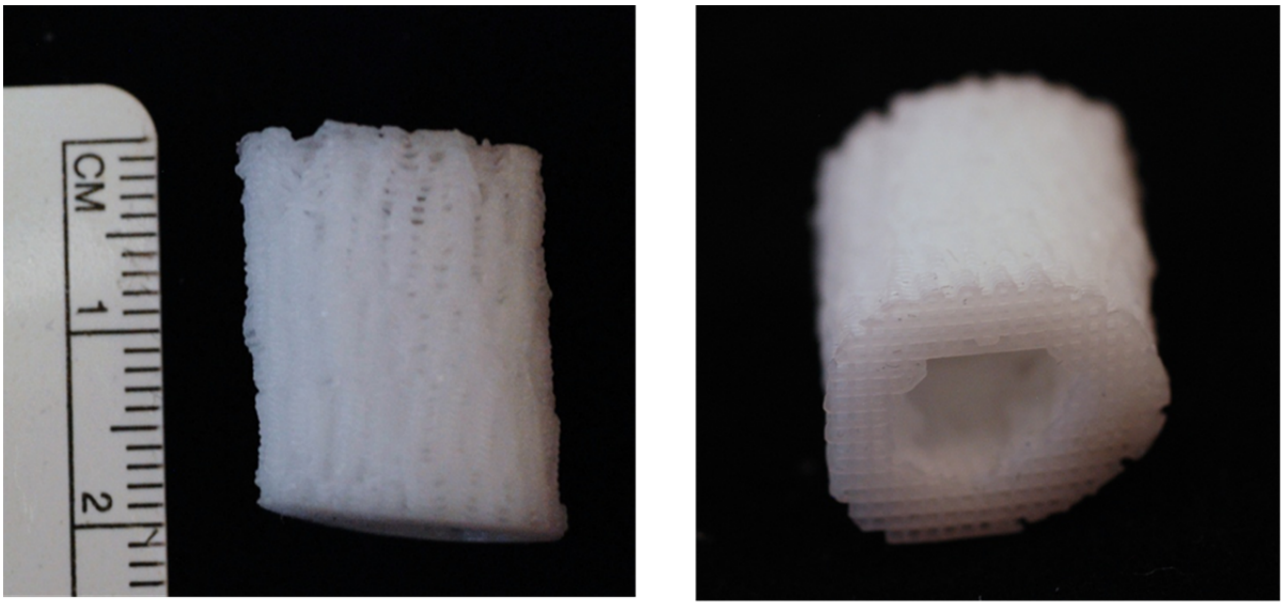

Figure 18: Photographs of two cm segmental defect scaffold showing no cortical shell

2.2.2 BMP-2 Microspheres Attachment to the Surface of Scaffolds

BMP-2 microspheres were synthesized with BMP-2 protein encapsulated into poly(DL-lactic-*co*-glycolic acid) (PLGA) microspheres through a double-emulsion procedure previously used by the co-PI of this grant (3). The microsphere attaching procedure incorporated a specified amount of hydrophobic microsphere powder suspended in pure ethanol followed by immersing the entire scaffold into the ethanol loaded with the microspheres and mixing for 20 minutes. The liquid soaked scaffolds were then placed on glass, and sprayed with the ethanol plus microspheres suspension. The scaffolds were air dried, followed by gas sterilization. The scaffolds with BMP-2 microspheres had the same apparent strength and a similar physical appearance as the unseeded scaffolds.

A BMP-2 attached segmental defect scaffold and an unseeded scaffold were selected for a scanning electron microscopic (SEM) imaging study. The scaffold was sliced and intersected to around 1 mm thickness pieces by a sterilized scalpel. A piece was then attached to a 10 mm diameter SEM specimen disk with special carbon double-side glue, and the specimen disk was dried overnight in a vacuum desiccator. The SEM test was done on a Zeiss Supra 55 SEM machine under 15 kV acceleration electron volts. The SEM images of unseeded scaffold piece and BMP-2 scaffold piece are shown in Figure 19 (a) and (b) separately. The surface of the unseeded scaffold had smooth surface with pore sizes of a few microns. The surface of the BMP-2 scaffold shows the attached microspheres. Because the specimen slices were specifically selected from the inner section of the scaffold, their SEM images prove that the BMP-2 microspheres can successfully enter into the body of the scaffold and attach to the surface of the inside walls.

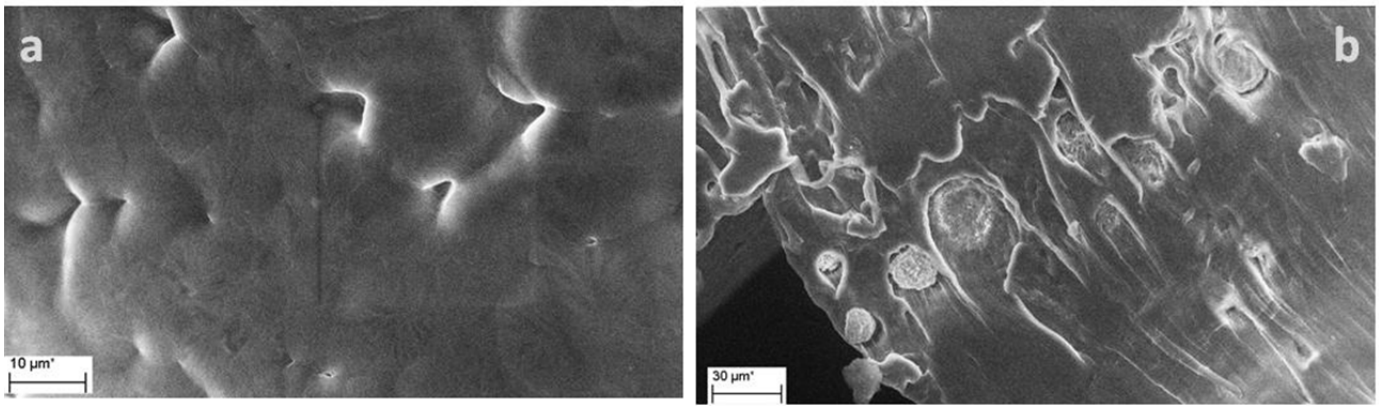

Figure 19: Scanning electron microscopic (SEM) image of the surface of the scaffolds in terms of (a) unseeded, and (b) seeded with BMP-2 microspheres.

2.2.3 Canine Stem Cell Expansion and Scaffold Seeding in-vivo Study

2.2.3.1 Methodology

In accordance with our approve IACUC protocol, bone marrow aspirate was obtained in a sterile fashion from the segmental defect dogs immediately post-mortem. The bone marrow aspirate was obtained bilaterally from the iliac crest of the dog and immediately cultured.

Canine BMSCs (Bone Marrow Derived Stem cells) derived from dog bone marrow were expanded in stem cell growth medium consisting of F12/DMEM (Life technologies Inc., MD, USA) supplemented with 20% (v/v) fetal bovine serum (Life technologies, USA) and 1% (w/v) Anti:Anti (Life technologies, USA). Osteogenic induction medium was prepared by adding 100 nM dexamethasone (Sigma) and 100 mg/ml L-ascorbic acid (Sigma) to the MEMα media) supplemented with 10% (v/v) fetal bovine serum (Life technologies, USA) and 1% (w/v) Penicillin: Streptomycin (Life technologies, USA). To induce osteogenic differentiation, BMSCs were seeded (10X5 cells/cm2) and cultured onto the PCL-HA scaffold in osteogenic induction medium with BMP-2 (50ng/ml) or without in 5% CO2 at 37°C. Cells were cultured in the stem cells growth medium for the first 10 days and in the osteogenic induction medium for the following day.

2.2.3.2 Live-Dead Staining

Initial cell viability was examined by fluorescence cell viability assay based on the simultaneous determination of live and dead cells with two probes that measure recognized parameters of cell viability (LIVE-DEAD Cell Staining Kit, Cambridge, MA, USA). After 7 day from seeding on the scaffold, cells were washed three times with PBS. The supplied cell-permeable green fluorescent dye (Ex/Em = 488/518 nm) and propidium iodide (PI), a cell non-permeable red fluorescent dye (Ex/Em = 488/615) was diluted with PBS and the cells on the scaffold were dyed using the aqueous working solution for 30 min in 5% CO2 at 37°C. After washing three times with PBS, the cells on the scaffold were placed on the cover glass and the observation was performed using a fluorescence microscope (Axiovert 2000, Carl Zeiss, Germany). These fluorescence images were shown in Figure 20. We found few dead cells.

2.2.3.3 Measurement of Cell viability on PCL-HA scaffold

To evaluate cell viability, we made a standard curve using optical density (OD) from MTT assay (Roche Applied Science, Indianapolis, IN, USA). We measured the OD use MTT assay and we converted the OD to a cell number relative to the standard curve. The BMSCs was used for cell viability assay. Four hundred µl of cell suspension was added to the scaffold at a density of 1×10^3 cells/scaffold. After 4 hours, 600 µl of growth medium was carefully added to the 12 wells plate. After culturing for 1 day in the plate, the cell/scaffold constructs were transferred to another 12 well plate, and added 100 µl of media that included 50 µl MTT reagent was added to each well and incubated at 37°C for 4 hours. An additional 500 µl of the solubilization solution was added to each well and incubated overnight. The absorbance at 570 nm was recorded using a Vermax microplate reader. The proliferation was evaluated after 7 days of culturing. The results shown in Figure 35 indicated the BMP positive group had higher cell numbers compared with BMP negative group at day 7 and day 14.

2.2.3.4 Immunocytochemistry

The canine BMSCs were seeded onto the scaffold at a density of 1×10^6 cells. Twenty-four hours later, media was replaced with fresh media. At indicated times, cells were fixed with 4% formaldehyde and permeabilized with 0.1% Triton X in PBS buffer. Non-specific binding was reduced by incubation in 1% BSA in PBST (0.1% Tween-20) at room temperature for 1 hour. The scaffolds were incubated overnight at 4°C with primary antibodies against COL1A1 primary antibody (1:100; Santa Cruz, USA), washed in PBST, and incubated with AF568-labeled secondary antibody (1:200; Life Technologies, USA) for 1 hour at room temperature. Nuclear staining was achieved with VECTASHIELD with DAPI (Vector Laboratories Inc., USA). Actin staining was achieved with FITC-phalloidin (Life Technologies, USA). The immunocytochemical fluorescence images at the same time point were shown in Figure 36.

2.2.3.5 Quantification of Osteogenic markers

Scaffolds were washed with PBS and total RNA was harvested using Trizol reagent (Life Technologies) according to the manufacturer's protocol. Total RNA (200 ng) was reverse-transcribed with Maxima First-Strand cDNA synthesis kit (Thermo Fisher Scientific Inc., USA). Real-time Quantitative PCR was performed with SYBR Select Master Mix UG (Life Technologies, USA) using QuantStudio 6 Flex (Life technologies, USA). Amplification conditions were 50°C for 2 min, 95°C for 10 min, followed by 40 cycles of denaturation (15s at 95°C), annealing (15s at 60°C) and elongation (20s at 72°C). Quantitative PCR results were normalized to the loading control (Beta-actin) transcript level to yield ΔCt, then normalized to control conditions (e.g., normoxia at the same time point) to generate ΔΔCt. Relative or fold

change in expression was subsequently calculated using the formula 2ΔCt or 2ΔΔCt, respectively. As shown from Figure 23, there was higher osteogenic gene expression level in BMP positive group than BMP negative group, which was according to the MTT assay result and the qualification results from fluorescence images.

2.2.3.6 Summary

A variety of growth factors control stem cell to osteogenic differentiation. In an *in-vitro* experiment, we tested a recombinant human bone morphogenetic protein-2 (rhBMP-2) with PCL-HA segmental defect scaffold to induce the differentiation of canine BMSCs towards osteogenic lineages, demonstrating the potential for scaffolds infused with canine BMSCs to promote bone infiltration and growth. Our approach was more efficient in the presence of rhBMP-2 rather than in the absence of rhBMP-2. The combined effects of biochemical signals from rhBMP-2 and scaffold stimulation on cell proliferation of canine BMSCs were examined in culture with and without soluble osteogenic factors (Figures 20 and 21). Furthermore, the rhBMP-2-added PCL-HA increased expression of RUNX2 and COL1A1 by the cells, compared to those without BMP-2 (Figures 22 and 23). We conclude that the combination of BMP-2 and the scaffold stimulated cell proliferation and differentiation in the *in-vitro* study.

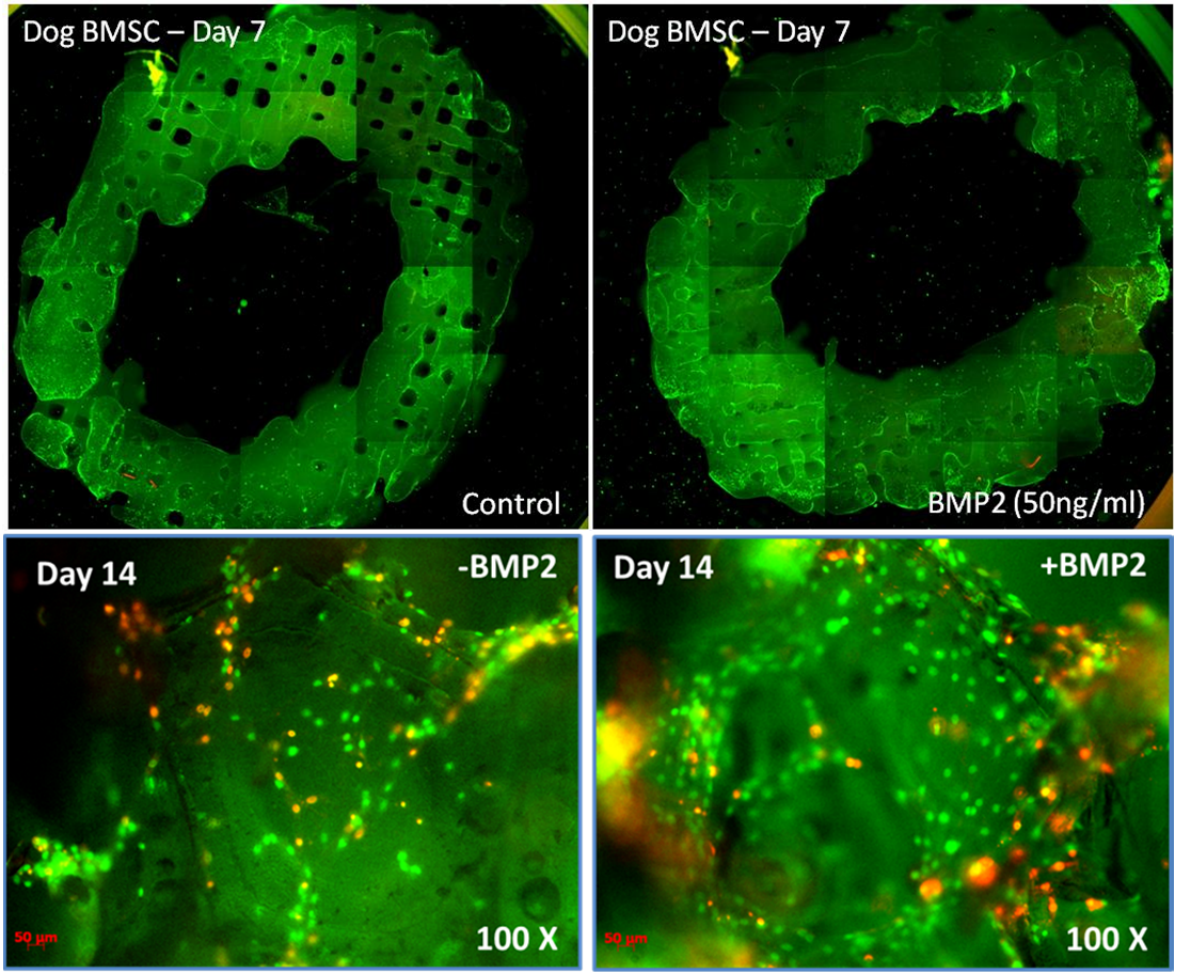

Figure 20: Live and dead assay of BMSCs on PCL-HA scaffold. Live cells were shown green and dead cells shown red. Most BMSCs were alive and gradually reached confluence at 14 days. Few dead cells were noted.

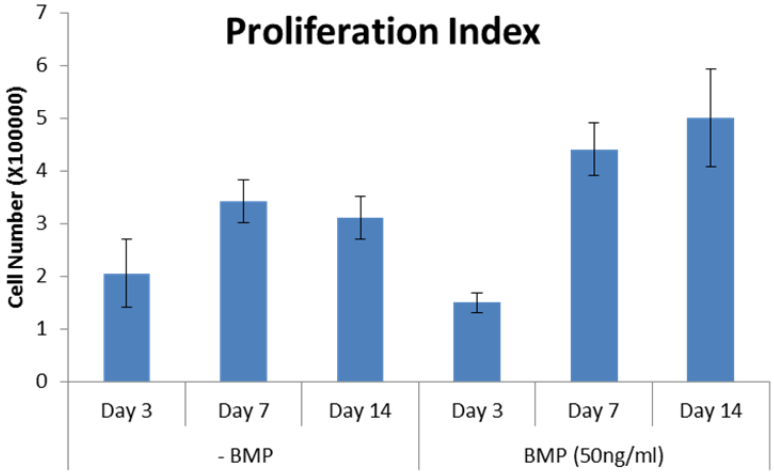

Figure 21: Quantification of viable cell number. There was significant difference in cell number between BMP with and without ($p < 0.05$).

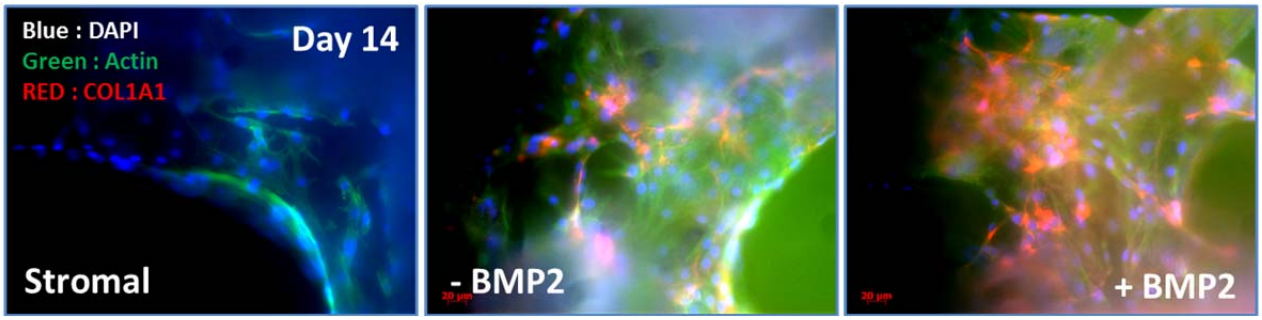

Figure 22: Fluorescence microscopic images of COL1A1 in BMSC cultured on PCL-HA scaffold for 14 days.

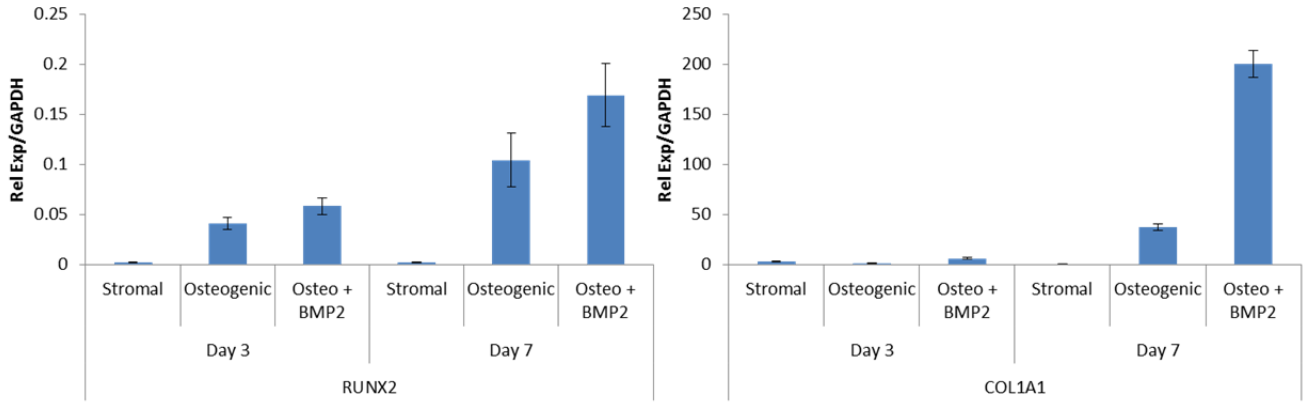

Figure 23: Related osteogenic gene expression levels in BMSC cultured on PCL-HA scaffold BMP2 with or without. Runx2 and Col1a1 gene expression levels were assessed by real-time PCR at days 3 and 7. GAPDH expression was also determined as an internal control. Significant difference between each groups are shown as ($p < 0.05$)

2.2.4 Segmental Defect Surgeries

The surgical approach and procedure were done in accordance to the approved IACUC protocol. The small fragment locking compression plate system from the Synthes® veterinary division (West Chester, PA) was used. To facilitate stability of the implant in a repaired critical size tibial defect, a 3.5 mm 8 hole locking compression plate (LCP) system was used. For segmental defect dogs, 1 through 7, a standard 3.5 mm LCP plate was used. However, because of instances of plate bending in 2 of the first 7 dogs, a broad 3.5mm LCP plate was used for dogs 8 through 28. No further problems with plate bending were observed.

Segmental defect surgeries were done in accordance to the approved IACUC protocol. The broad 3.5-mm-8-hole locking compression plate (LCP) system from the Synthes® veterinary division (West Chester, PA) was used for dogs 8 through 28. None of the dogs experienced any untoward events. A very slight amount of plate bending in one of the dogs was observed, but this very slight bend did not demonstrate any significant clinical manifestations and did not progress with time. Therefore, it was concluded that the use of broad LCP was a significant improvement to the standard plate.

The surgical procedure used to repair a segmental defect in the canine tibia was to perform a block excision of the middle 1/3 of the tibial shaft with an ORIF (open reduction, internal fixation) LCP (locking compression plated) and synthetic scaffold bone insertion. An anterolateral incision was made on the lateral side of the tibia, with the incision carried down to the periosteum, which was reflected back for later placement on top of the scaffold prior to closure. The long extensor digitorum were elevated laterally. The inferior check ligament was displaced laterally. A 2 cm tibial shaft cut was made half-way through the circumference of the medial side using an oscillating saw. An 8-hole (105 mm) locking compression plate was applied using 6 screws (3 superior, 3 inferior, all into native bone, none into the scaffold). All screws were sized to span both cortices. Locking screws were used wherever possible. A 2.8 mm drill bit was used for the 3.5 mm self-tapping locking screws. Once plate fixation was achieved, the superior and inferior cuts to the tibia were completed and a 2 cm bone piece was removed and replaced with a synthetic 2 cm bone graft (scaffold, Figure 24). One cortical screw was placed obliquely through the scaffold to maintain its stability. A 2.5 mm drill bit was used without a tap for the cortical screw. The incision was then closed and the wound bandaged with sterile dressing.

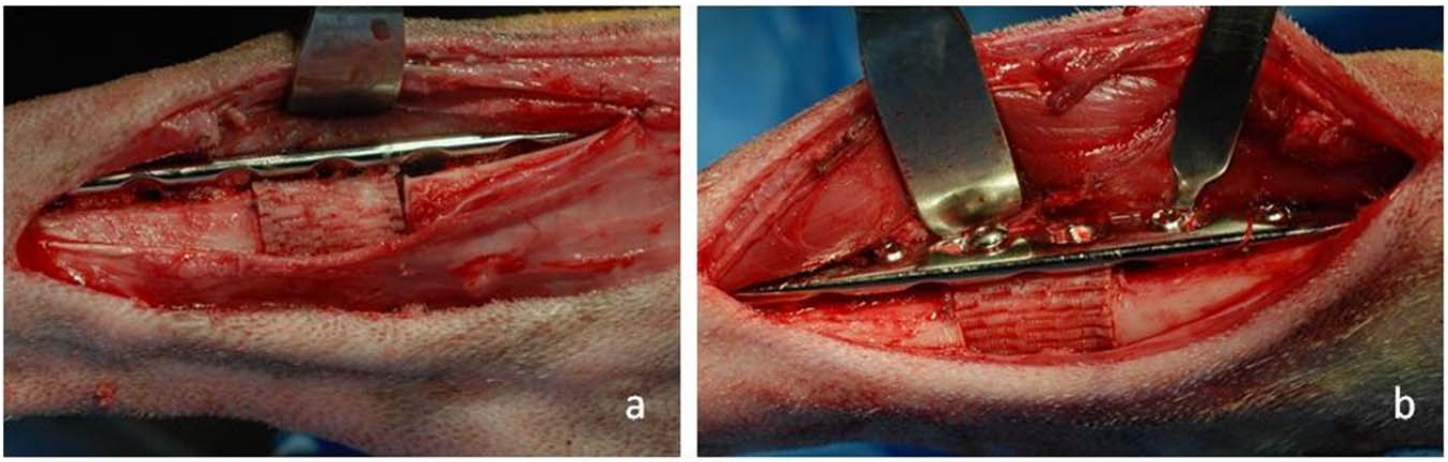

Figure 24: Operative photo showing sterile field, locking plate, and placement of scaffold in segmental defect in the exposed lateral side of the right tibia of Segmental Defect Dog 1 (a) and Dog 2 (b).

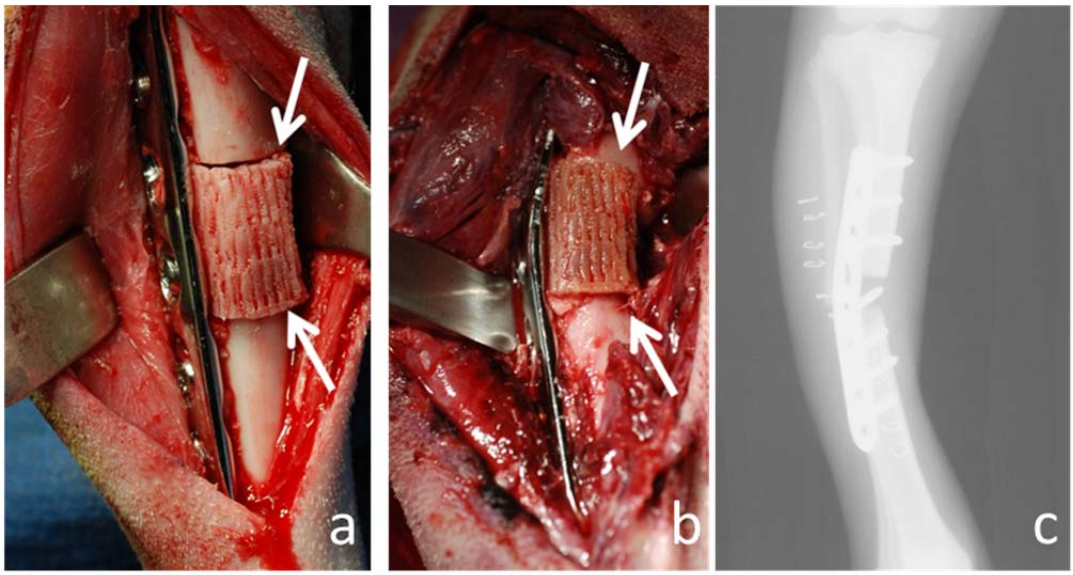

Figure 25: Segmental Defect Dog 3 right tibia a) scaffold placement during surgery, arrows denote misalignment of scaffold with transected bone ends, b) exposure following sacrifice showing bent plate with arrows denoting subsidence of proximal and distal bone edges in scaffold, c) radiograph of bent plate prior to dissection.

Segmental Defect Dogs 1 and 2 experienced no post-surgery problems. However, Dog 3 experienced an adverse event. The dog appeared to be recovering as expected after surgery, with moderate weight bearing on the operated limb. On post-op day 4, there was minimal right hind leg weight bearing, the incision site was erythematous, swollen, and hot to touch. The treatment with additional antibiotic was initiated. On the morning of post-op day 5, it was noticed that there was excessive flexion of the stifle, no weight bearing, and lateral deviation of the tibia. The dog was sedated, and radiographs of the right hind leg were taken. Radiographs showed a bent stabilization plate, fractured fibula, and deformed osteotomy site. The dog was euthanized with an overdose of euthanasia solution by the attending veterinarian.

Figure 26: Lateral view of excised tibiae of a) Segmental Defect Dog 1 with fibula still attached. Note the significant amount of bony callus surrounding the plate. b) Segmental Defect Dog 2 with part of the fibula near the middle of the plate not yet removed. Note significantly less bony callus surrounding the plate than for Dog 1.

After careful dissection of the affected limb and review of all surgery photographs and radiographs (Figure 25), it was concluded that the cause of the plate failure was malalignment of the scaffold with the transected bone ends, which in this dog had rougher edges than in the first two dogs due to the need for repeated cutting of the bone ends to properly fit the scaffold. It is postulated that the combination of malalignment and rough bone edges caused the bone ends to effectively cut their way through the scaffold due to their sharpness and the fact that the stress was high because the annulus of the transected bone ends was not fully supported by the malaligned scaffold. As the bone ends subsided into the scaffold, they effectively pushed the scaffold into the plate causing it to bend. Once the effective length of the tibia was shortened because of the plate bending, the fibula received too great a percentage of the load supported by the limb, causing it to fracture, resulting in further deformation of the limb. Another possible confounding factor is that an increase in associated leg pain might have made it difficult for the dog to ambulate, increasing the likelihood of a fall, which would have further aggravated the problem.

To avoid this complication in future segmental defect surgeries, two primary corrective plans were proposed in a modification to the IACUC protocol. First and foremost, more care was exercised during surgery to ensure that the scaffold was properly placed and aligned with the transected tibia. Secondly, the

dog was sling-walked immediately following surgery to preclude any possibility of a fall. Sling-walking was continued until the attending veterinarian determined that the dog was properly and safely ambulating.

Sixteen weeks post-surgery, the animals were humanely sacrificed and both hind limbs removed by disarticulating at the hip. The tibiae were then carefully excised and all soft tissue removed in preparation for biomechanical testing. The fibulae of both experimental (right limbs) were found to be adhered to the tibia in the immediate vicinity of the plate via callus formation. Using sharp dissection, and, where necessary, a small oscillating power saw, the adhered fibulae were carefully removed without damaging or putting undue stress on the tibiae. There was callus formation around the edges of the plate and in the screw holes of the plate for both dogs, more so for Dog 1 than for Dog 2 (Figures 26a and b). All locking screws were found to be tight upon removal. The cortical screws in each of the scaffolds were not loose, but nor where they tight. They had not backed out, maintaining the same position on the plate as during initial insertion.

2.2.5 Segmental Defect Radiographs

Digital radiographs were taken of all segmental defect dogs every two to four weeks. The dogs with BMP-2 scaffolds (segmental defect dog 8, 9, 10 12, 13 and 14) qualitatively demonstrated more callus formation than the dogs with unseeded scaffolds (segmental defect dog 1, 2, 4, 11, 15, 18, 19 and 21) four weeks post-surgery. Slight bending was observed for Segmental Defect Dog 15, possibly because less than optimal scaffold placement during surgery. The bending first appeared at four weeks (Figure 27) and did not progress the remaining twelve weeks to sacrifice.

2.2.5.1 Allograft Segmental Defect Radiographs

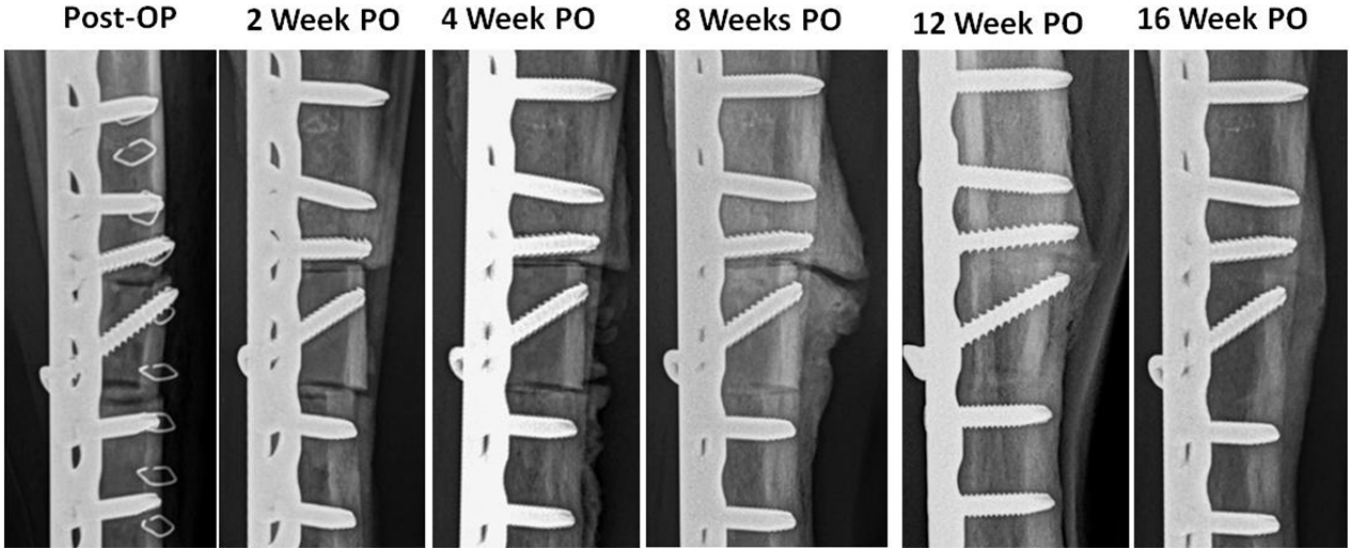

Figure 27: Radiograph of lateral view for Segmental Defect Dog 5 (allograft) as a function of time showing progress of callus formation in the vicinity of the allograft (the area between the two cuts with an oblique screw). By post-op week 8 the gaps between both superior and inferior ends of the allograft was clearly narrowing.

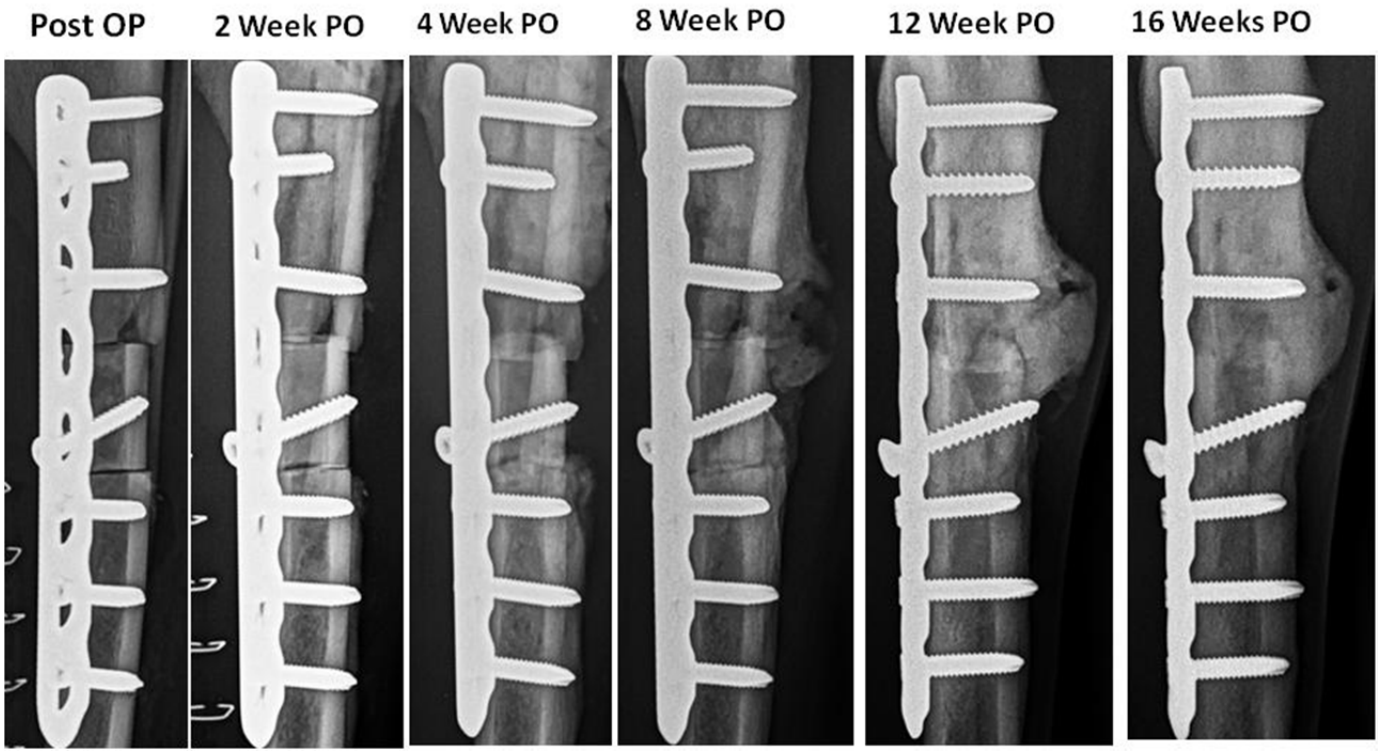

Figure 28: Radiograph of lateral view for Segmental Defect Dog 6 (allograft) as a function of time showing progress of callus formation in the vicinity of the allograft (the area between the two cuts with an oblique screw). As for Dog 5, by post-op week 8 the gaps between both superior and inferior ends of the allograft was clearly narrowing

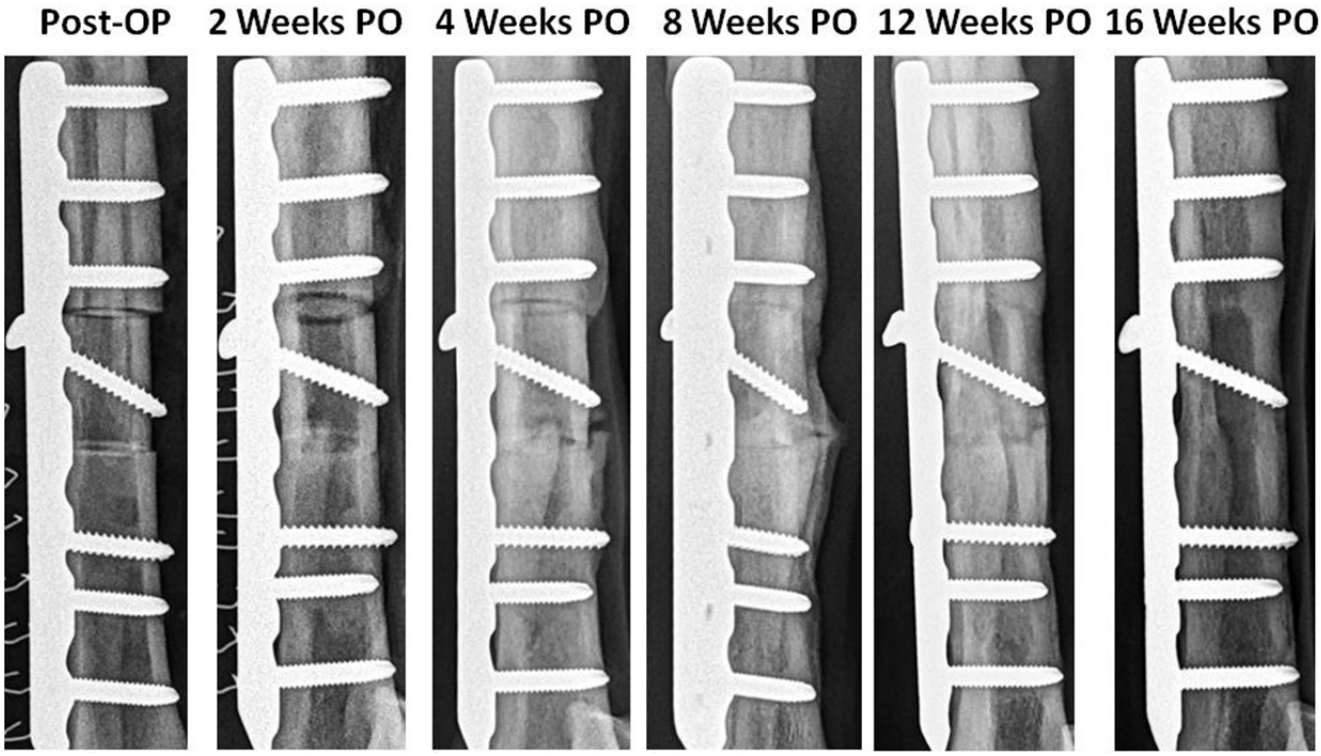

Figure 29: Radiographs of lateral view for Segmental Defect Dog 16 (allograft) as a function of time.

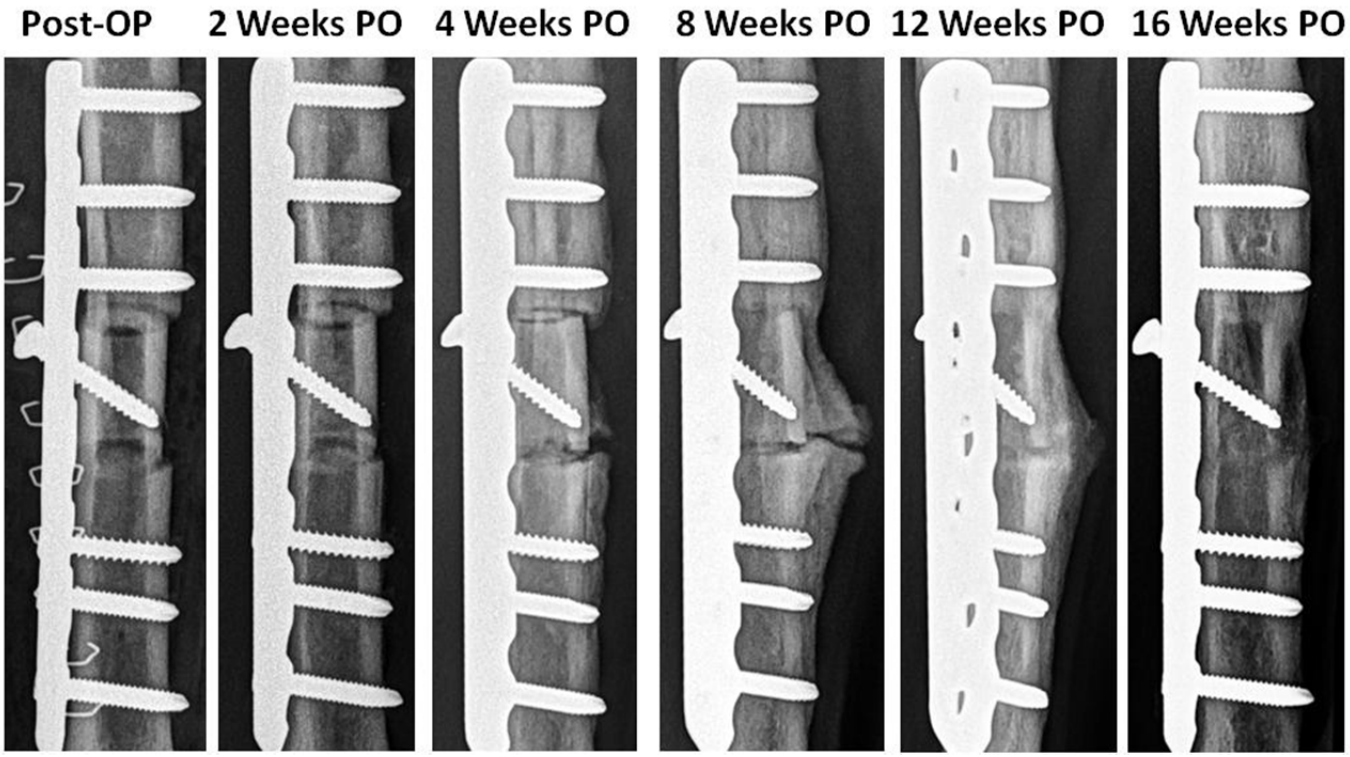

Figure 30: Radiographs of lateral view for Segmental Defect Dog 17 (allograft) as a function of time.

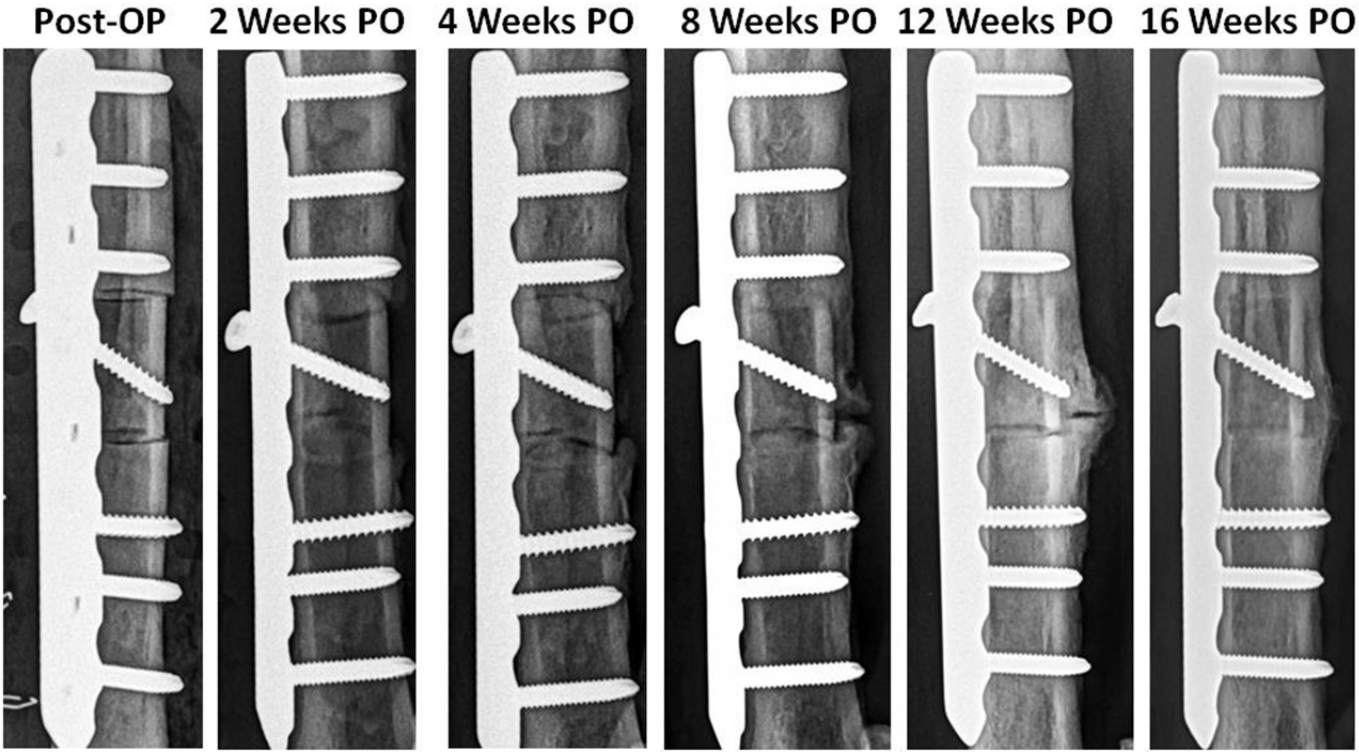

Figure 31: Radiographs of lateral view for Segmental Defect Dog 20 (allograft) as a function of time.

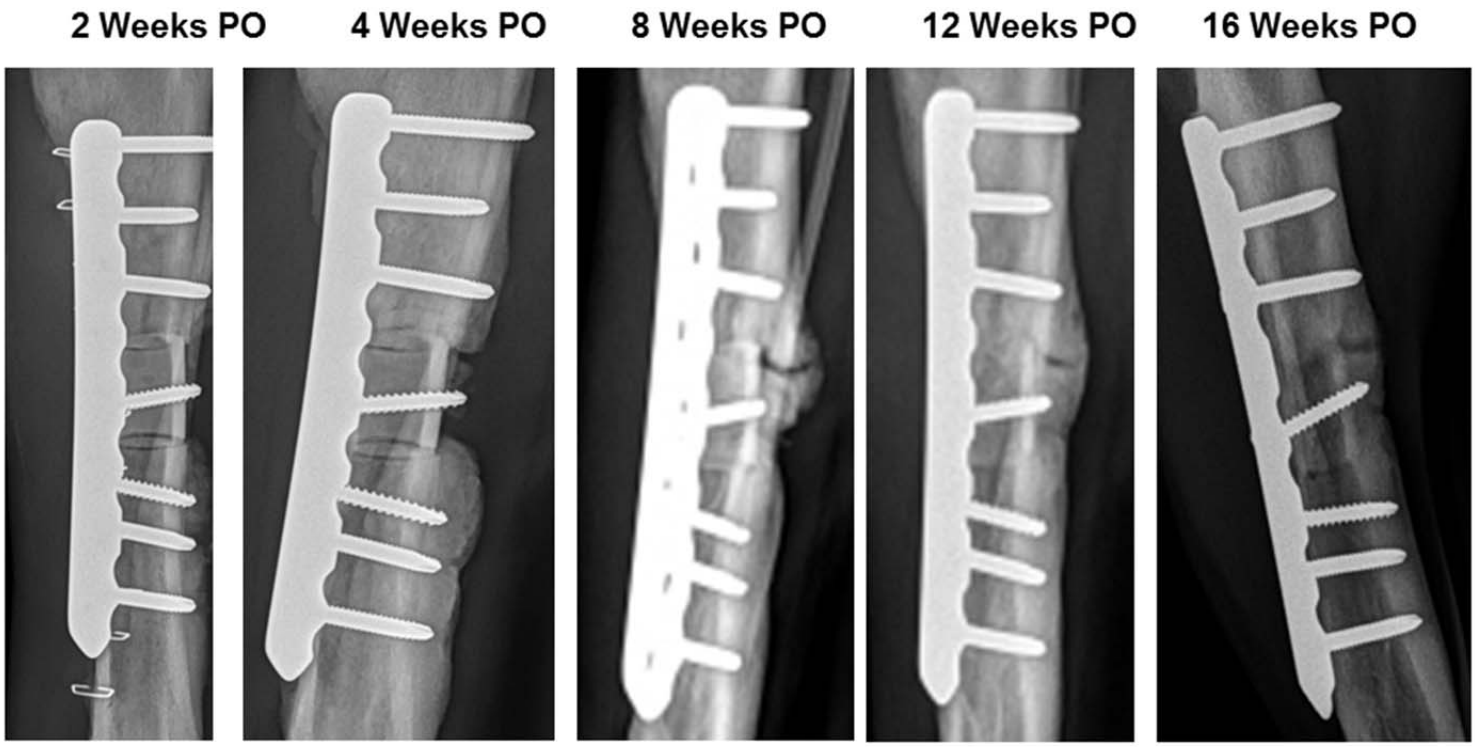

Figure 32: Radiographs of lateral view for Segmental Defect Dog 22 (allograft) as a function of time

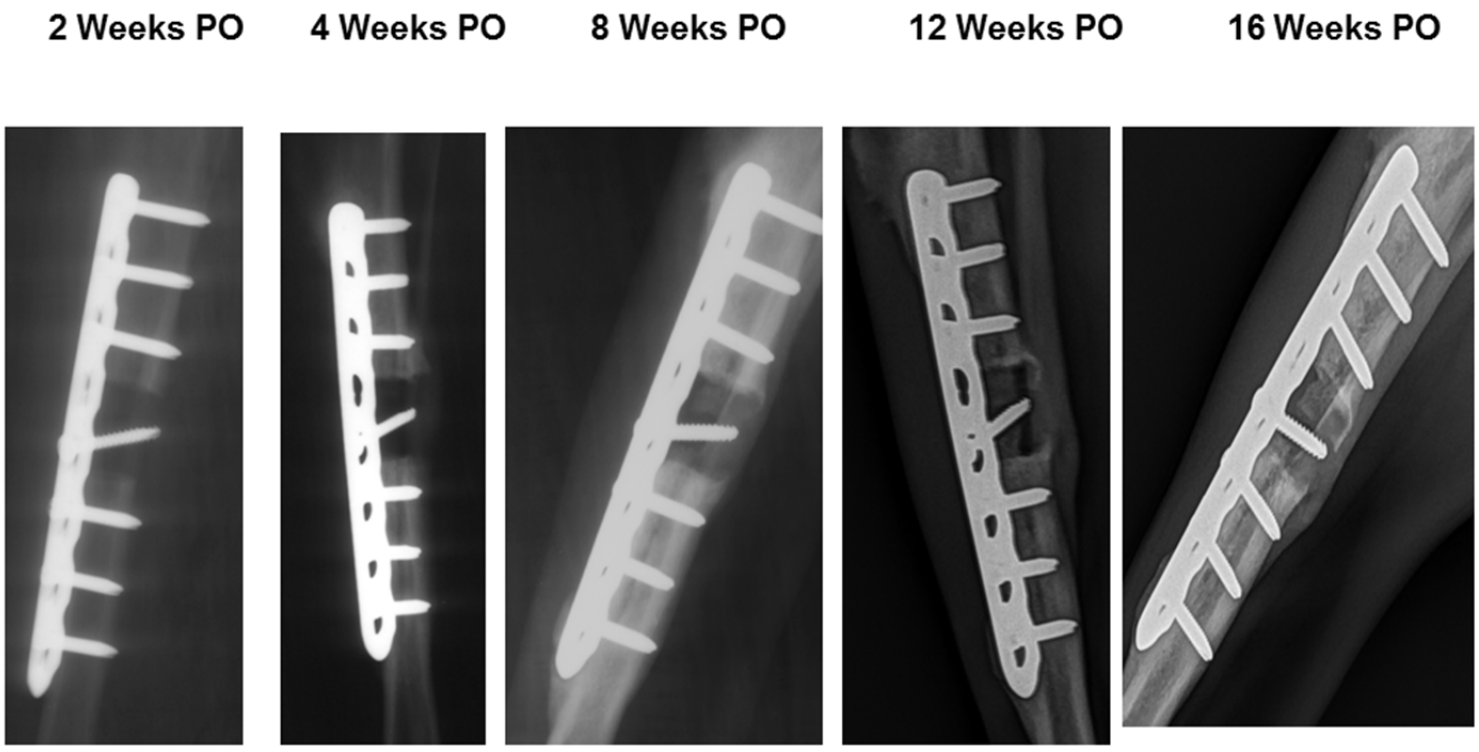

2.2.5.2 Unseeded Scaffold Segmental Defect Radiographs

Figure 33: Radiographs of lateral view for Segmental Defect Dog 1 (unseeded scaffold) as a function of time showing the progression of callus formation in the vicinity of the scaffold (relatively dark area with oblique screw through it).

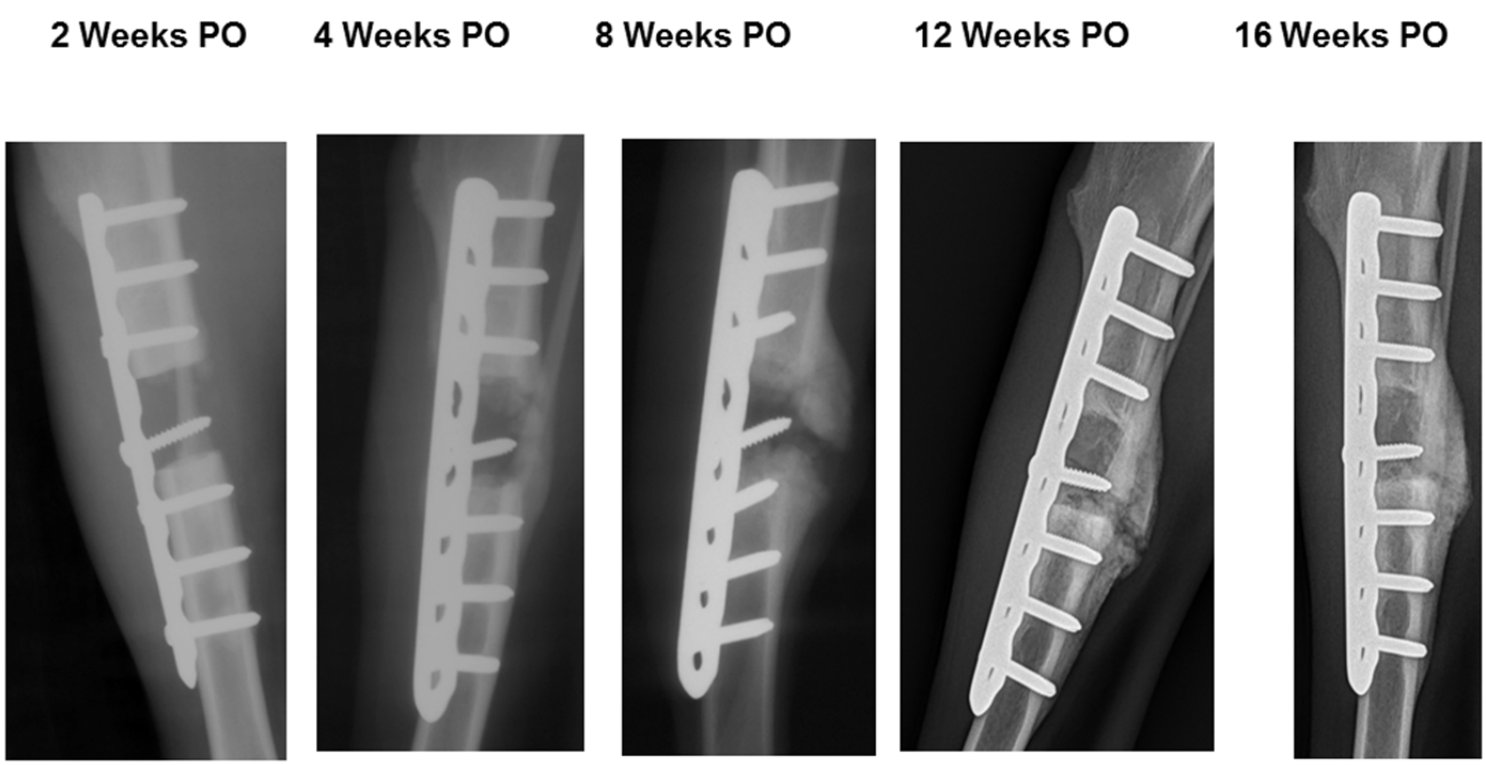

Figure 34: Radiographs of lateral view for Segmental Defect Dog 2 (unseeded scaffold) as a function of time showing the progression of callus formation in the vicinity of the scaffold (relatively dark area with oblique screw through it).

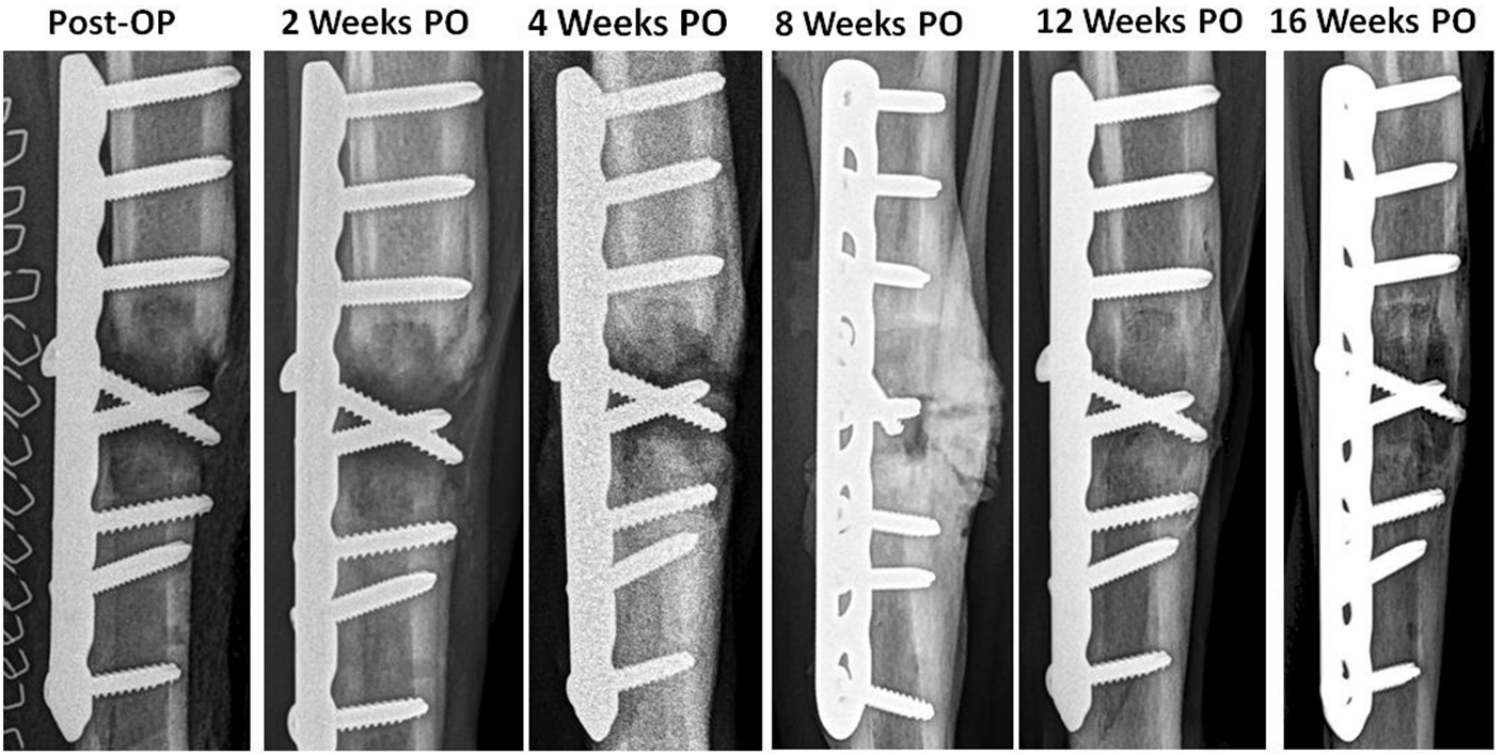

Figure 35: Radiograph of lateral view for Segmental Defect Dog 4 (unseeded scaffold) as a function of time showing the progression of callus formation in the vicinity of the scaffold (relatively dark area with oblique screw through it).

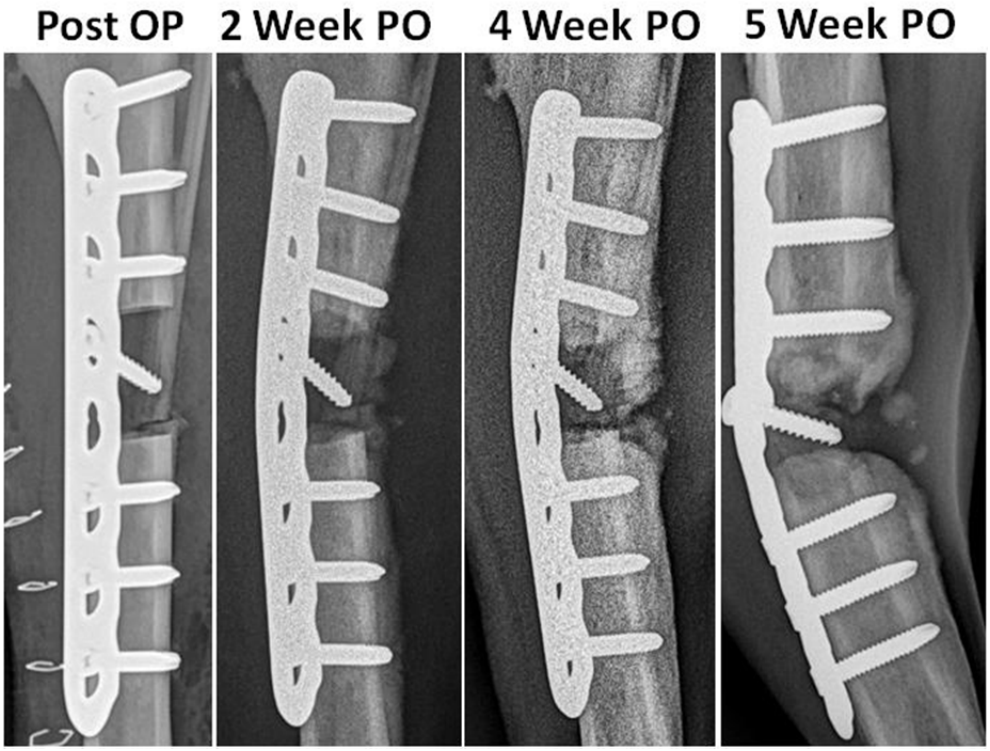

Figure 36: Radiograph of lateral view for Segmental Defect Dog 7 (unseeded scaffold) as a function of time showing. Slight bending of the plate is apparent by week 2, with catastrophic plate failure occurring at week 5 PO.

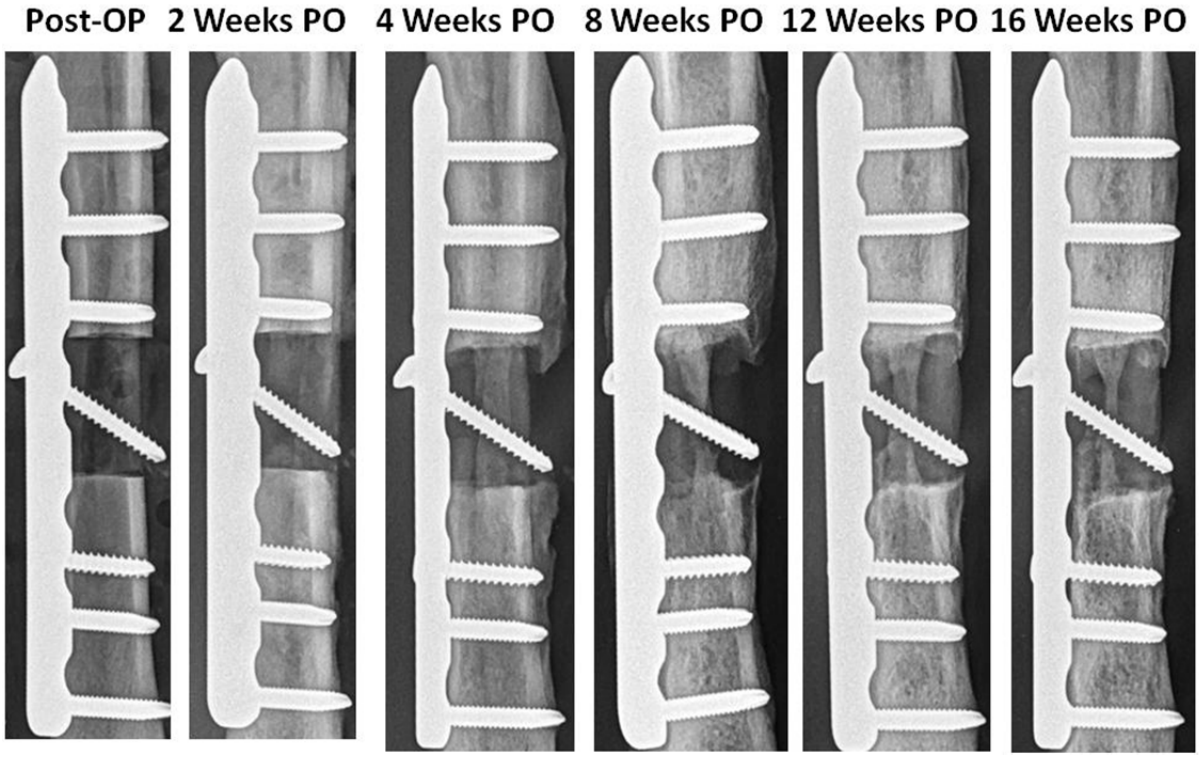

Figure 37: Radiographs of lateral view for Segmental Defect Dog 11 (unseeded scaffold) as a function of time.

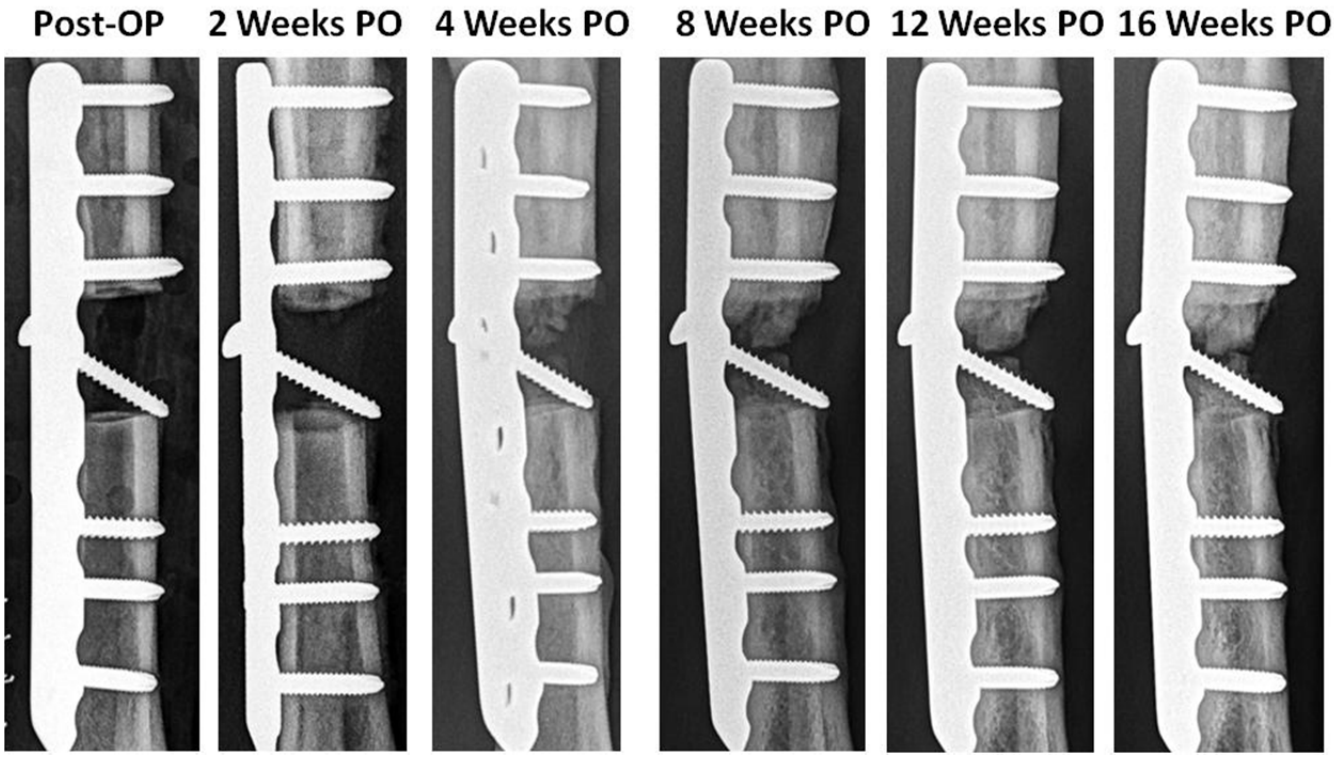

Figure 38: Radiographs of lateral view for Segmental Defect Dog 15 (unseeded scaffold) as a function of time.

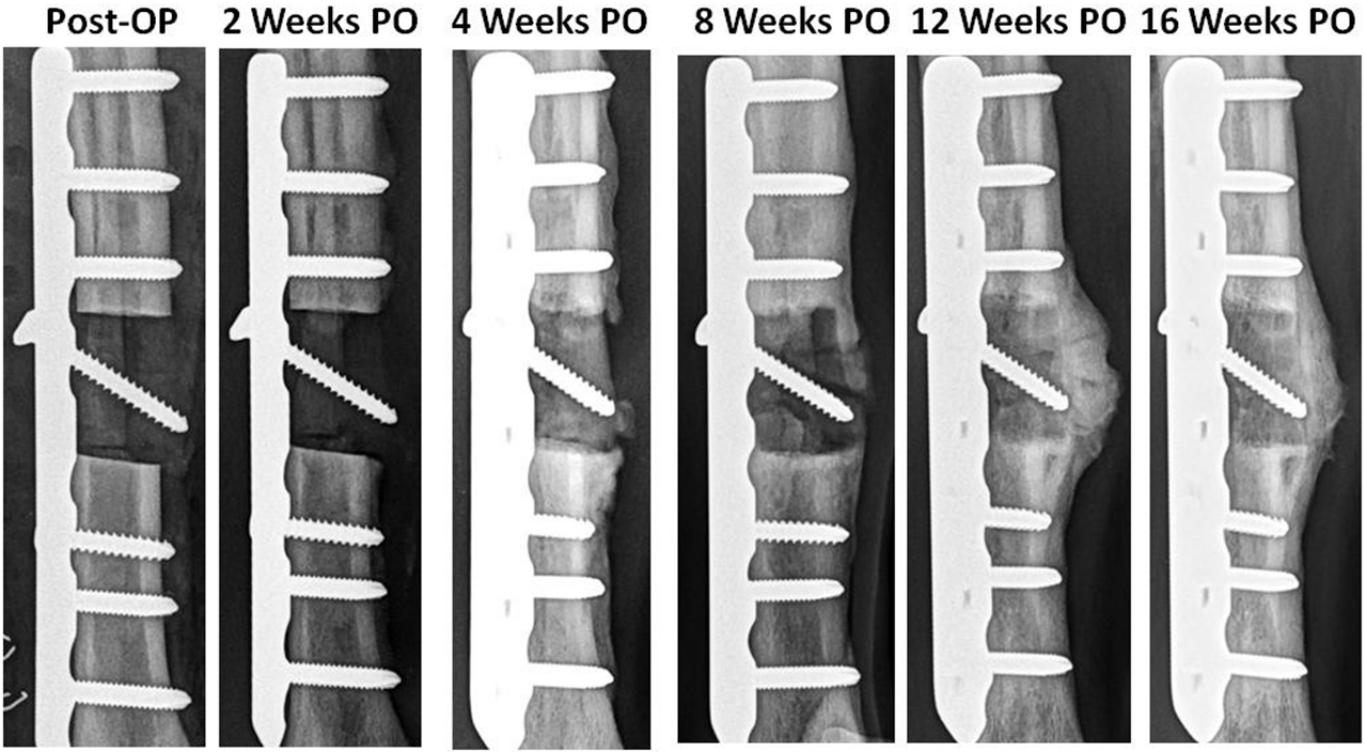

Figure 39: Radiographs of lateral view for Segmental Defect Dog 18 (unseeded scaffold) as a function of time.

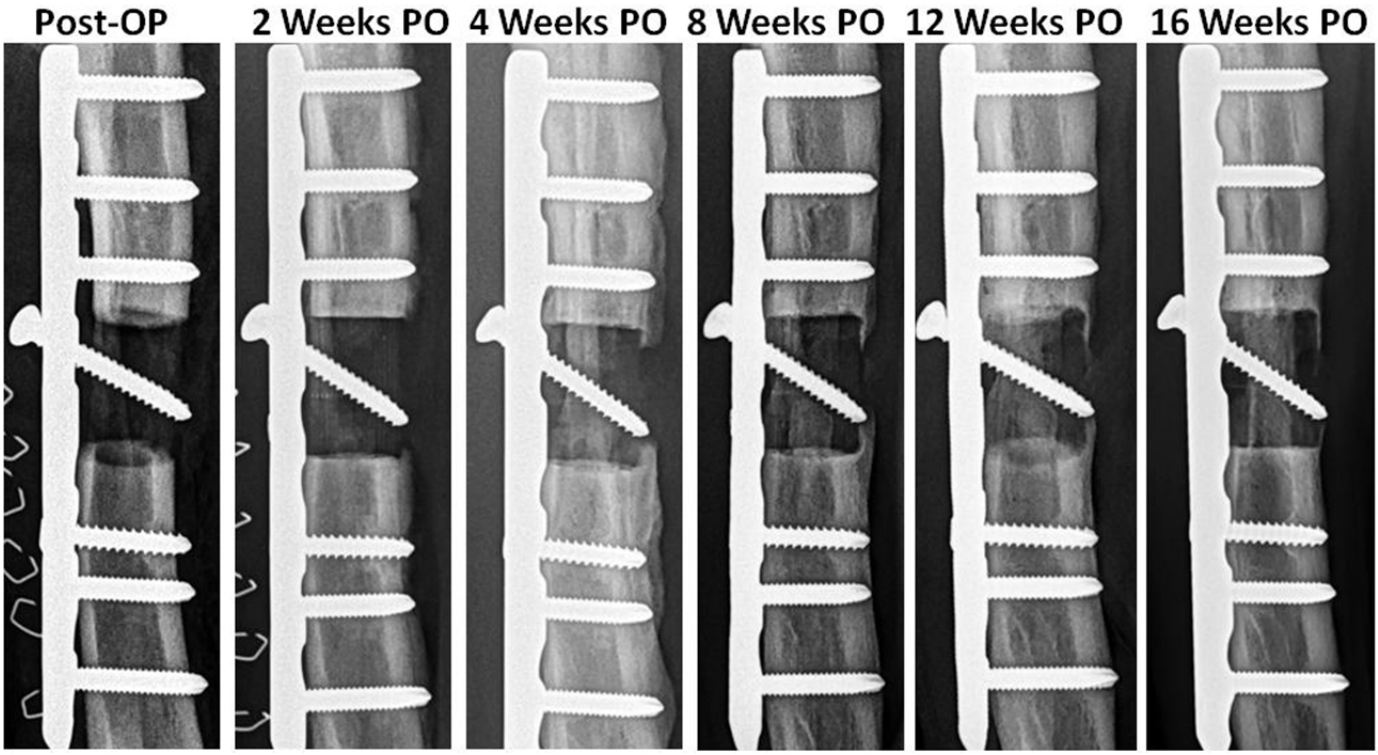

Figure 40: Radiographs of lateral view for Segmental Defect Dog 19 (unseeded scaffold) as a function of time.

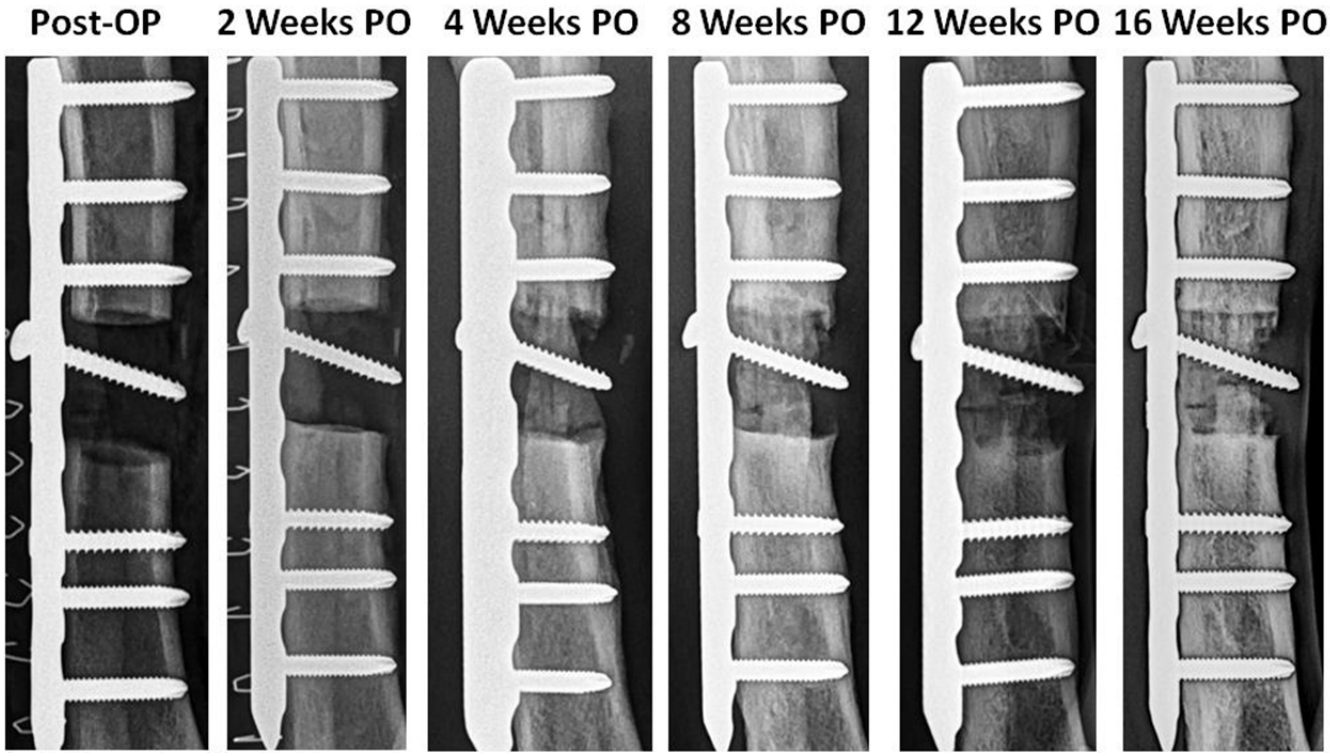

Figure 41: Radiographs of lateral view for Segmental Defect Dog 21 (unseeded scaffold) as a function of time.

2.2.5.3 BMP-2 Seeded Scaffold Segmental Defect Radiographs

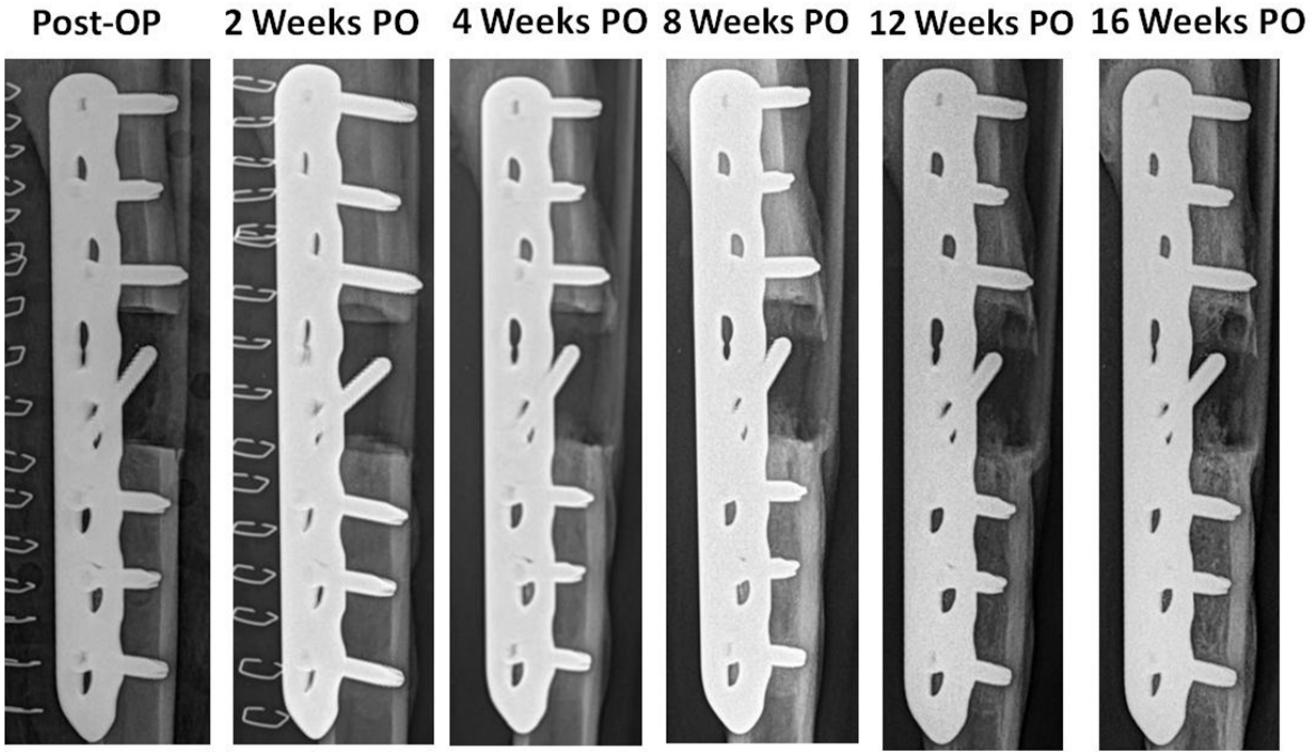

Figure 42: Radiographs of lateral view for Segmental Defect Dog 8 (BMP-seeded scaffold) as a function of time.

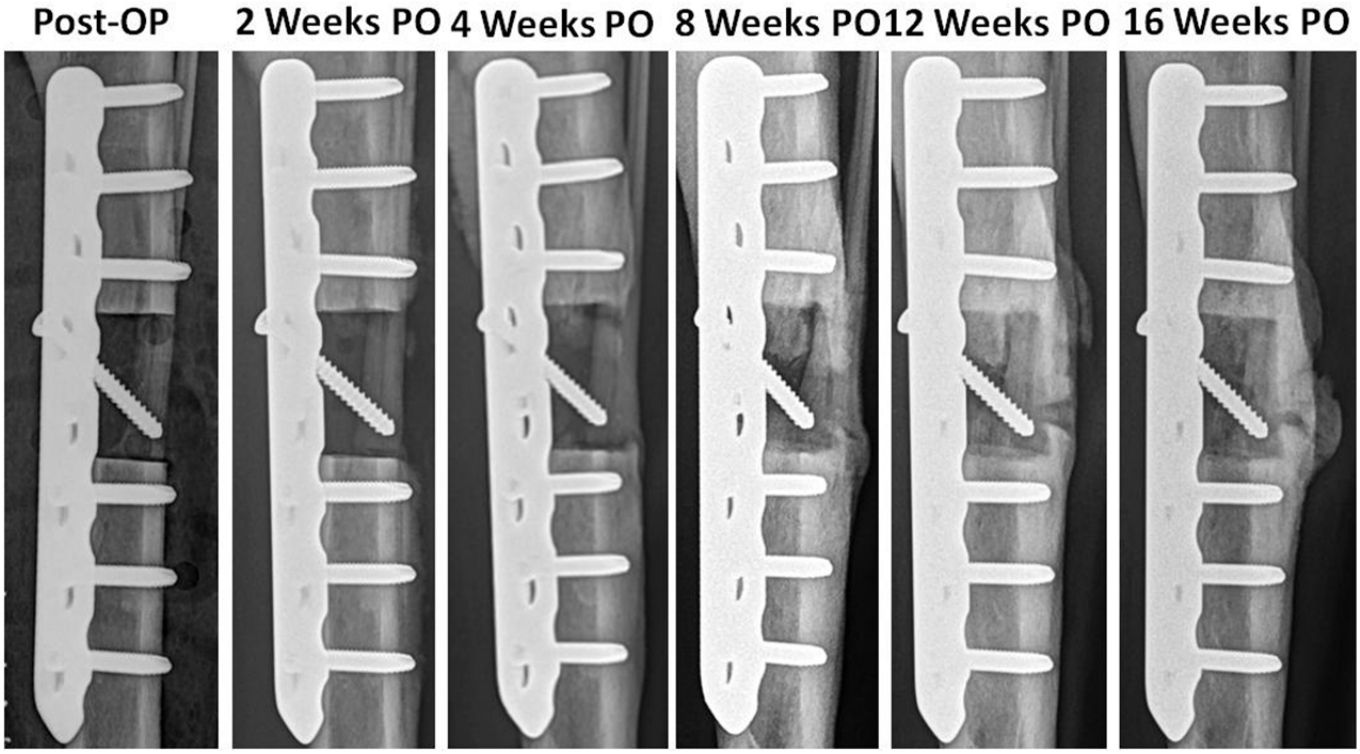

Figure 43: Radiographs of lateral view for Segmental Defect Dog 9 (BMP-seeded scaffold) as a function of time.

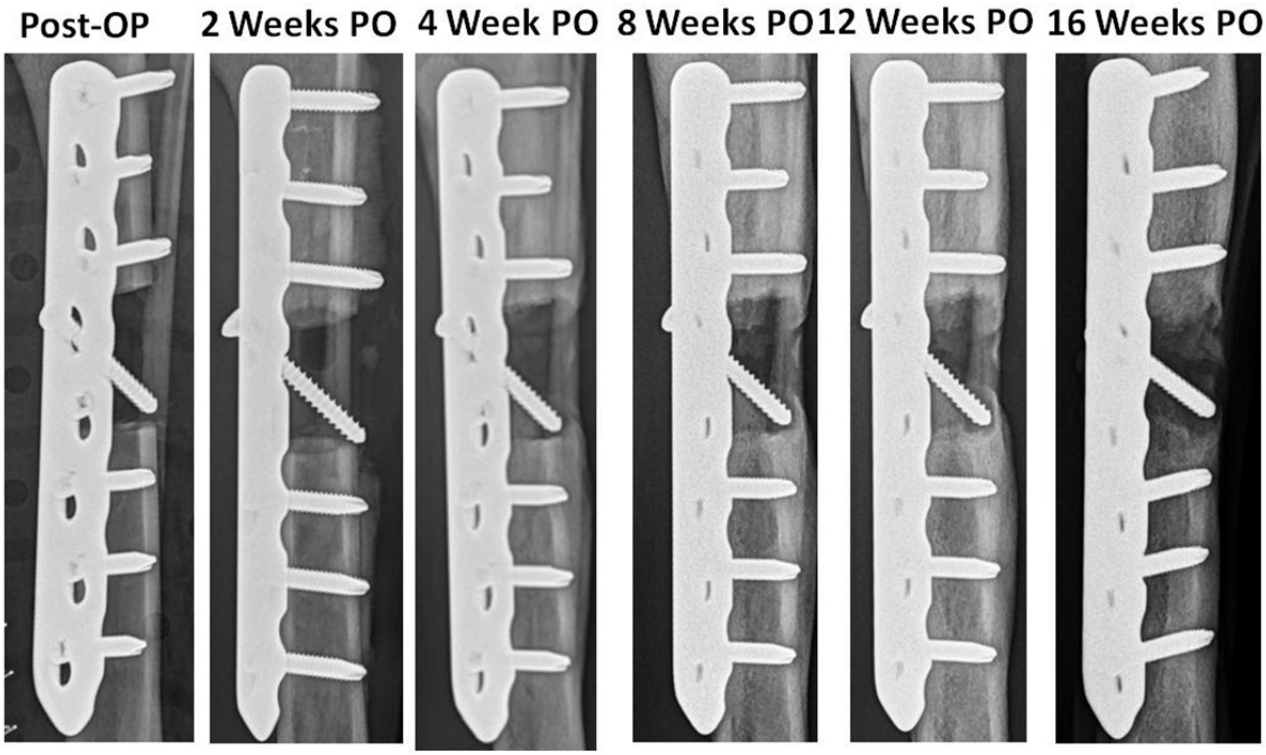

Figure 44: Radiographs of lateral view for Segmental Defect Dog 10 (BMP-seeded scaffold) as a function of time.

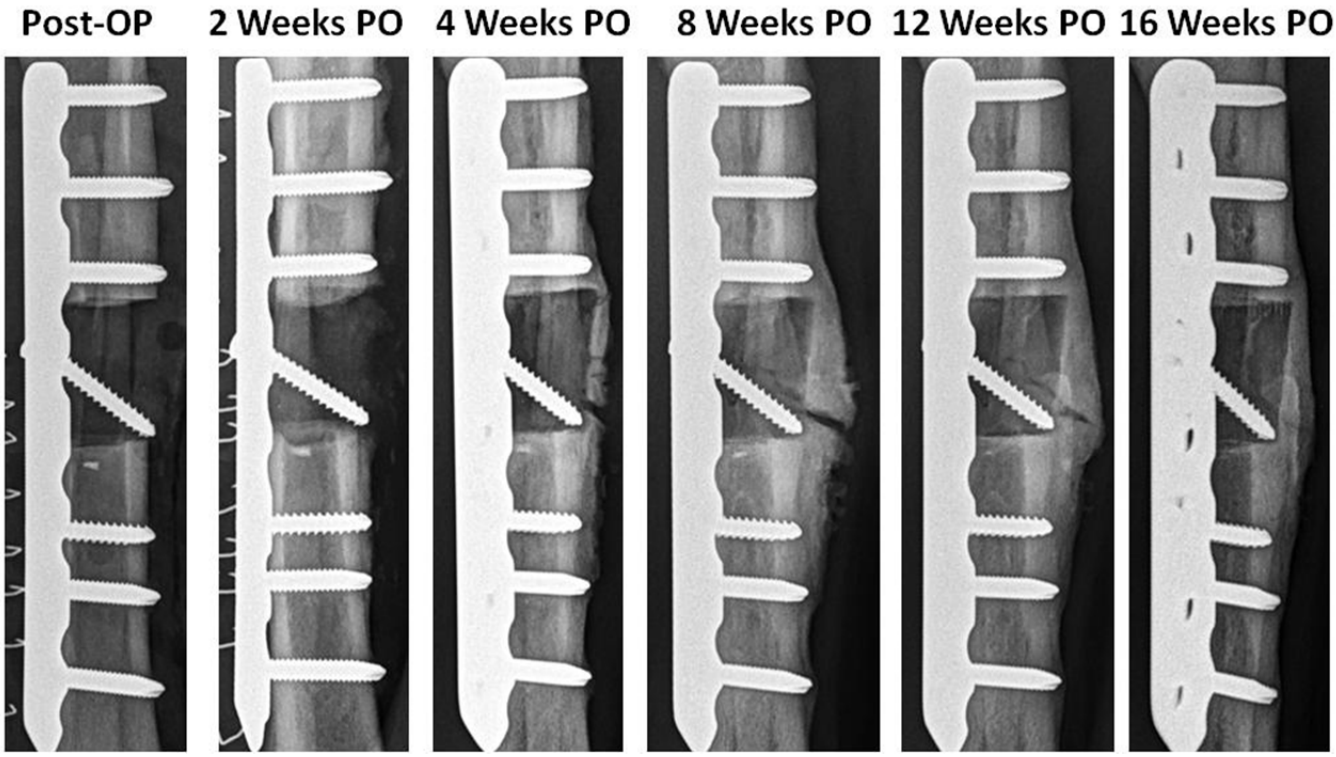

Figure 45: Radiographs of lateral view for Segmental Defect Dog 12 (BMP-seeded scaffold) as a function of time.

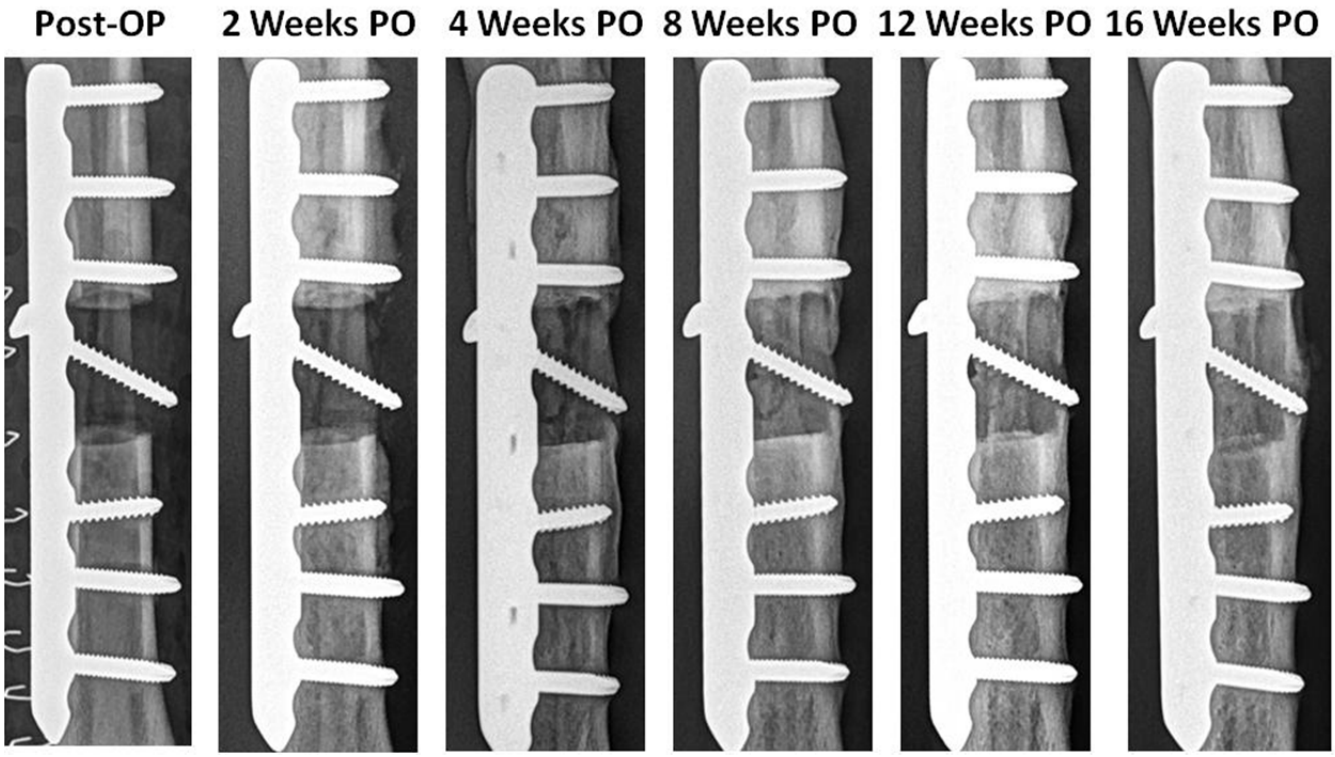

Figure 46: Radiographs of lateral view for Segmental Defect Dog 13 (BMP-seeded scaffold) as a function of time.

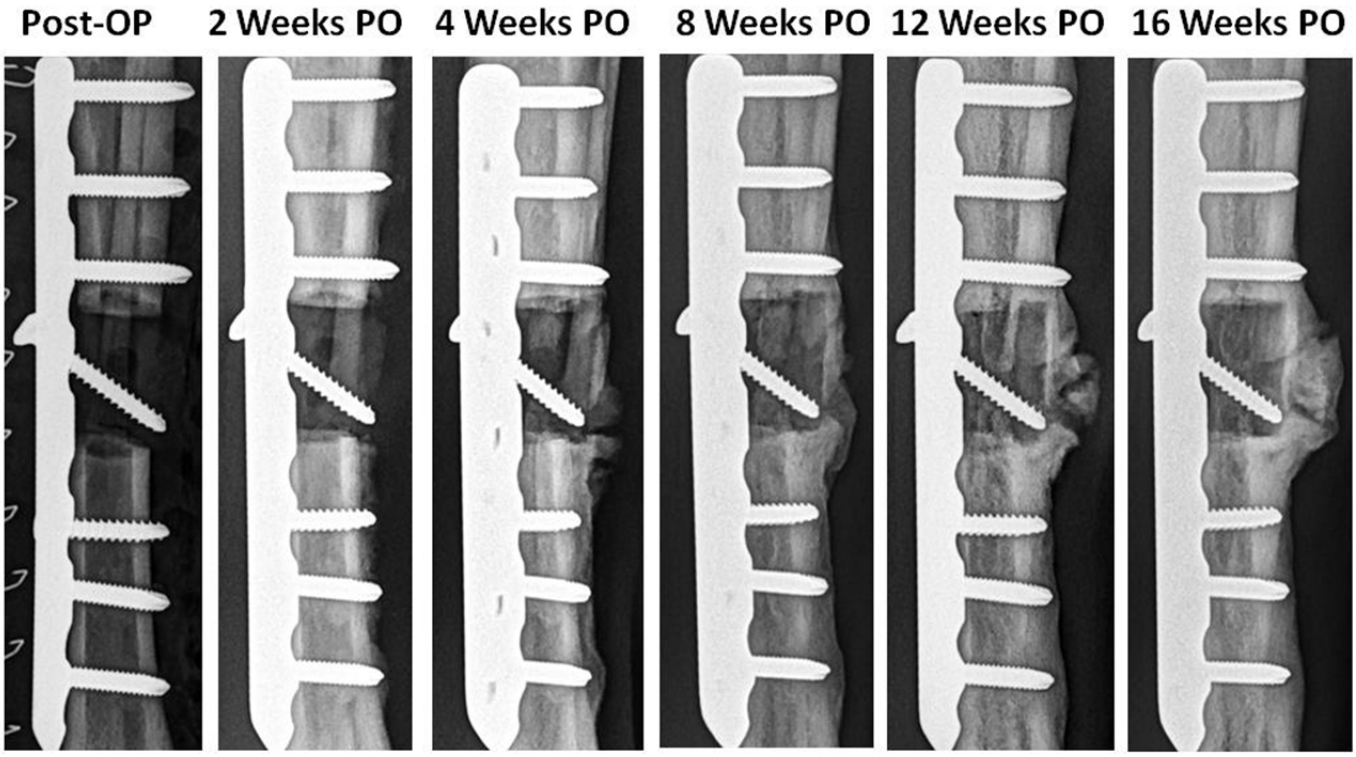

Figure 47: Radiographs of lateral view for Segmental Defect Dog 14 (BMP-seeded scaffold) as a function of time.

2.2.5.4 cMSC Seeded Scaffold Segmental Defect Radiographs

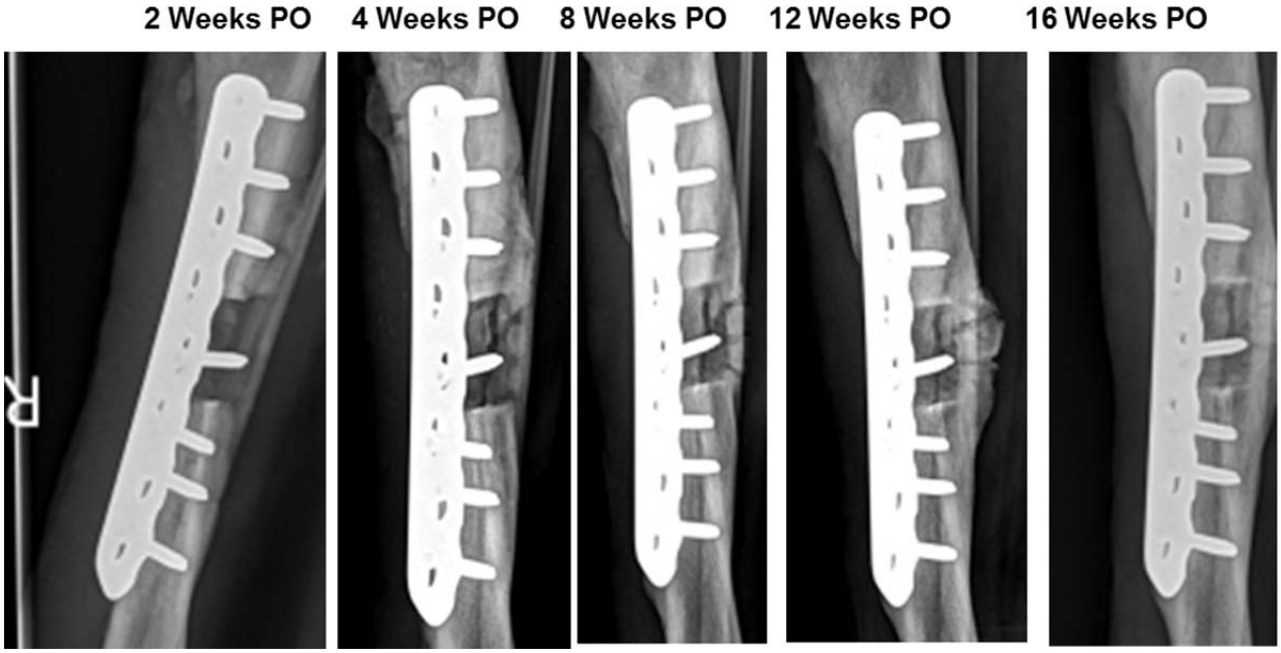

Figure 48: Radiographs of lateral view for Segmental Defect Dog 23 (cMSC-seeded scaffold) as a function of time.

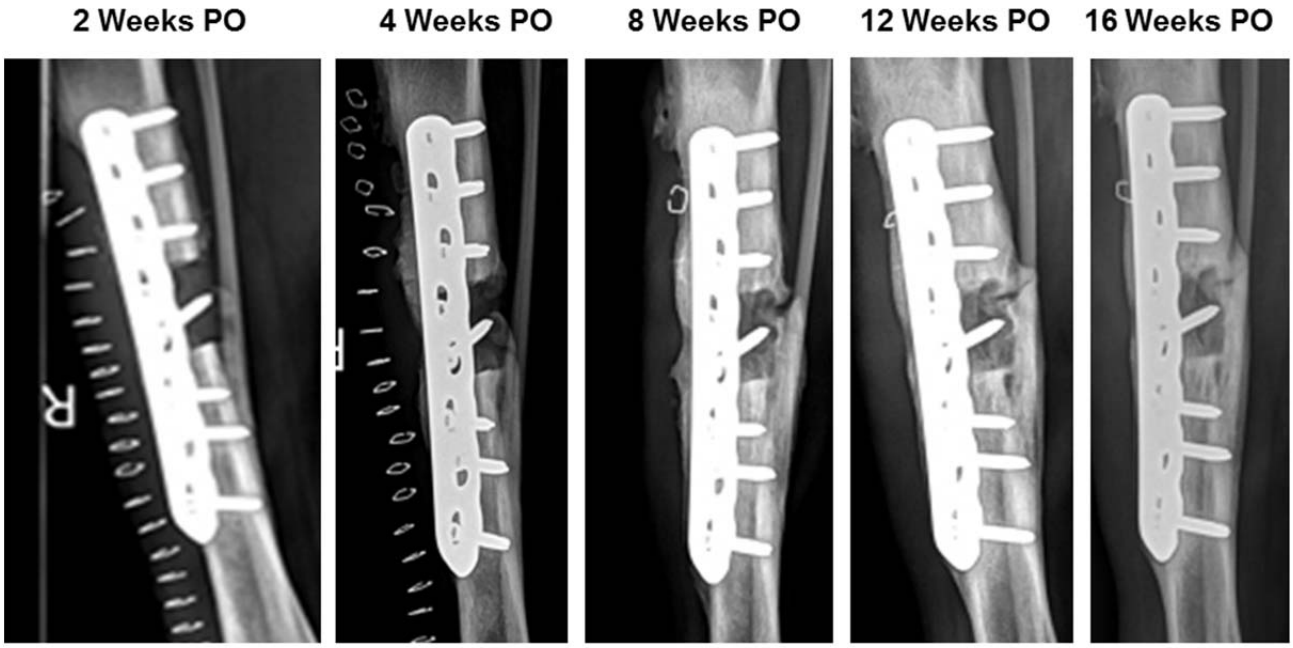

Figure 49: Radiographs of lateral view for Segmental Defect Dog 24 (cMSC-seeded scaffold) as a function of time.

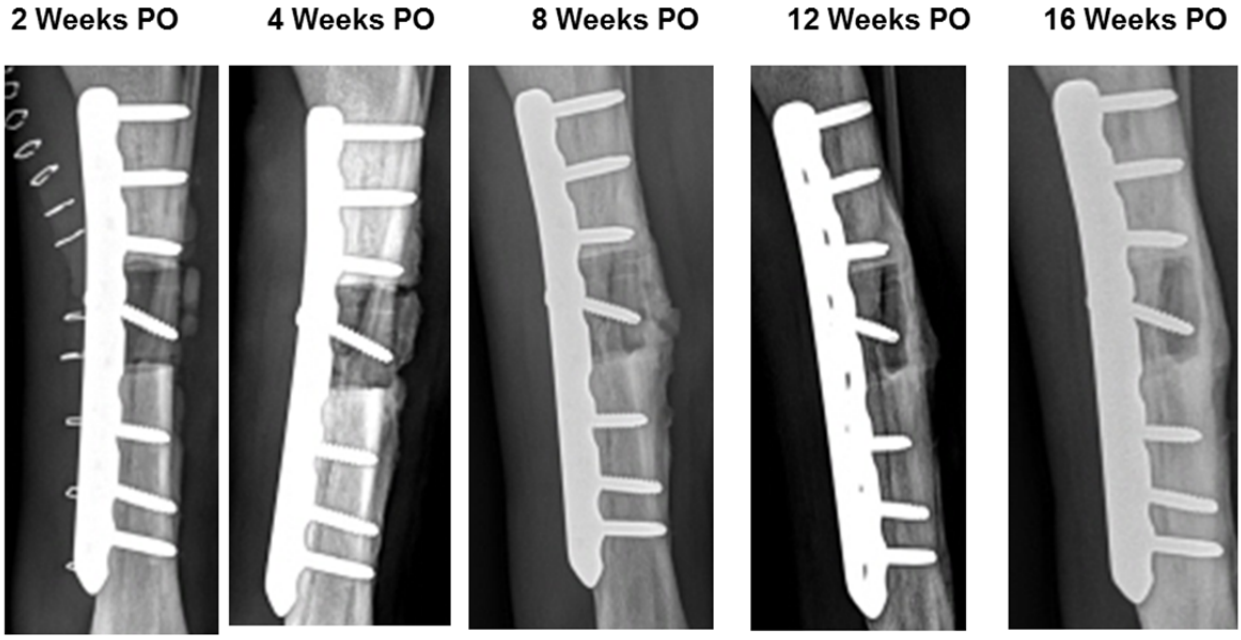

Figure 50: Radiographs of lateral view for Segmental Defect Dog 25 (cMSC-seeded scaffold) as a function of time.

Figure 51: Radiographs of lateral view for Segmental Defect Dog 26 (cMSC-seeded scaffold) as a function of time.

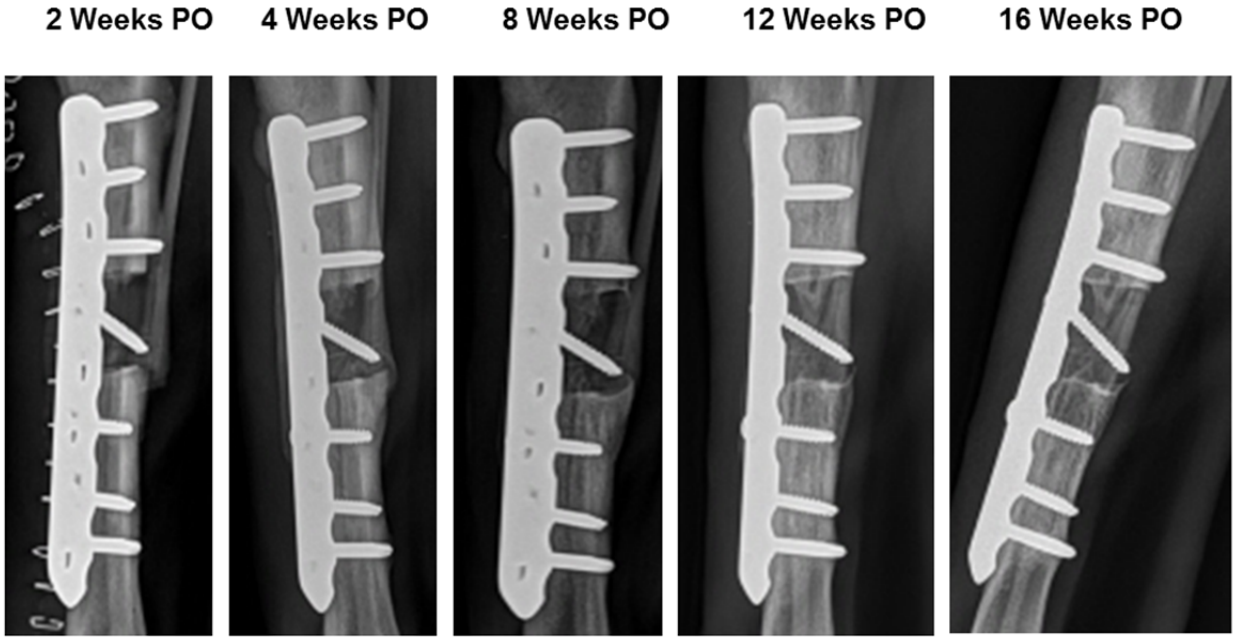

Figure 52: Radiographs of lateral view for Segmental Defect Dog 27 (cMSC-seeded scaffold) as a function of time.

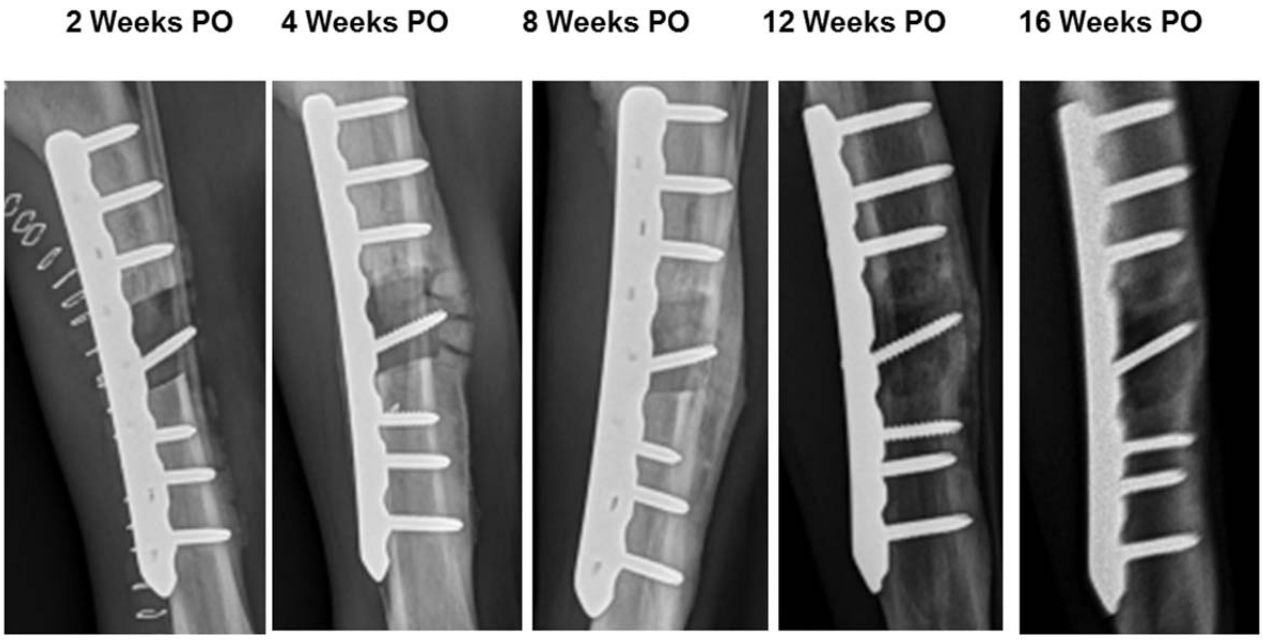

Figure 53: Radiographs of lateral view for Segmental Defect Dog 28 (cMSC-seeded scaffold) as a function of time.

2.2.6 Segmental Defect Outcome Measures

Outcome measurements were gathered as a facet of post-operative care. We sought to assess functional outcomes based on gait, lameness, pain, and knee motion. Gait was scored from 0-2 based on the amount of weight borne by the limb. The amount of limping during ambulation was determined from 0-2 on the Lameness scale. Pain was determined from 0-2 by the dog's reaction to the limb being touched, from guarding and withdrawing behavior to no reaction. Knee motion was graded from 0-3, based on reduction of range of motion, from significant reduction (0-30%), moderate (30-60%), slight (60-80%), and normal range of motion. A total score of 9, indicated a normal, or fully recovered patient. Outcome measures of gait, lameness, pain, knee motion and an aggregate of these measures were nominally recorded for each dog every weekday (refer to Table 2 for criteria), excluding Saturdays and Sundays.

Dogs from Scaffold, Allograft, Scaffold+BMP2, and Scaffold+cMSC groups were monitored daily from a couple days before surgery up until one day before the animal was sacrificed and the limb harvested. Daily scores were charted for each dog of each group, which gave us a visual representation of the functional outcomes. From these charts, we

observe the gradual rise and plateau of function between the groups. All groups experienced eventual functional restoration and healing, with differences arising in duration to restoration, and functional relapses. The most significant functional restoration came from the Scaffold+cMSC group, where a total score of 9 was achieved – often in as little as 30-40 days post-surgery. The cultured stem cell group also illustrated a more resolute functional plateau, i.e. the function did not dip as was observed in other groups. The gradual increase in function and duration of the full function scoring in the cMSC subjects leads to analysis favoring the defect healing achieved from a combination of our scaffold and cultured mesenchymal stem cells over the other experimental groups.

The allograft group (Figure 23, 24, 27) also entered the good range at around the twenty-second day, which was earlier than the dogs in the unseeded group. The Segmental Defect Dog 15 that had a slight amount of plate bending that seemed to delay its bone healing and may have made it more uncomfortable as demonstrated by fluctuation of the scores between seventy and eighty days, however the overall scores of this dog remained in good range.

Outcome	Criteria	Range
Gait	Non weight-bearing	0
	Partial weight-bearing	1
	Full weight-bearing	2
Lameness	Does not use limb during walking	0
	Partial use of affected limb, walks with noticeable limb	1
	No lameness when walking	2
Pain	Severe reaction to touch, withdraws upon the slightest touch with guarding behavior and/or vocalization	0
	Mild reaction to touch, withdraws limb upon touch	1
	No reaction to touch of affected limb	2
Knee Motion	Significant reduction in range of motion (0-30%)	0
	Moderate reduction in range of motion (30-60%)	1
	Slightly reduced range of motion (60-80 %)	2
	Normal range of motion (90-100%, preoperative range)	3
Total		0-9

Table 2: Criteria used to grade Outcome Measures for Segmental Defect Dogs.

2.2.6.1 Allograft Segmental Defect Outcome Measures

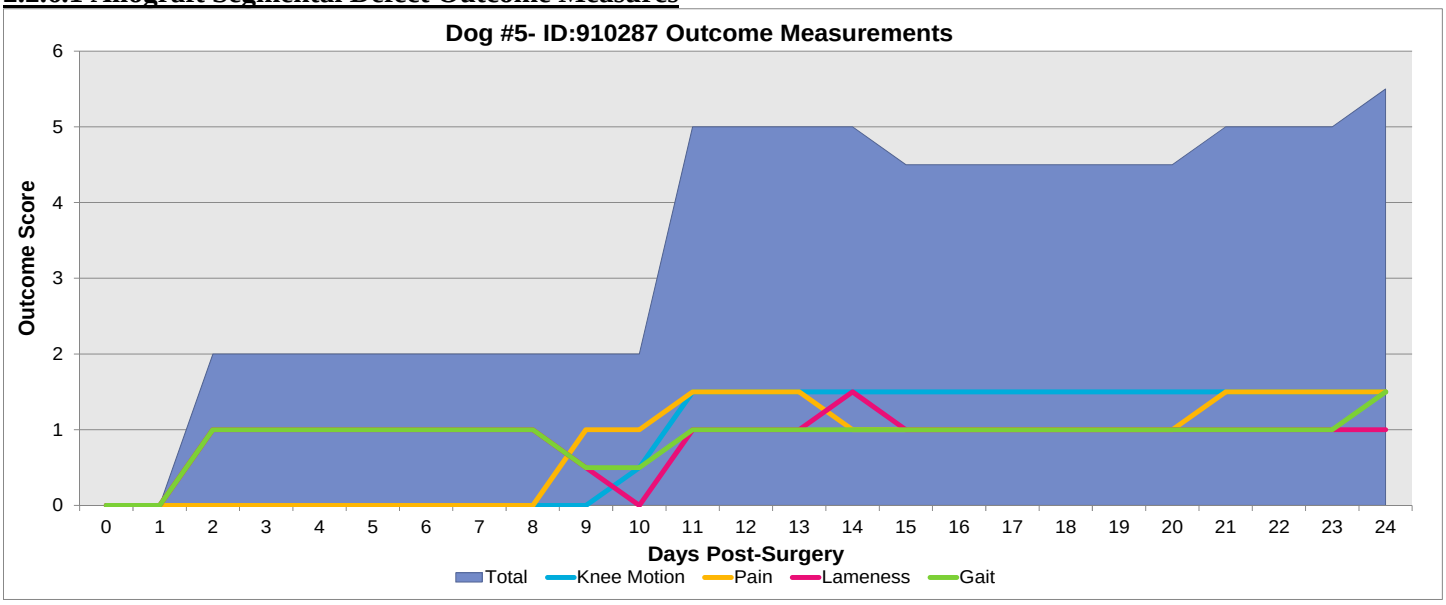

Figure 54: Outcome measurements for Segmental Defect Dog 5 (Allograft).

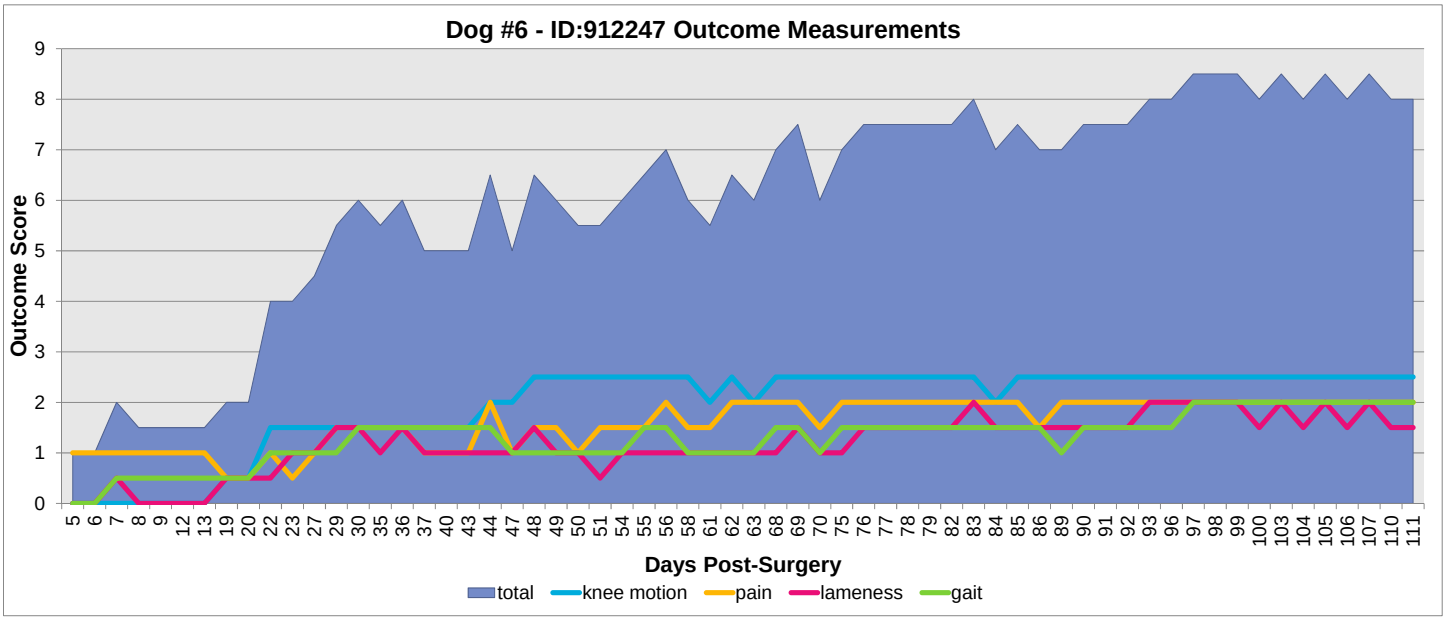

Figure 55: Outcome measurements for Segmental Defect Dog 6 (Allograft).

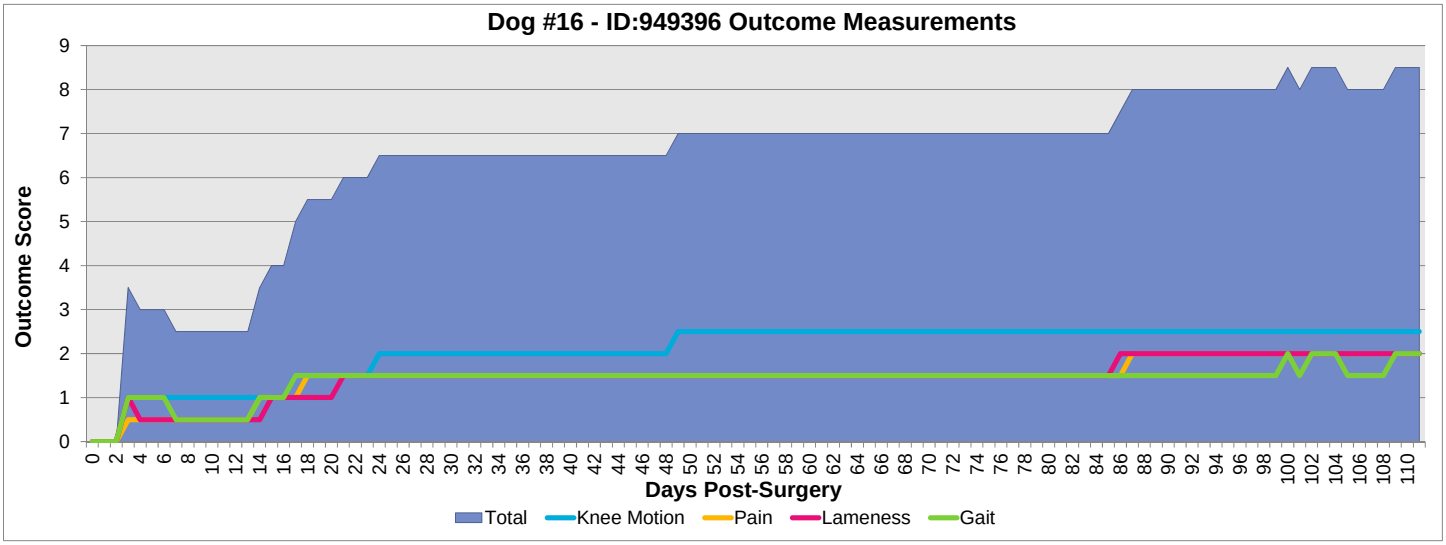

Figure 56: Outcome measurements for Segmental Defect Dog 16 (Allograft).

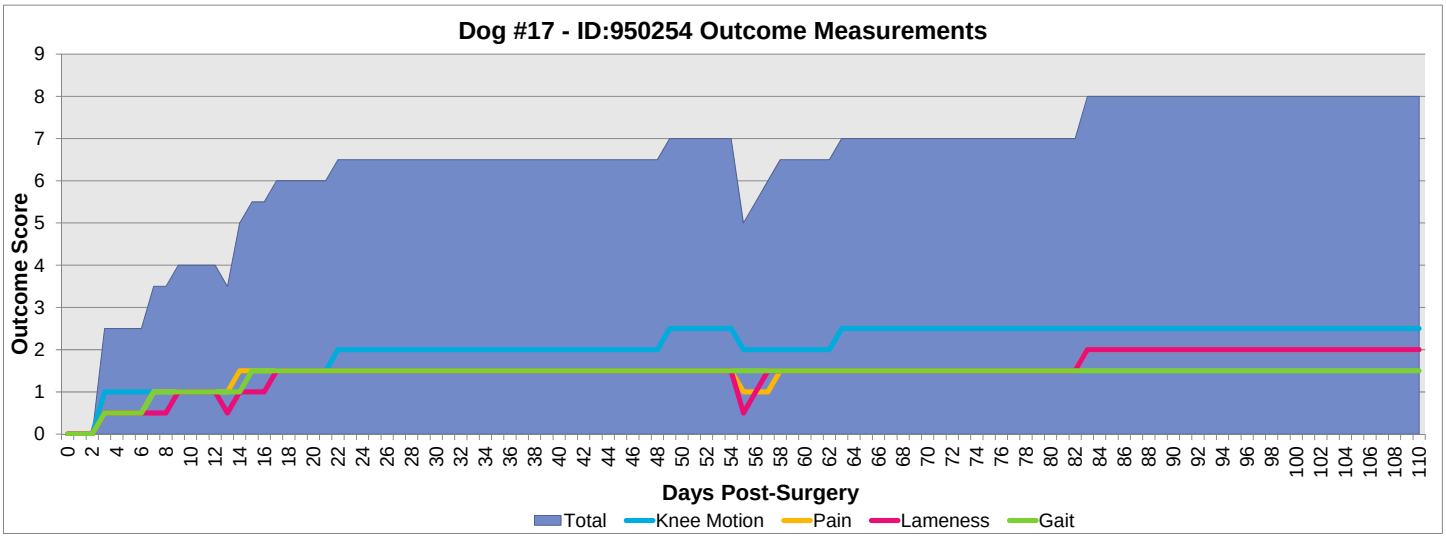

Figure 57: Outcome measurements for Segmental Defect Dog 17 (Allograft).

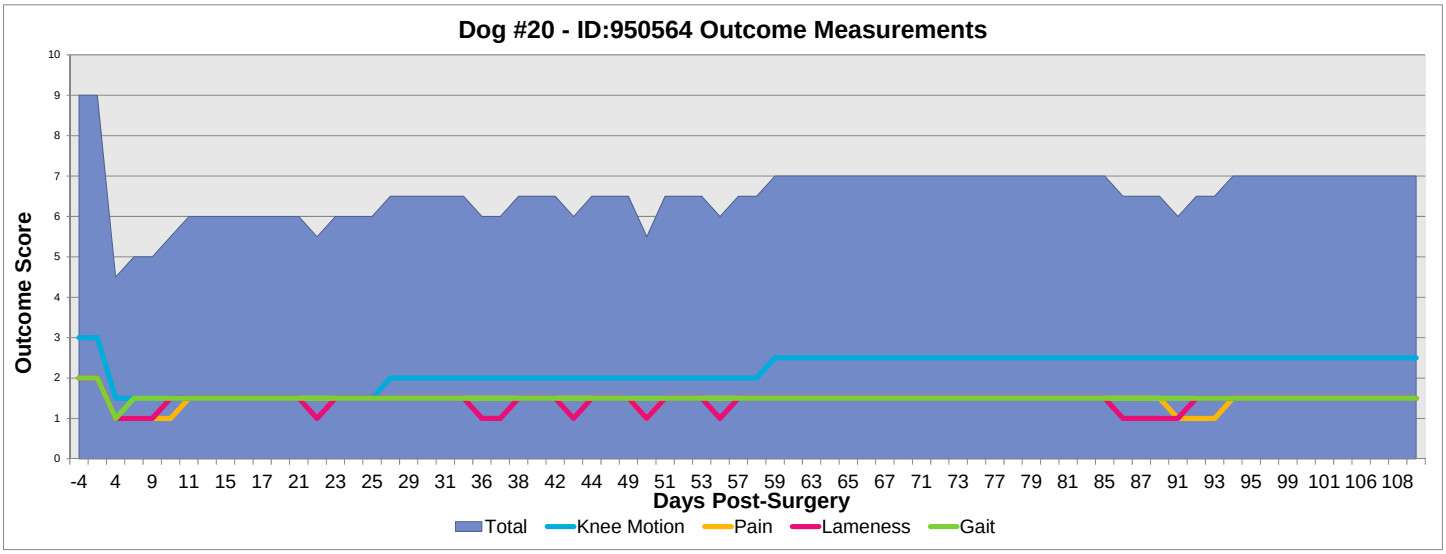

Figure 58: Outcome measurements for Segmental Defect Dog 20 (Allograft).

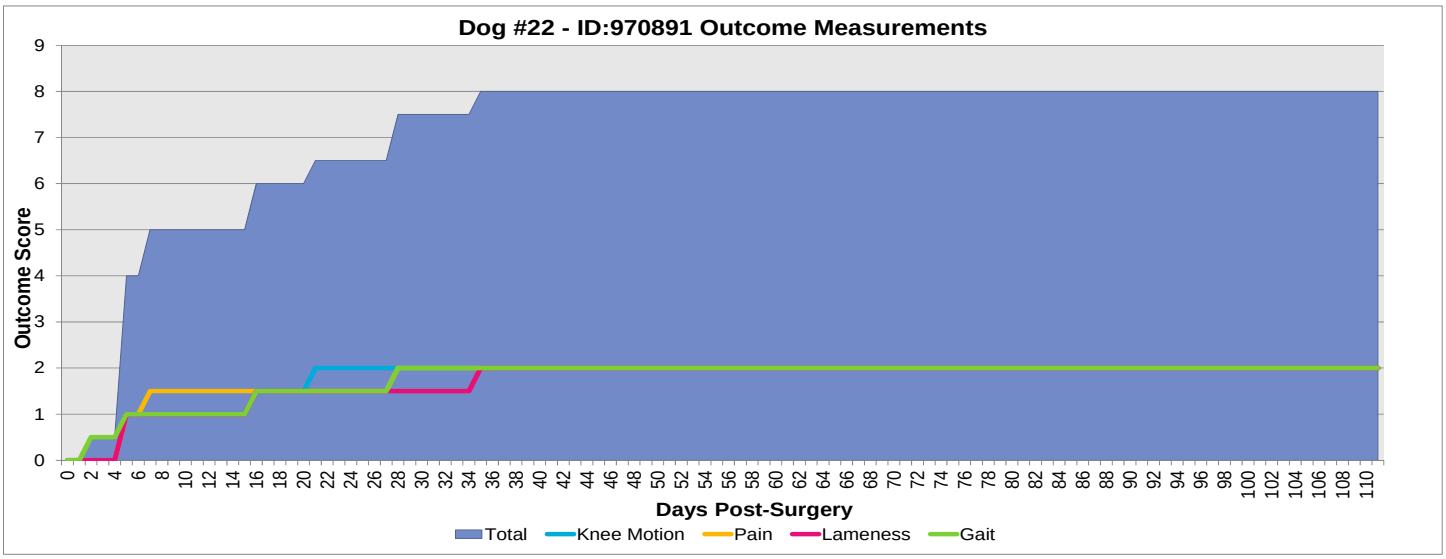

Figure 59: Outcome measurements for Segmental Defect Dog 22 (Allograft).

2.2.6.2 Unseeded Scaffold Segmental Defect Outcome Measures

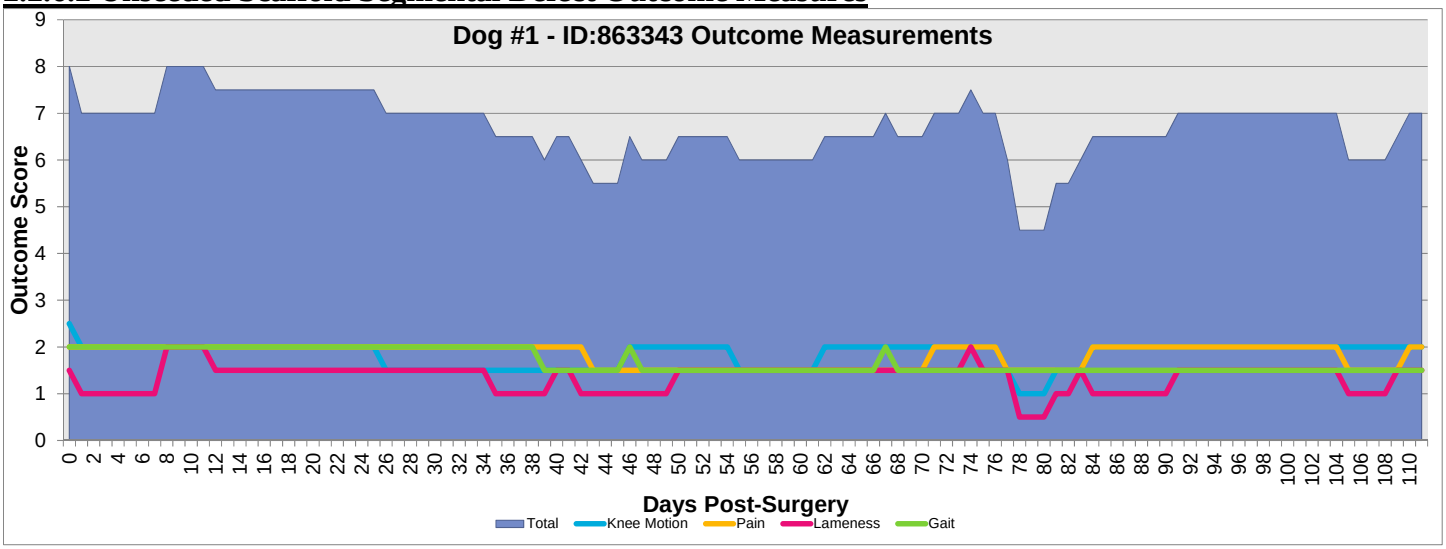

Figure 60: Outcome measurements for Segmental Defect Dog 1 (Unseeded scaffold).

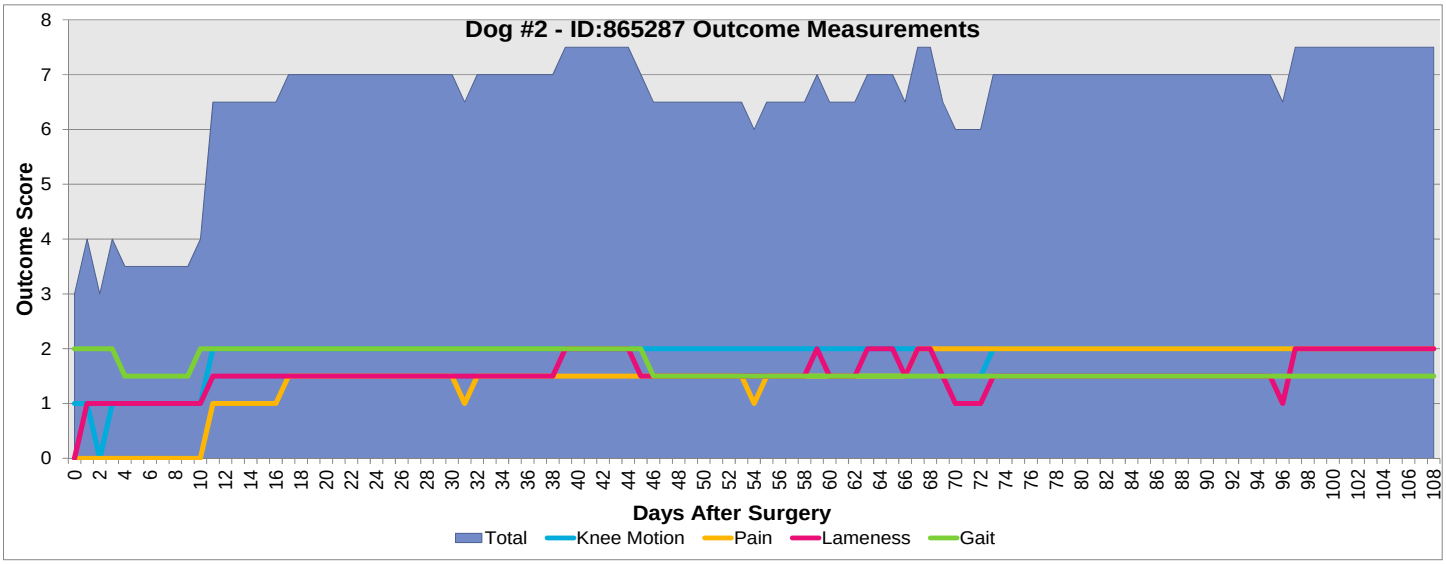

Figure 61: Outcome measurements for Segmental Defect Dog 2 (Unseeded scaffold).

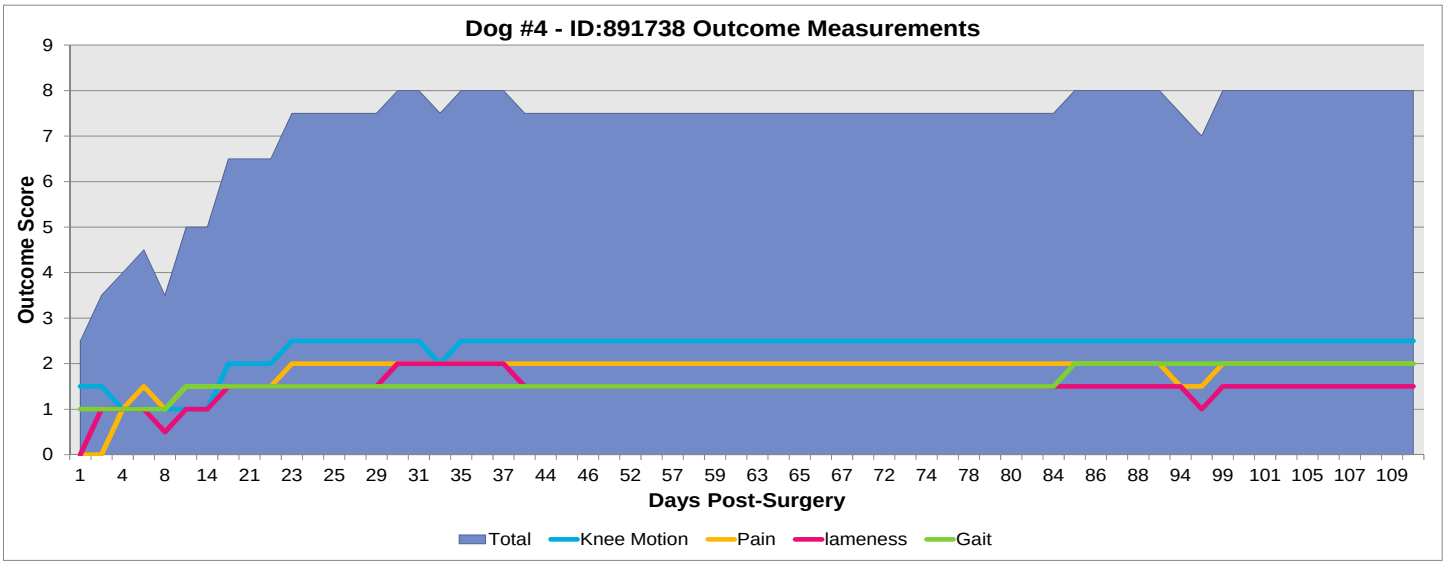

Figure 62: Outcome measurements for Segmental Defect Dog 4 (Unseeded scaffold).

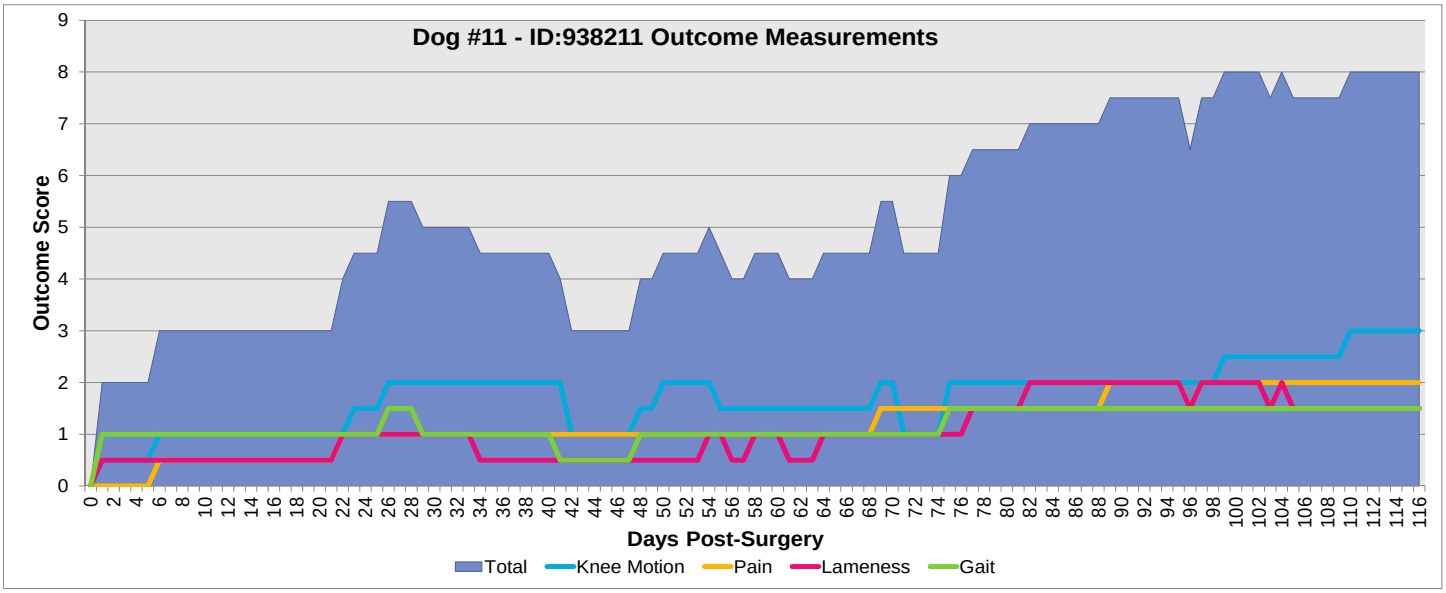

Figure 63: Outcome measurements for Segmental Defect Dog 11 (Unseeded scaffold).

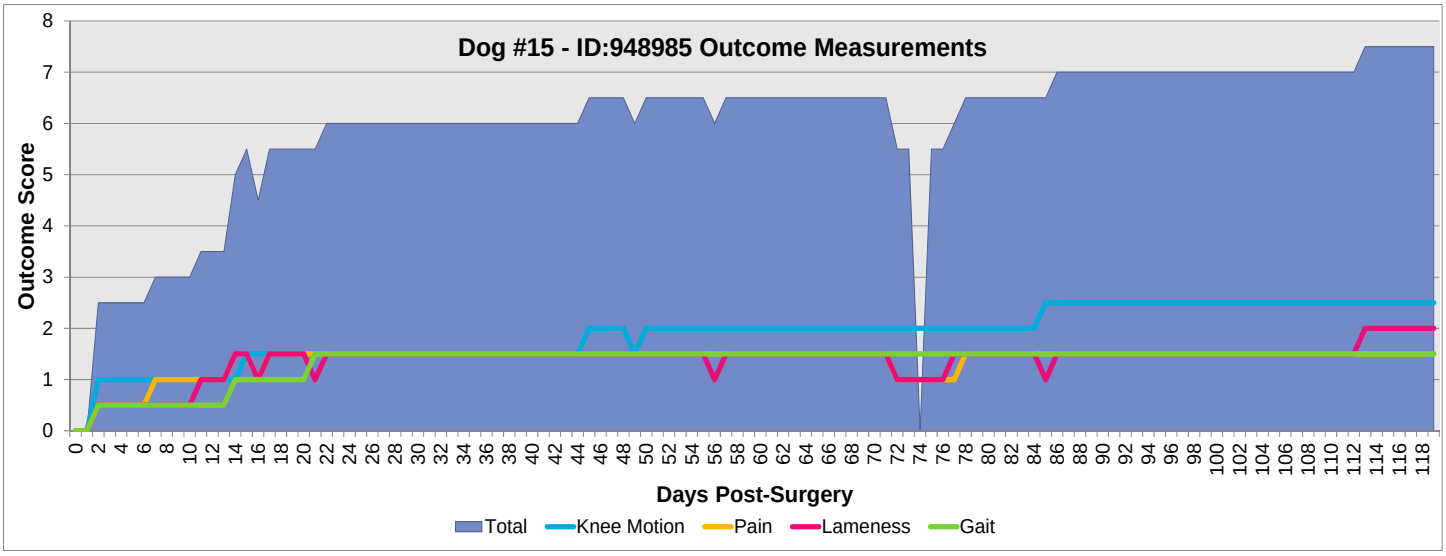

Figure 64: Outcome measurements for Segmental Defect Dog 15 (Unseeded scaffold).

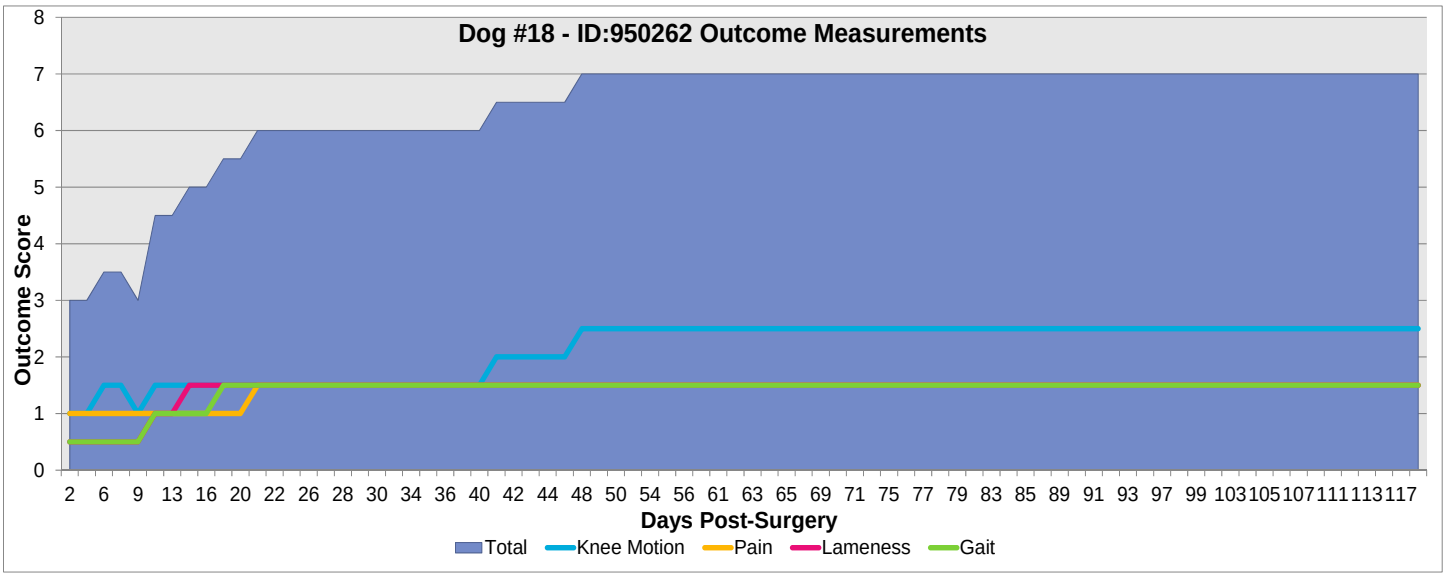

Figure 65: Outcome measurements for Segmental Defect Dog 18 (Unseeded scaffold).

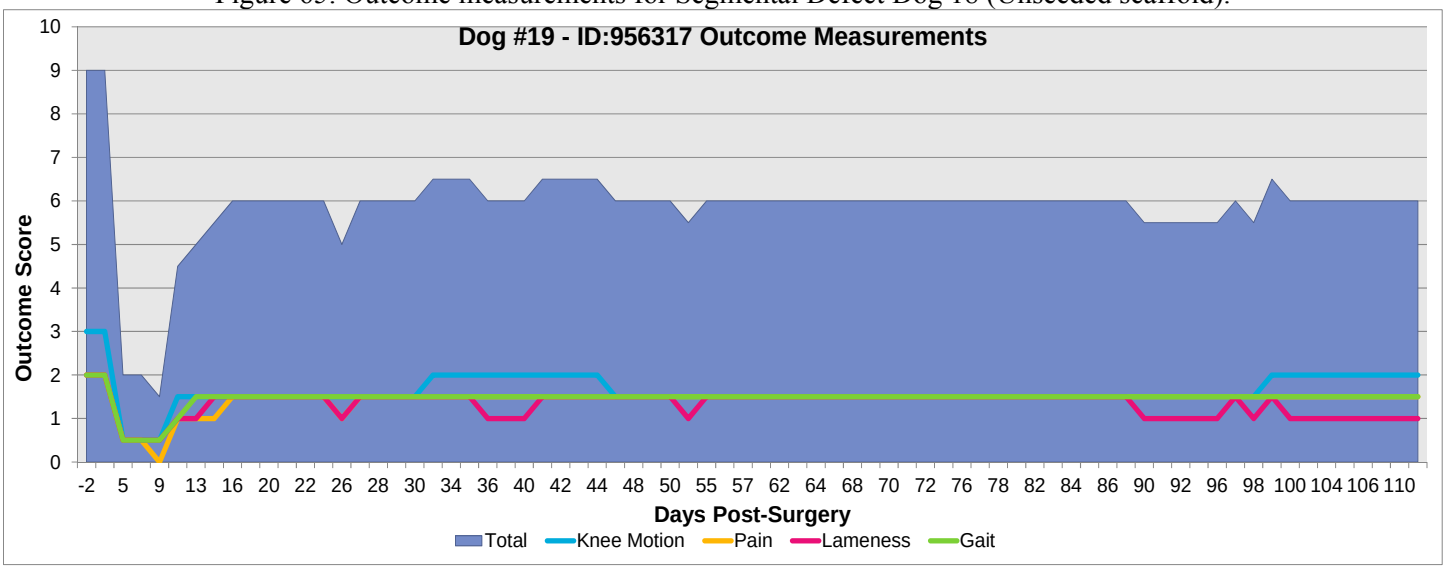

Figure 66: Outcome measurements for Segmental Defect Dog 19 (Unseeded scaffold).

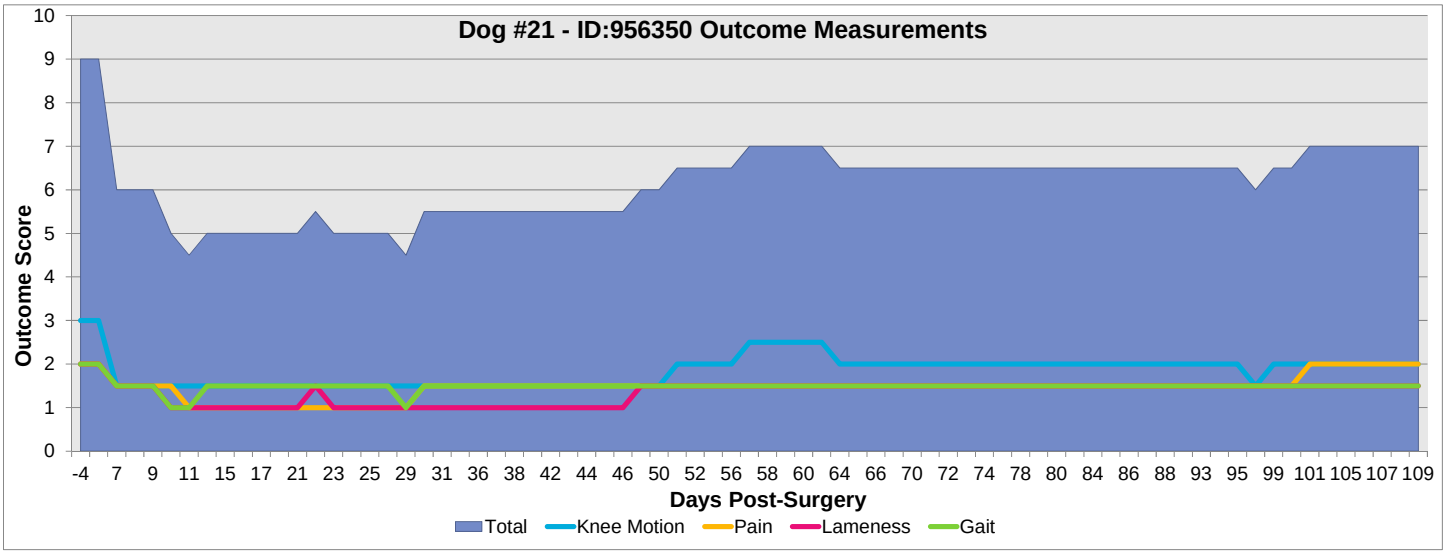

Figure 67: Outcome measurements for Segmental Defect Dog 21 (Unseeded scaffold).

2.2.6.3 BMP-2 Seeded Scaffold Segmental Defect Outcome Measures

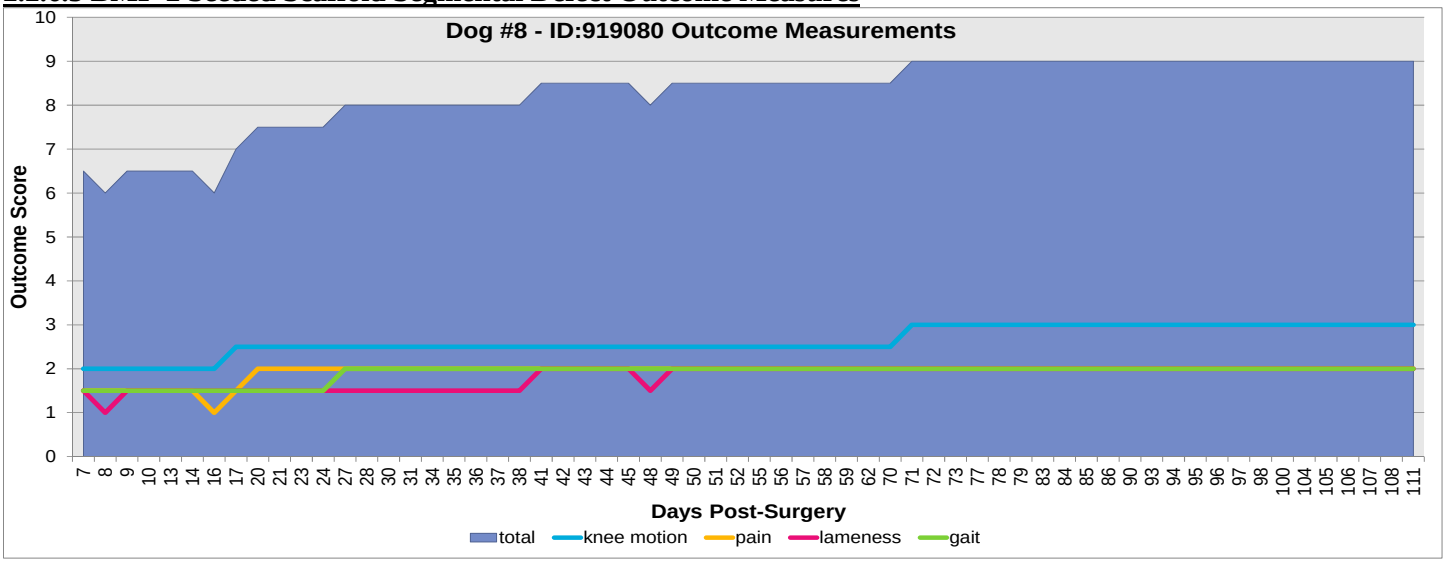

Figure 68: Outcome measurements for Segmental Defect Dog 8 (BMP2 seeded scaffold).

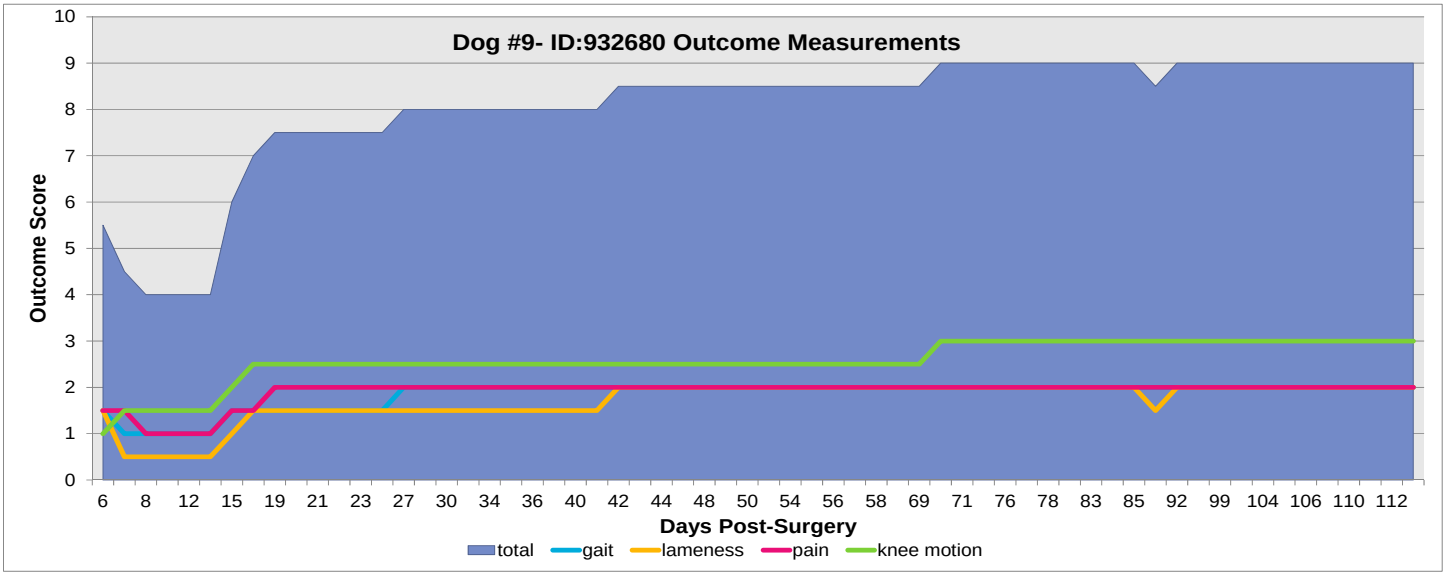

Figure 69: Outcome measurements for Segmental Defect Dog 9 (BMP2 seeded scaffold).

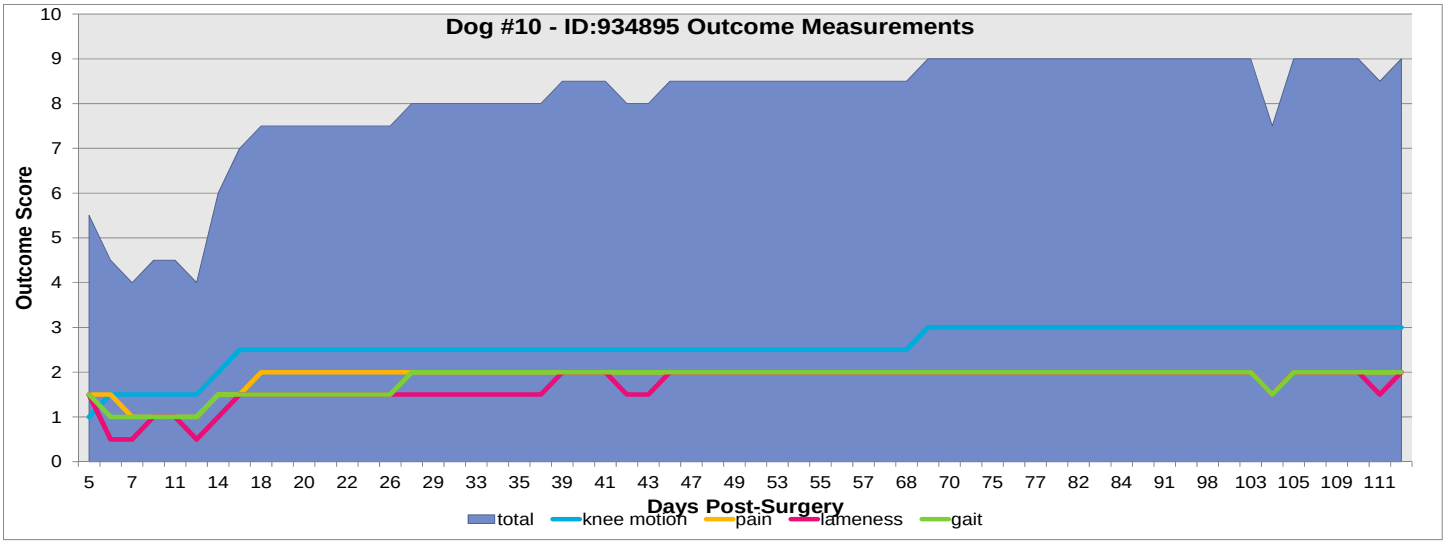

Figure 70: Outcome measurements for Segmental Defect Dog 10 (BMP2 seeded scaffold).

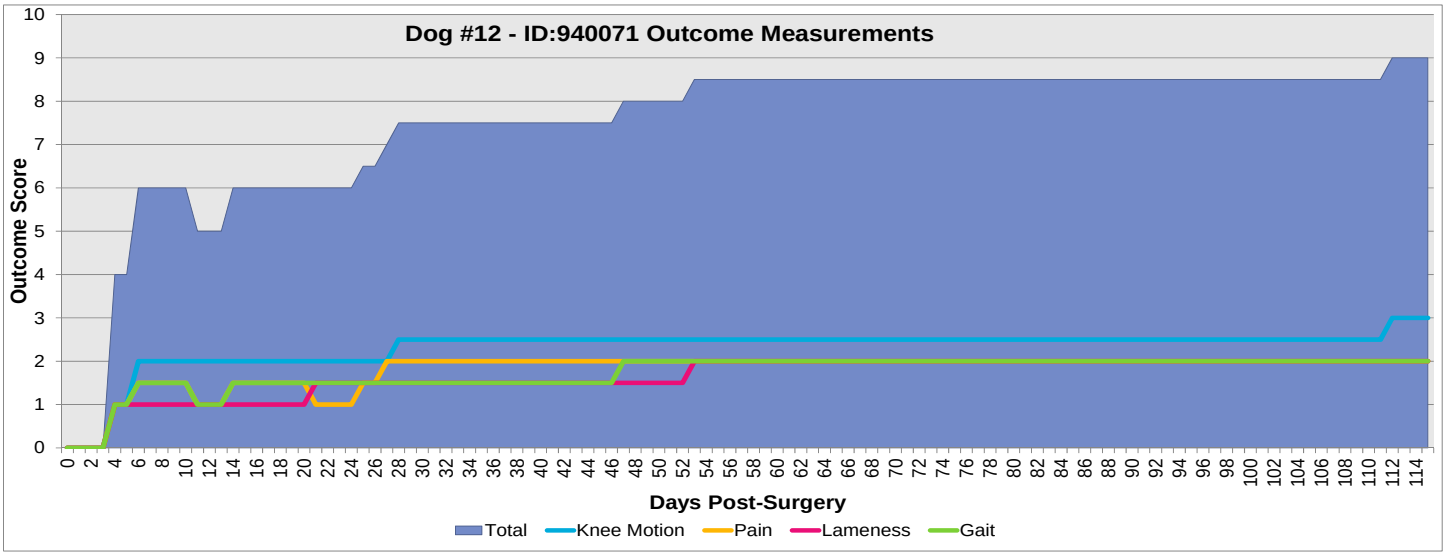

Figure 71: Outcome measurements for Segmental Defect Dog 12 (BMP2 seeded scaffold).

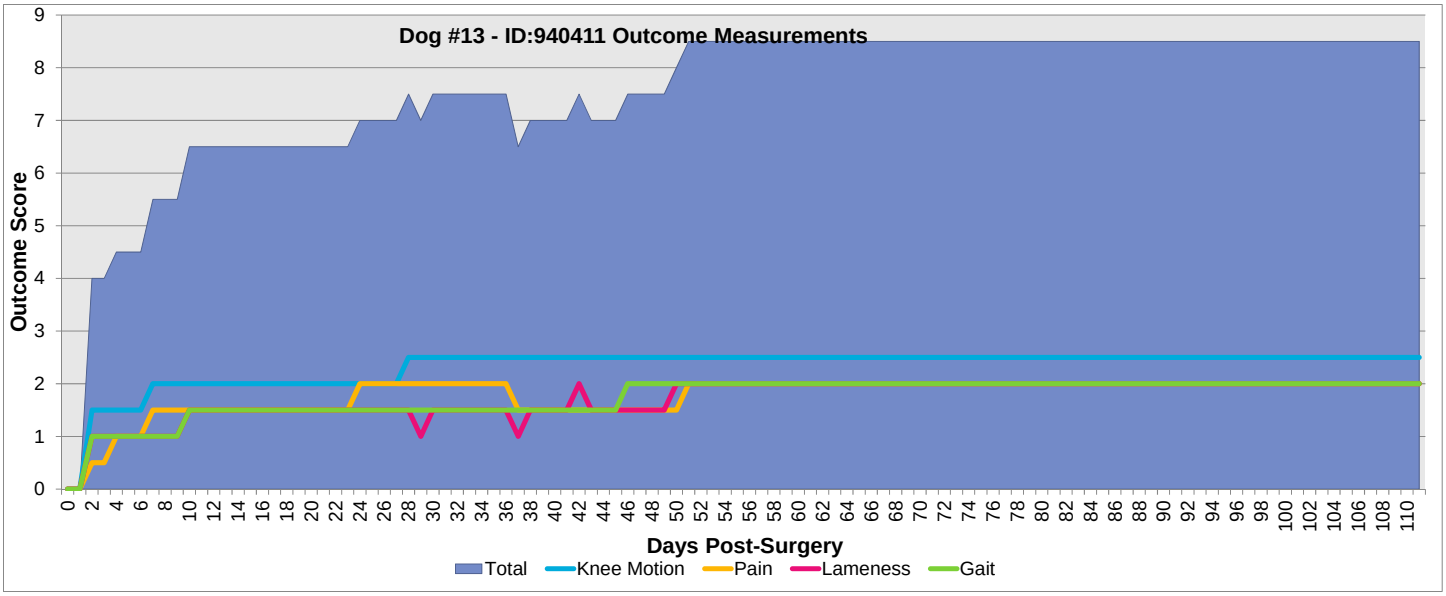

Figure 72: Outcome measurements for Segmental Defect Dog 13 (BMP2 seeded scaffold).

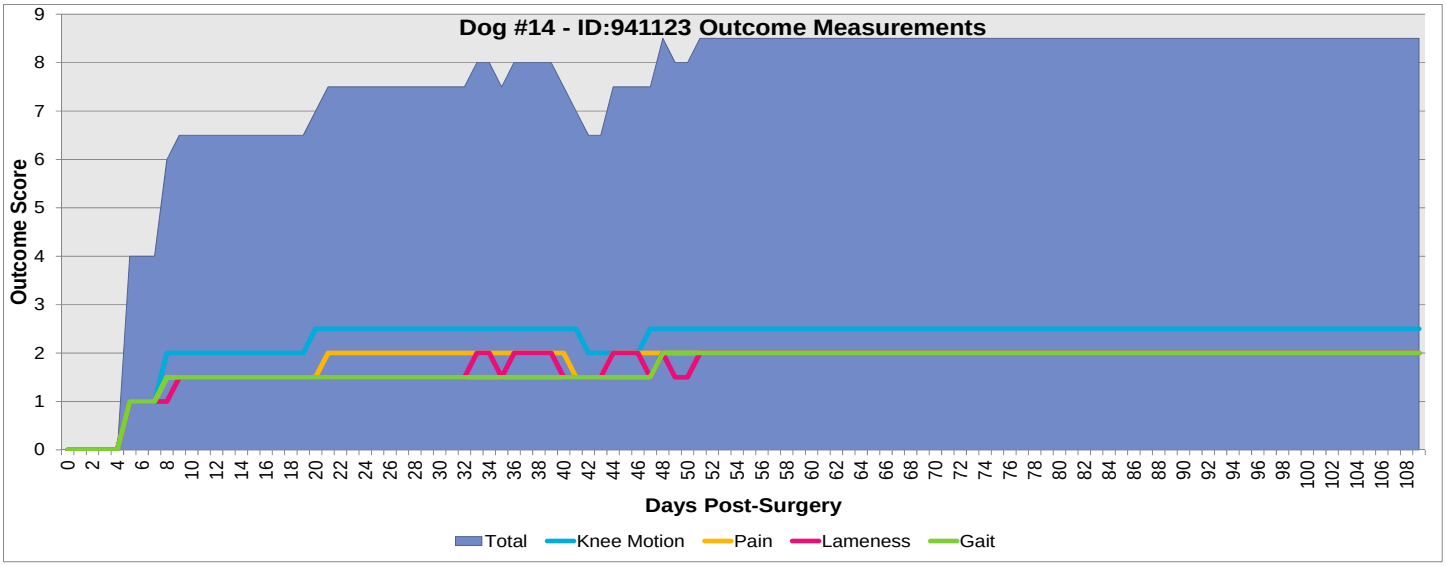

Figure 73: Outcome measurements for Segmental Defect Dog 14 (BMP2 seeded scaffold).

2.2.6.4 cMSC Seeded Scaffold Segmental Defect Outcome Measures

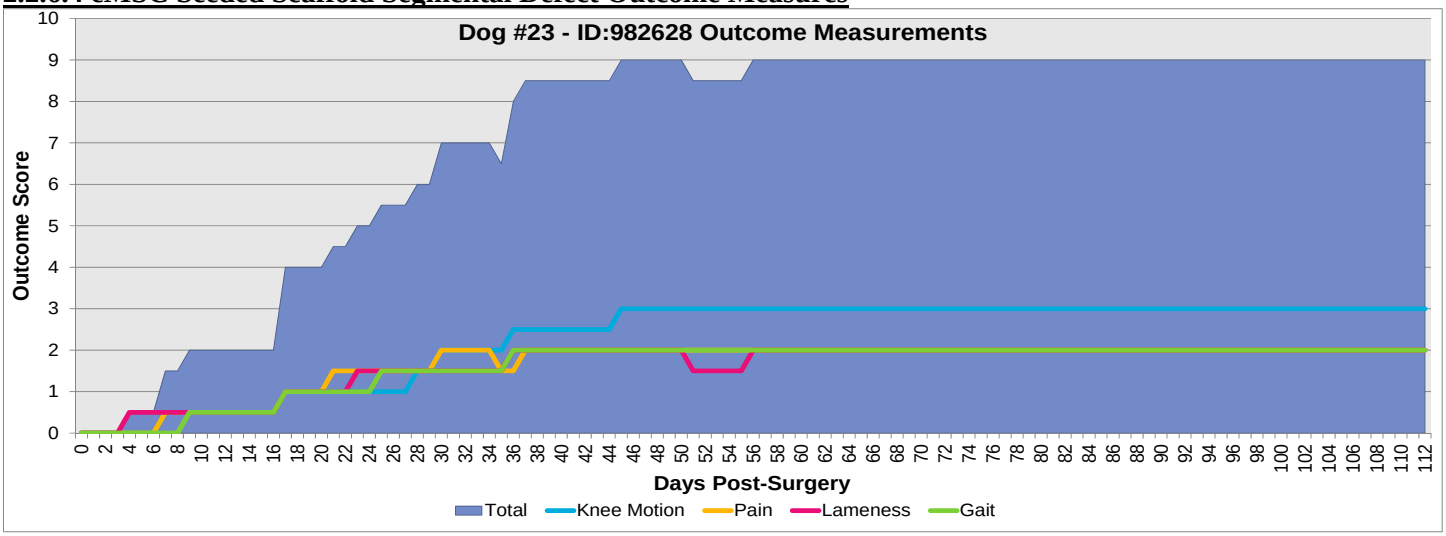

Figure 74: Outcome measurements for Segmental Defect Dog 23 (cMSC seeded scaffold).

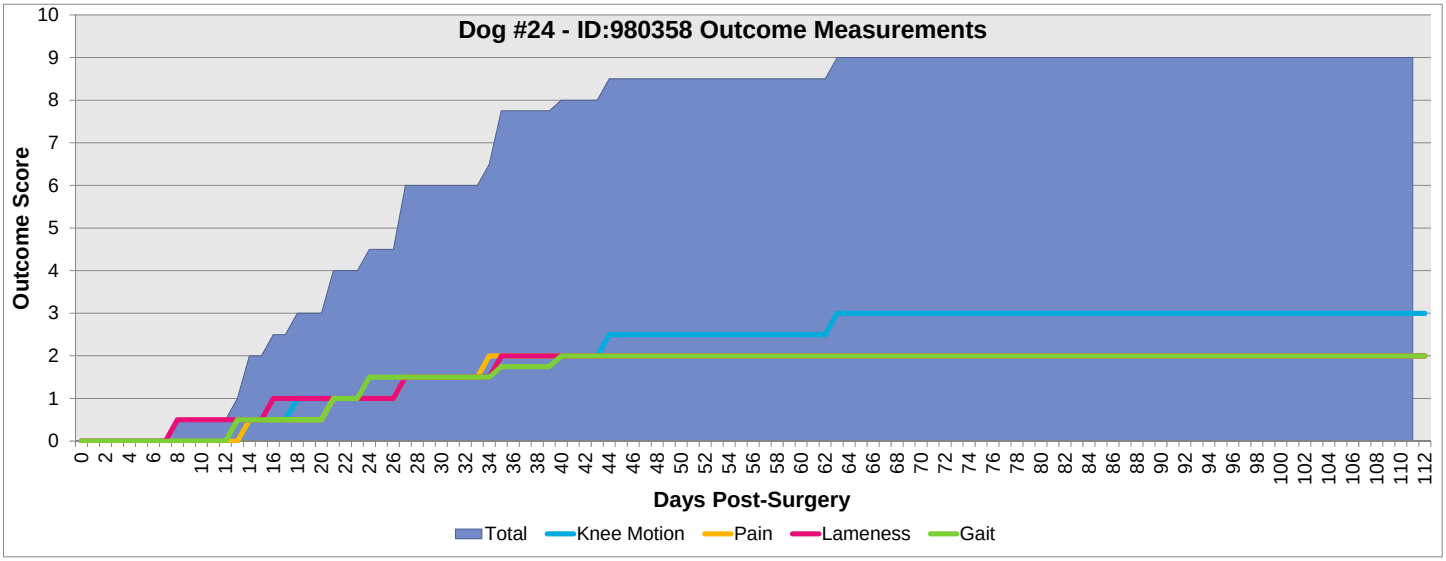

Figure 75: Outcome measurements for Segmental Defect Dog 24 (cMSC seeded scaffold).

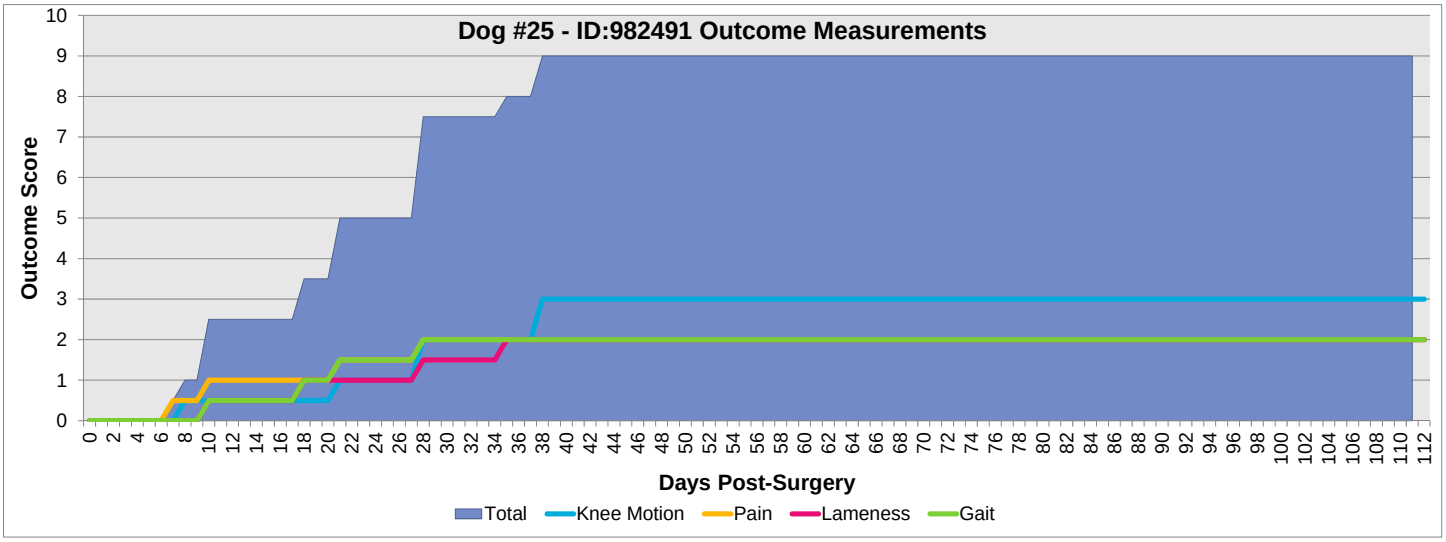

Figure 76: Outcome measurements for Segmental Defect Dog 25 (cMSC seeded scaffold).

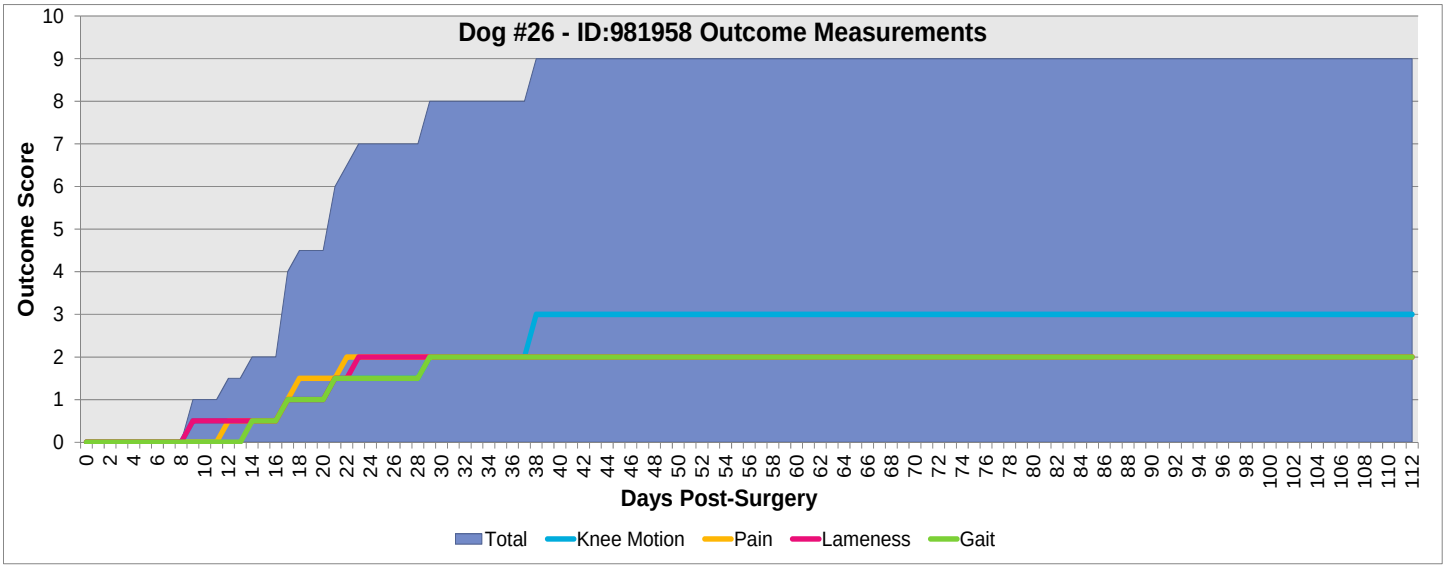

Figure 77: Outcome measurements for Segmental Defect Dog 26 (cMSC seeded scaffold).

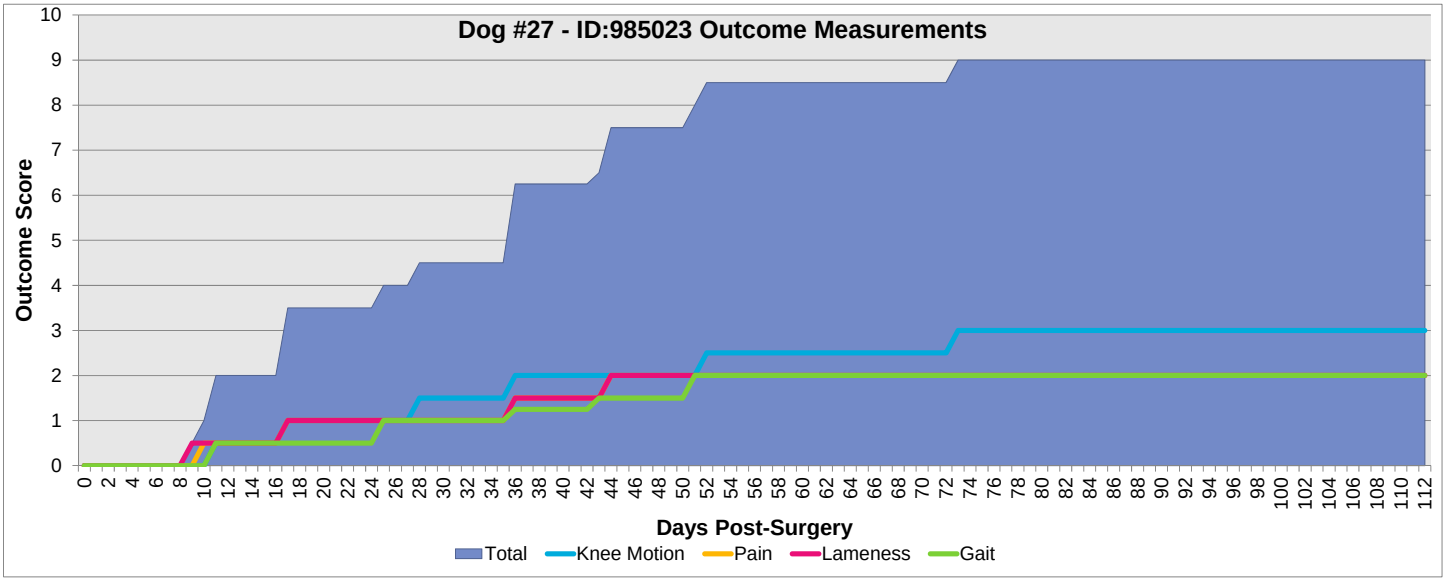

Figure 78: Outcome measurements for Segmental Defect Dog 27 (cMSC seeded scaffold).

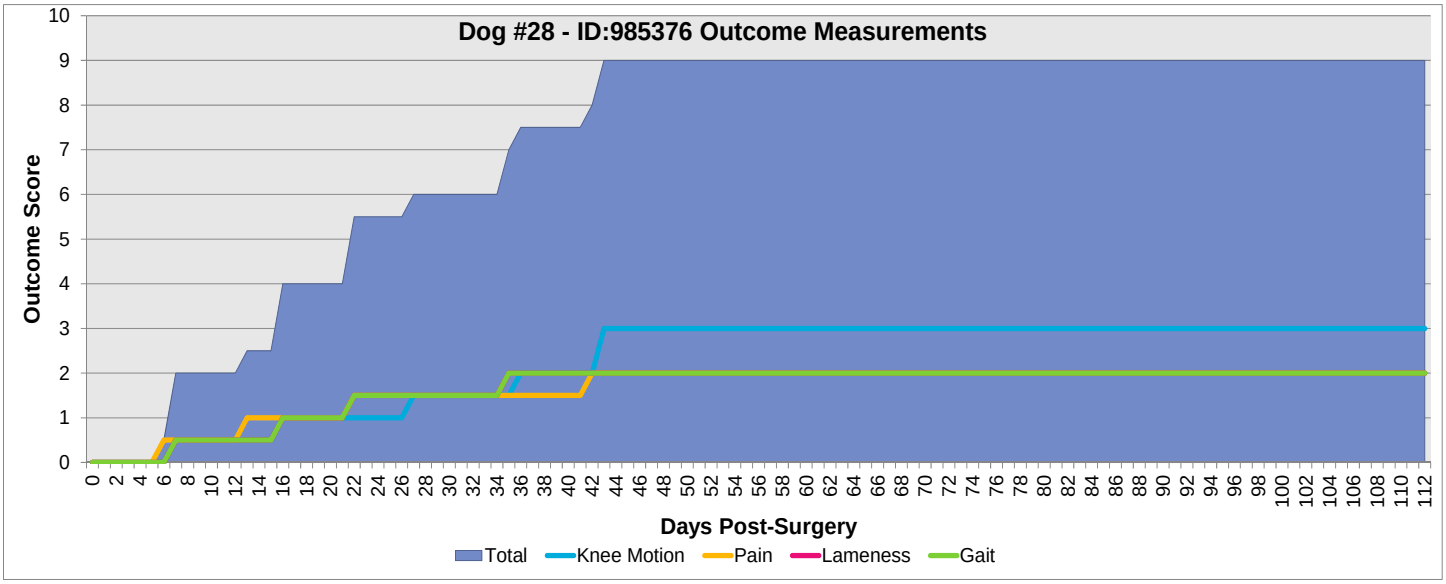

Figure 79: Outcome measurements for Segmental Defect Dog 28 (cMSC seeded scaffold).

2.2.7 Biomechanical Testing of the Segmental Defect Dogs

Mechanical testing in axial compression (2 dogs with allografts, 3 dogs with unseeded scaffold repairs and 2 dogs with BMP-2 seeded scaffolds) with the plate attached. Following axial testing, the plates were removed and the limbs were tested by torsion in internal rotation with the plate carefully removed until failure. A total of 6 tests to torsional failure were performed for Segmental Defect dogs (2 each for allograft, unseeded scaffold (one experimental limb that was used for axial testing was damaged during plate removal and consequently not included in the tests to torsional failure) and BMP-2 seeded scaffold dogs). The experimental test set-up is shown in Figure 80.

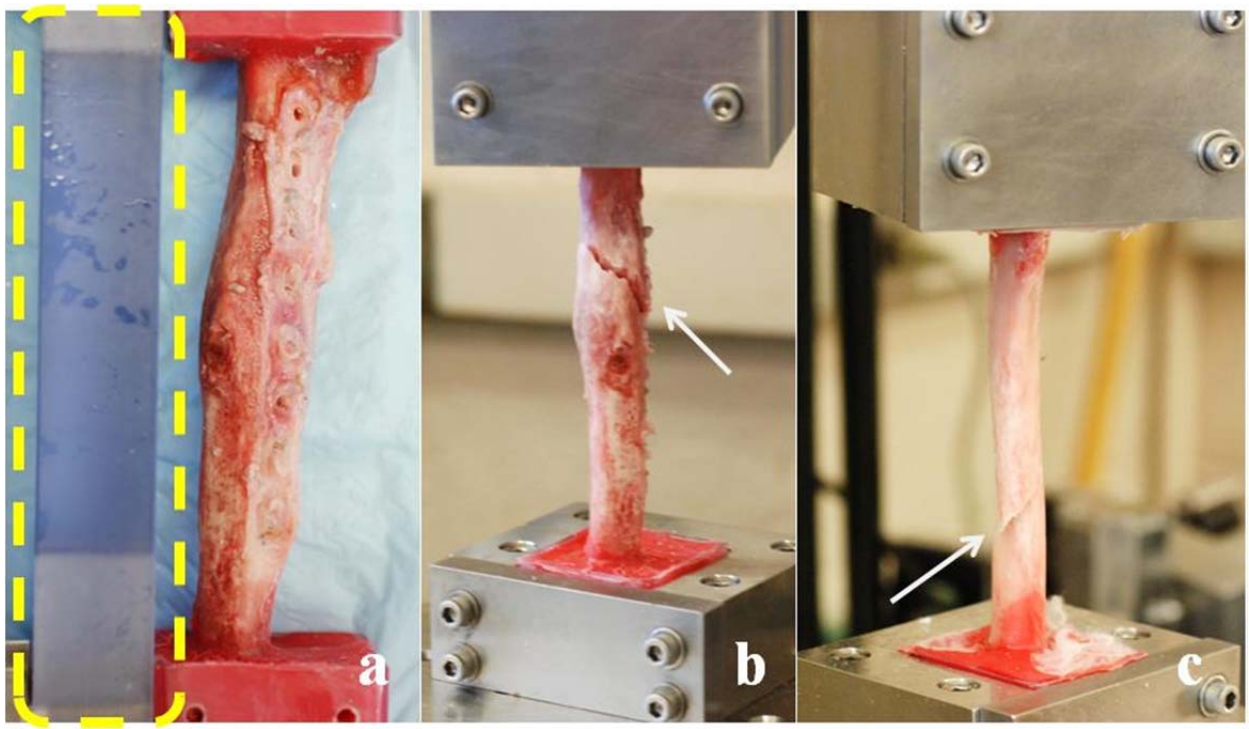

Figure 80: (a) The rigid polycarbonate support attached to the potted blocks to secure the tibia during removal of screws and plate is highlighted by the dashed region; biomechanical testing of the Segmental Defect canine tibiae (b) experimental tibia with hardware removed and (c) contralateral control tibia. Similar spiral fractures, denoted by arrows, are apparent on both tibiae.

2.2.7.1 Biomechanical Testing of the Segmental Defect Dogs – Test Design

Torsional testing to failure of tibiae from both the experimental hind limb (right) and contralateral control hind limb (left) was performed. Special torsional testing clamps and jigs to stabilize the joints during dissection were manufactured. In addition to the required torsional testing, non-destructive axial testing of the limbs was also performed prior to the torsional testing to compare the axial stiffness of the experimental limb with the locking plate in place to that of its contralateral control limb. Following sacrifice of the animal, both hind limbs were disarticulated at the hip and CT images obtained. The limbs were then dissected down to the tibia, wrapped in physiologic saline soaked gauze and frozen at -20˚C until the day of testing. On the day of testing, the limbs were thawed to room temperature and the proximal and distal ends of the tibia cleaned of any soft tissue, wiped clean with acetone and proximal and distal potting blocks applied. The potting blocks were 2" square by 1.5" high polycarbonate rectangular tubes. The proximal end of the tibia was placed in a vertical position in the tube, and a 1.6 mm diameter stainless steel Kirschner wire (Zimmer, Warsaw IN) was driven through the wall of the tube, through the bone and then out through the opposite wall of the tube. In a similar fashion, a second, similar wire was driven at right-angles to the first wire. Following wire insertion, the tube and K-wires were filled with PMMA to create a stable construct to resist torsion. A small depression was drilled in the center of the top of the proximal mounting block to accept a steel ball used during axial testing. Once the PMMA hardened in the proximal mounting block, the proximal block was placed in the material testing system and then carefully lowered into the distal mounting block to ensure that the tibia was centered and in a vertical position in the testing machine. K-wires and then PMMA were then applied to the distal mounting block in the same fashion as was done for the proximal mounting block. The tibia was kept wrapped in physiologic saline soaked gauze throughout the entire potting process to ensure that it did not dehydrate.

Mechanical testing was done in an MTS 858 Bionix material testing machine (MTS, Eden Prairie MN) with a biaxial (axial/torsional) load cell. The torsional range of the load cell is ± 50 N-m. The full axial range of the load cell is ± 5000 N. To ensure maximum accuracy of the axial loading, the gain of the axial range of the load cell was set to ± 500 N. Axial testing was done by applying a ramp load to 125 N, representing approximately one-half of the dog's body weight at a rate of 10 N/s (3-5). The compressive axial load was applied by pressing down with a flat plate onto a large steel ball bearing (Figure 80) which was placed in a small depression that was drilled into the top of the PMMA filled proximal mounting block. The loading was repeated three times. Following the compressive testing, the proximal mounting block was placed into the square top clamp (Figure 80). The sides of the proximal mounting block were sanded prior to testing to ensure a close but not tight fit in the top mounting clamp. Grease was also placed around the sides of the proximal clamp prior to placing it in the top clamp. Fitting the proximal mounting block and applying grease to the block were done to allow for axial displacement of the proximal clamp to minimize any axial loading during the torsional testing. A rotation rate of 1 N/s was applied to the tibia. This rate was less than the 3 N/s rate stated in the original grant proposal because further review of the literature (3, 6, 7) indicated that this rate would lessen any viscoelastic effect and allow comparison to similar data in the literature which used the 1 N/s loading rate. A lateral-to-medial (internal rotation) direction of loading was used. The distal end of the tibia was fixed and the torsion was applied to the proximal end of the tibia. Time history data were collected at a frequency of 10 Hz for axial and 20 Hz for torsional testing.

Axial testing was done for the control (left) tibia and experimental limb (right). Axial testing was done with the stainless steel plate and screws intact for the experimental limb. Torsional testing for the experimental limb was performed following removal of the plate to properly measure the strength of the bone-scaffold interface that may have formed during the 16 weeks of healing. For some of the dogs, CT images were obtained prior to axial testing of the experimental limb with the plate intact, but the metal artifact made the resulting CT images of questionable value. Therefore, additional CT images were obtained following plate removal and prior to torsional testing so that metal artifact free CT images of the healed bone-scaffold-bone construct were recorded. To ensure that the bone-scaffold-bone construct was not damaged during plate removal and CT imaging, a special external fixation device was used. After axial testing of the experimental limb, 2 threaded screw holes were placed in both the proximal and distal mounting blocks while the tibia was still in the testing machine. A polycarbonate block was then attached to the proximal and distal mounting blocks using 4 thumb screws. This resulted in an extremely stable construct that allowed for removal of the locking plate without imposing loading on the healed bone, as well as transport to the CT while maintaining the rigidity of the clamped tibia. Following plate removal and CT imaging, the tibia was placed back in the testing machine and the polycarbonate support plate removed. Immediately following plate removal, and before torsional testing, the 6 screw holes in the bone (3 proximal to the segmental defect and 3 distal to the segmental defect) were filled with PMMA.

Axial stiffness is shown in Figures 81 and 82 for both the loading and unloading phases. Ratios of the axial stiffness (experimental/control limb) are shown in Figure 83. In terms of percentage for failure torque, angular rotation at failure and rotational energy to failure are shown in Table 2. Neither the allograft nor scaffold implants fully restored the mechanical strength of the experimental limb to that of the control (non-operated) limb by the end of the 16 week

recovery period. However, the mechanical results of the PCL-HA scaffolds for one dog were very comparable to that of the allograft dogs with the other scaffold dog somewhat lower, indicating that the PCL-HA scaffold can perform similarly to that of an allograft.

2.2.7.2 Biomechanical Testing of the Segmental Defect Dogs – Results

Axial stiffness was comparable between the control and experimental limb for both loading and unloading for allografts, unseeded scaffold and BMP-2 + scaffold as seen in Figures 81 and 82. However both the unseeded scaffold and BMP-2 + scaffold dogs had lower stiffness than the allograft dogs in both loading and unloading. Accordingly, the ratios of experimental to control limb stiffness were higher for the allograft dogs than for either the unseeded scaffold dogs or the BMP-2 + scaffold dogs as seen in Figure 83.

Failure torques for the control limbs were all very comparable for the allograft, unseeded scaffold and BMP-2 + scaffold dogs. However, for failure torque for the experimental limbs, the unseeded scaffold dogs were slightly less than those of the allografts, whereas failure torques for the BMP-2 + scaffold dogs were much less than either the allograft or unseeded scaffold dogs as seen in Figure 84. Failure angles were very similar for both the control and experimental limbs for allograft, unseeded scaffold and BMP-2 + scaffold dogs as shown in Figure 85. Rotational energy to failure was similar for the control limbs for the allograft, unseeded scaffold and BMP-2 + scaffold dogs, and exhibited the same trend for the experimental limbs, with the allograft dogs having the largest value, followed by the unseeded scaffold dogs and the BMP-2 + scaffold dogs having the lowest value, as seen in Figure 86. Torsional stiffness was similar for the control limbs for the allograft, unseeded scaffold and BMP-2 + scaffold dogs. Torsional stiffness for the experimental limbs of the allograft and unseeded scaffold dogs was very similar to that of the control limbs. However, the torsional stiffness of the experimental limbs for BMP-2 + scaffold dogs was much lower, as seen in Figure 87. Finally, when comparing the ratios of the experimental to the control limb for all torsional parameters measured, Figure 88, it is seen that the for both the allograft and unseeded scaffold dogs, the ratios are close to 1 for torque to failure, torsional failure angle and torsional stiffness, where the BMP-2 + scaffold dogs are significantly less than 1 for these measurements. At face value, the mechanical testing results may imply that the allograft and unseeded scaffold treatments may be better at restoring mechanical properties to the contralateral limb (control) values than the BMP-2 + scaffold treatment.

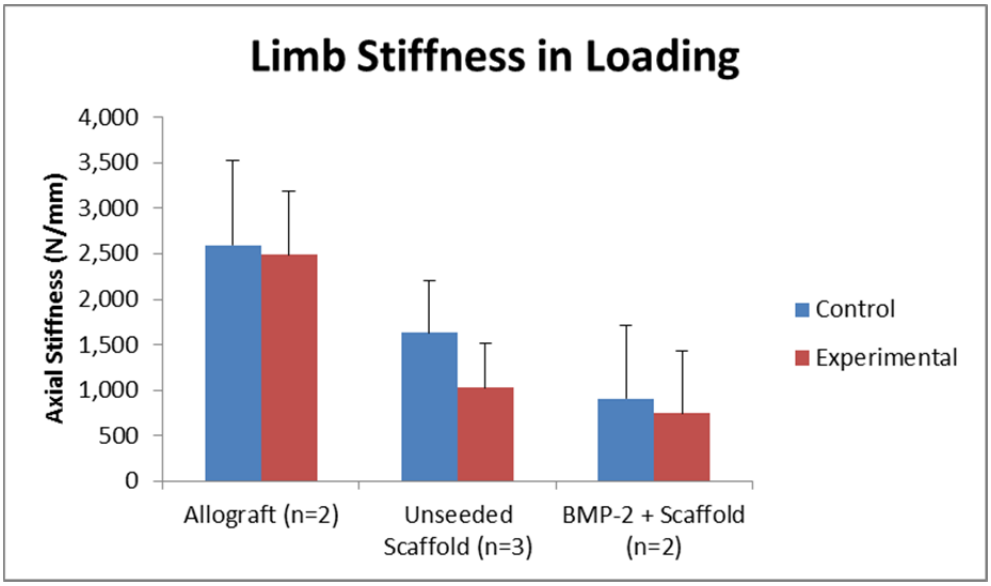

Figure 81: Axial compressive stiffness in loading as a function of repair type. Error bars denote standard deviations. Note that the plate is on the experimental limb whereas the control (contralateral) limb is in its native state (i.e. no plate).

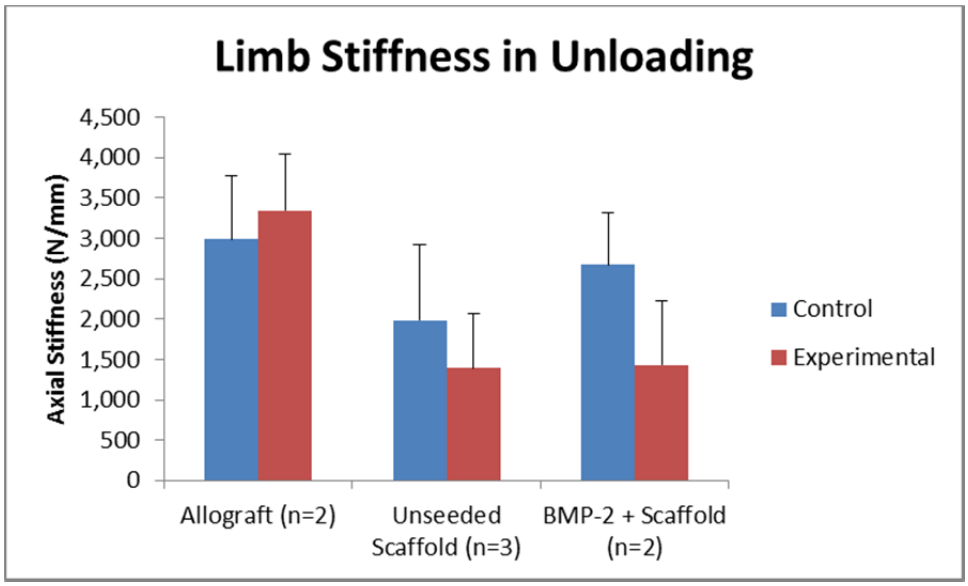

Figure 82: Axial compressive stiffness in unloading as a function of repair type. Error bars denote standard deviations. Note that the plate is on the experimental limb whereas the control (contralateral) limb is in its native state (i.e. no plate).

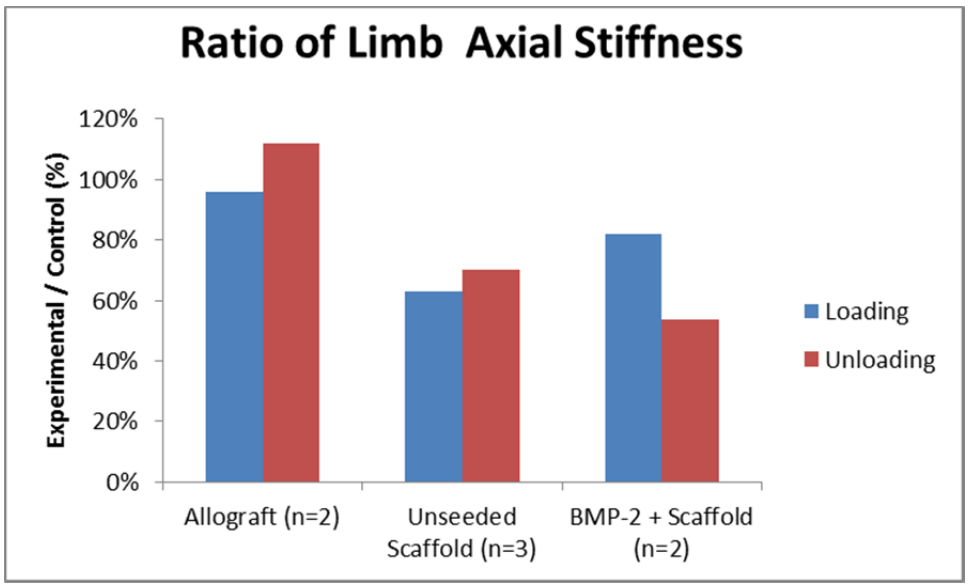

Figure 83: Ratio of axial stiffness of experimental limb to the control limb as a function of repair type. Note that the plate is on the experimental limb whereas the control (contralateral) limb is in its native state (i.e. no plate).

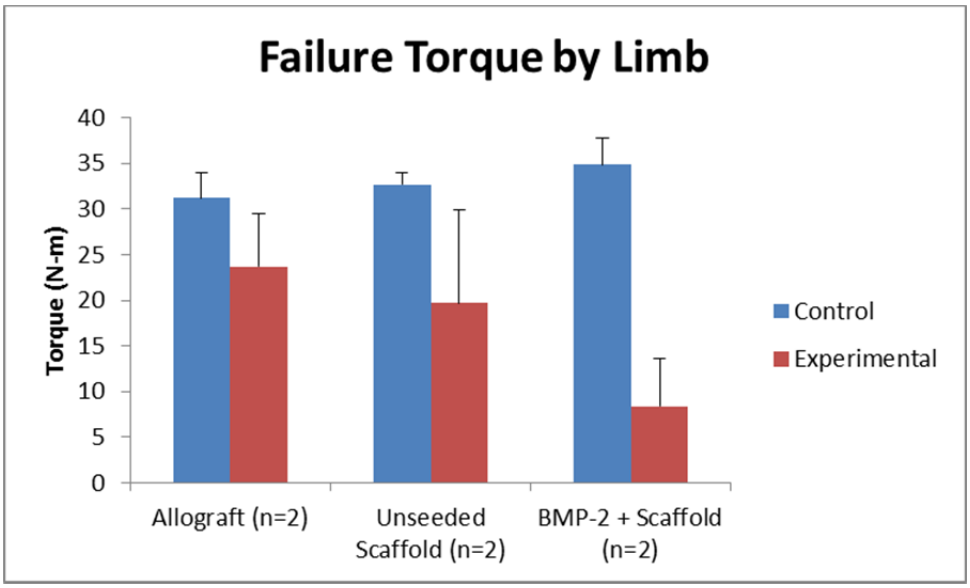

Figure 84: Failure torque for the control and experimental limbs as a function of repair type. Note that the plate was removed from the experimental limb whereas the control (contralateral) limb is in its native state. Error bars denote standard deviations.

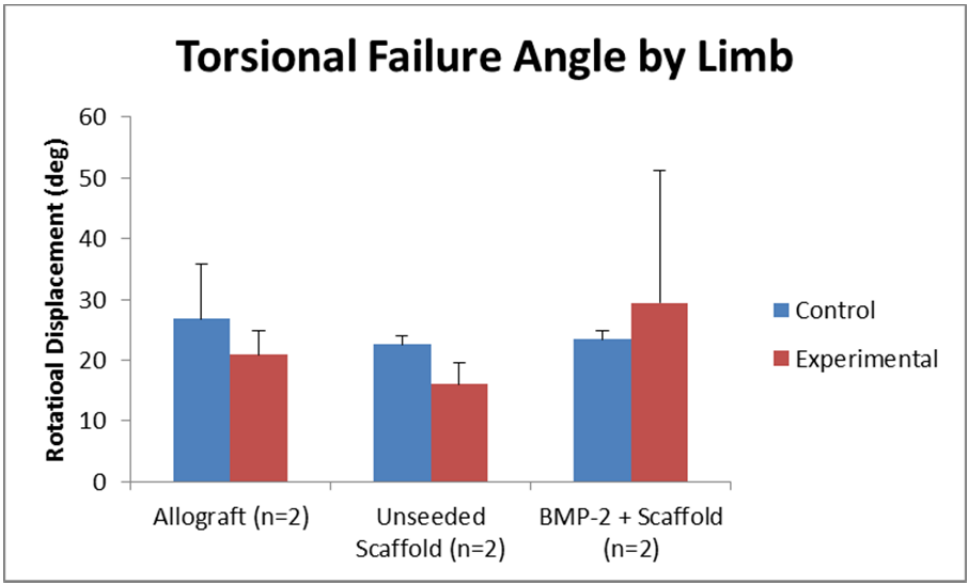

Figure 85: Rotation angle at which torsional failure occurred for the control and experimental limbs as a function of repair type. Note that the plate was removed from the experimental limb whereas the control (contralateral) limb is in its native state. Error bars denote standard deviations.

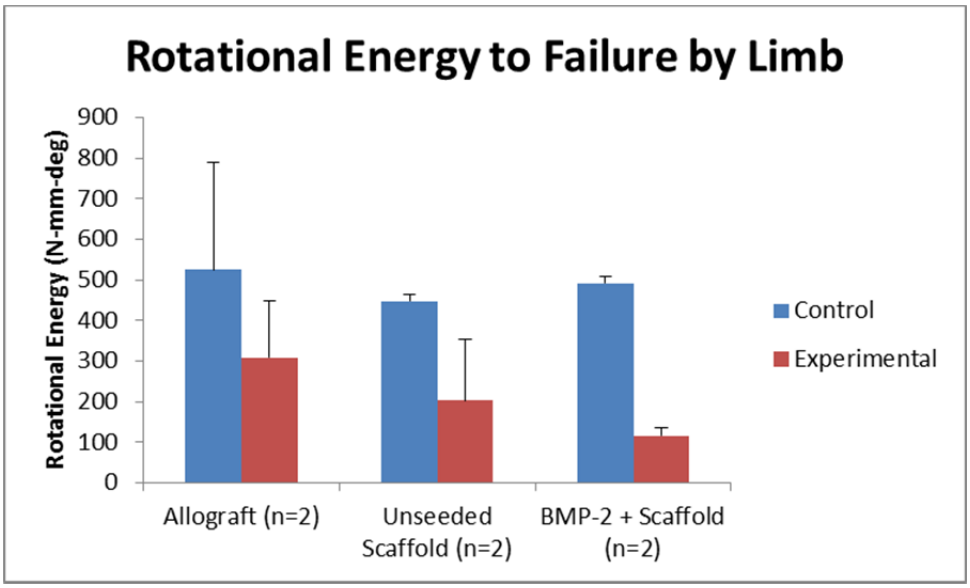

Figure 86: Rotational energy to torsional failure for the control and experimental limbs as a function of repair type. Note that the plate was removed from the experimental limb whereas the control (contralateral) limb is in its native state. Error bars denote standard deviations.

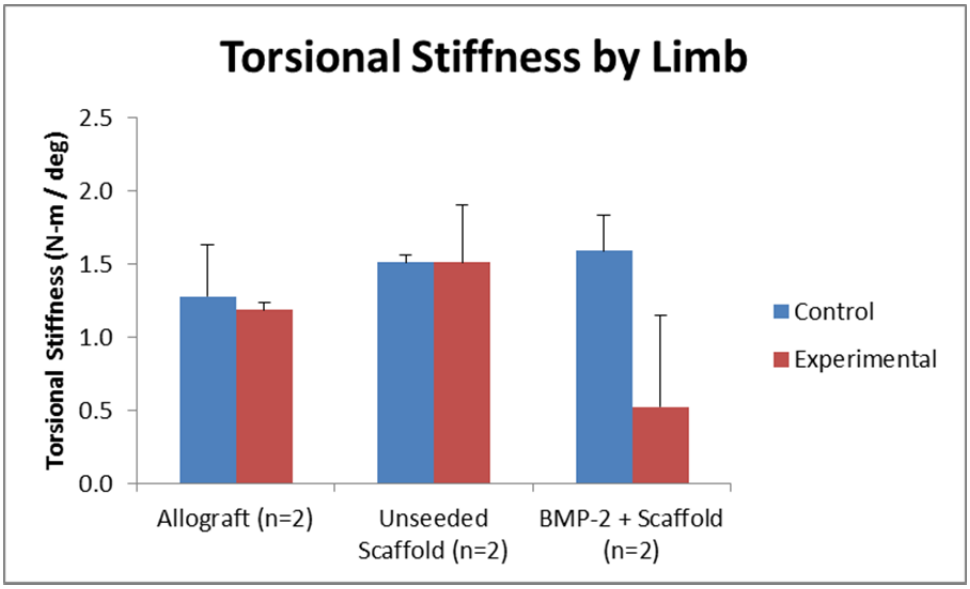

Figure 87: Torsional stiffness prior to torsional failure for the control and experimental limbs as a function of repair type. Note that the plate was removed from the experimental limb whereas the control (contralateral) limb is in its native state. Error bars denote standard deviations.

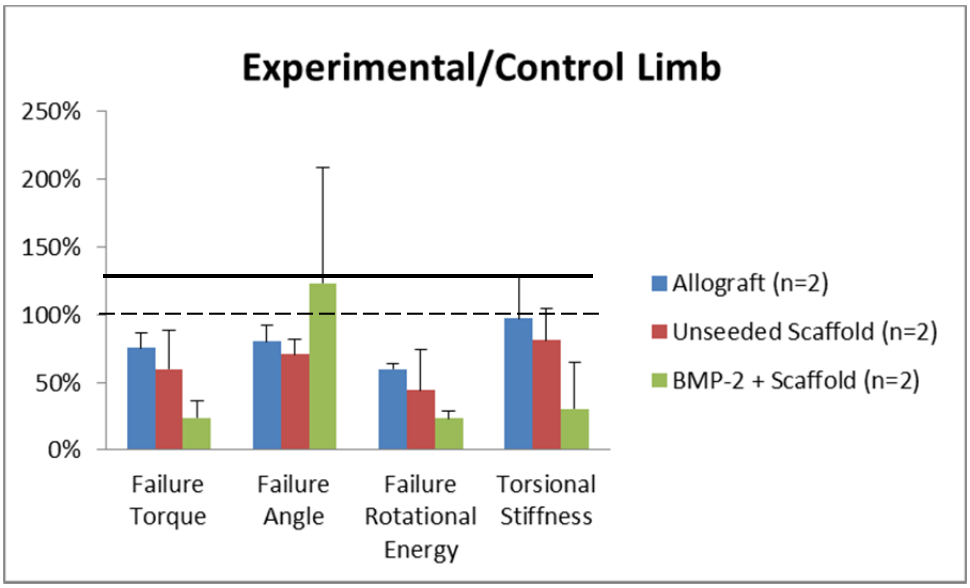

Figure 88: Ratio of experimental tibia (right) to its contralateral control tibia (left) as a percentage for the experimentally measured values. Note that the plate was removed from the experimental limb whereas the control (contralateral) limb is in its native state. Error bars denote standard deviations.

2.2.8 Segmental Defect Hard Sectioning Histology Study

Immediately following the mechanical testing, the leg was removed from the testing jig and the resulting diaphyseal portion of the tested bone was then soaked in 10% formalin solution for over two months for fixation for future histological evaluation. Following fixation, the condyles underwent automatic dehydration and plastic infiltration (Leika TP 1020, Germany). The samples were put in a mold and covered with Technovit 7200 media (EXAKT, Germany). The submersed samples were than exposed to yellow and blue wavelengths via the Light Polymerization Utility (EXAKT, Germany) for a period of two days to create a hard specimen block. The specimen block was then trimmed with a band saw (EXAKT, Germany), and the cut surface was ground smooth with 800 or 1000 grit sandpaper. The smoothed side was then glued to a 4"× 2" plastic template slide by Technovit 7210 and the glue was hardened on a Light-Polymerization-Block-Sandwich machine (EXAKT, Germany) with blue light for 5 min. The process was repeated for the other side to create a specimen block sandwich. The block was then cut on a band saw with a 1 cm-wide diamond blade (EXAKT, Germany). The cut direction was parallel to the surface to be stained resulting in a 800~1000 μm thick slide specimen. To prepare the specimen for staining, the surface underwent a series of progressively finer polishing using 800 grit paper, 1000 grit paper and 1200 grit paper until only a 50~80 μm specimen layer was left. To eliminate scratches from cutting and grinding and to improve transparency of the slide surface, the specimen surface was polished with 4000 polish paper for more than one hour on the same grinding machine. The entire protocol followed the method provided by the EXAKT company(2). The slides were then stained with the standard Haematoxylin & Eosin (H&E) Stain or Masson's Trichrome Stain to distinguish connective tissues. The specimen for Dog 4 (shown in Figure 31 and 32) and Dog 5 (shown in Figure 29 and 30) were stained with both methods.

Figure 89 (a) and 90 (a) are of the entire mid-diaphysis of the tibia, including the scaffold and associated callus. The scaffold region can be distinguished from the region between the spiral screws marks at both ends and bone growth into most of the voids of PCL-HA scaffold and the lumen. The bone covering of the scaffolds is mostly cancellous bone, which can be clearly identified from Figure 89 (c), and cartilage, which is apparently shown in Figure 90 (c). Cancellous bone and cartilage are both present on the inside scaffold wall as shown in Figures 89 (d) and 90 (b). The hard section histological images of Segmental Defect Dog 1 and Dog 2 show the bony growth induction of the unseeded scaffold. In order to differentiate the bony growth from microscopic images, dynamic bone staining in live post-surgery dogs is highly recommended. A modification to the IACUC protocol to include this will be submitted shortly.

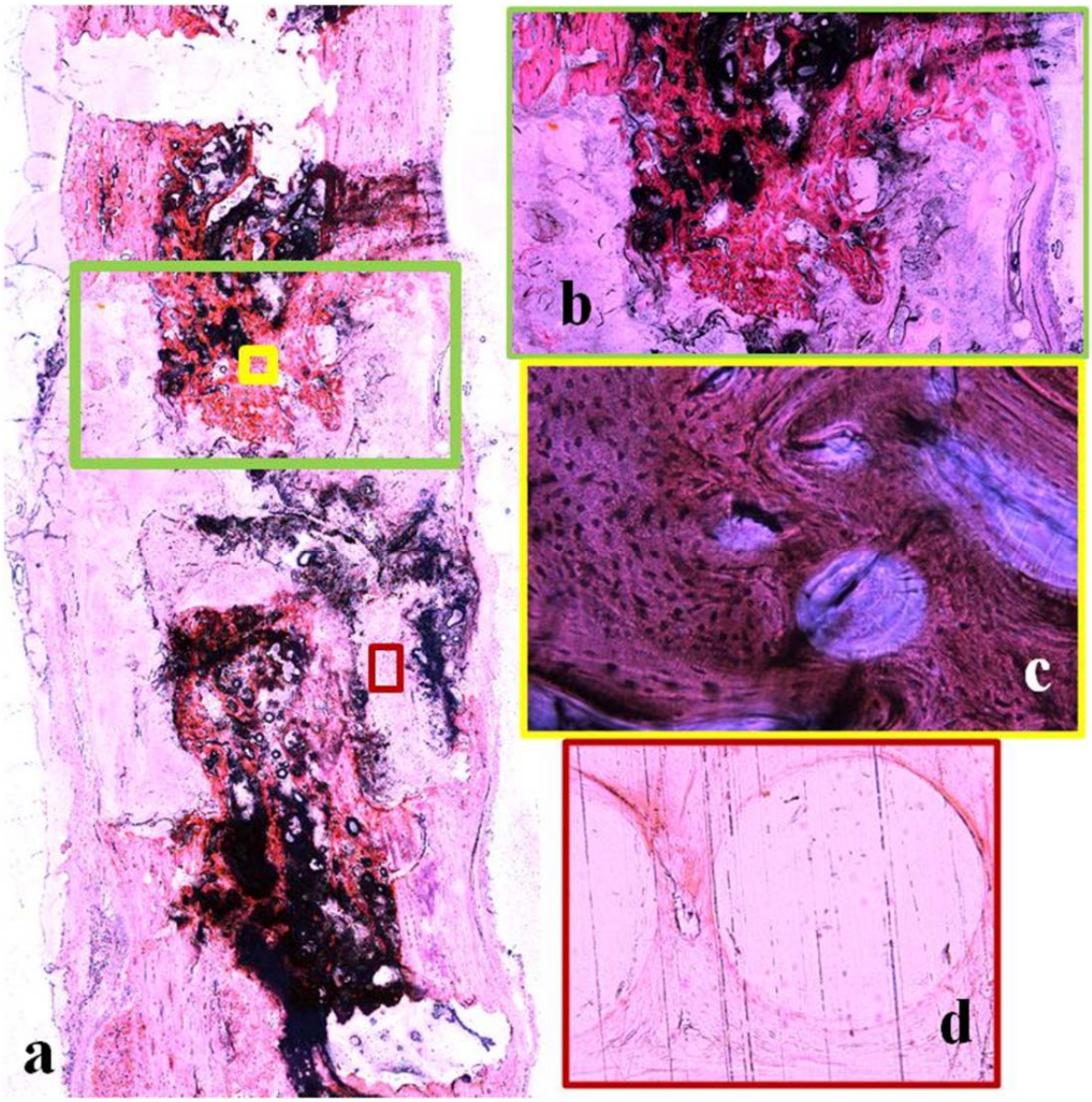

Figure 89: Hard sectioning histology image of Segmental Defect Dog 1, stained by H&E method. (a) Overview of middle right tibia with scaffold; the locking screws marks are the two blank regions both at the top and at the bottom of the image. (b) close-up of green rectangle region, the lumen region of the scaffold, (c) close-up of yellow rectangle region in 40X magnification, showing cancellous bone growth into the hole of the scaffold, (d) high magnification (20X) image of red rectangle region.

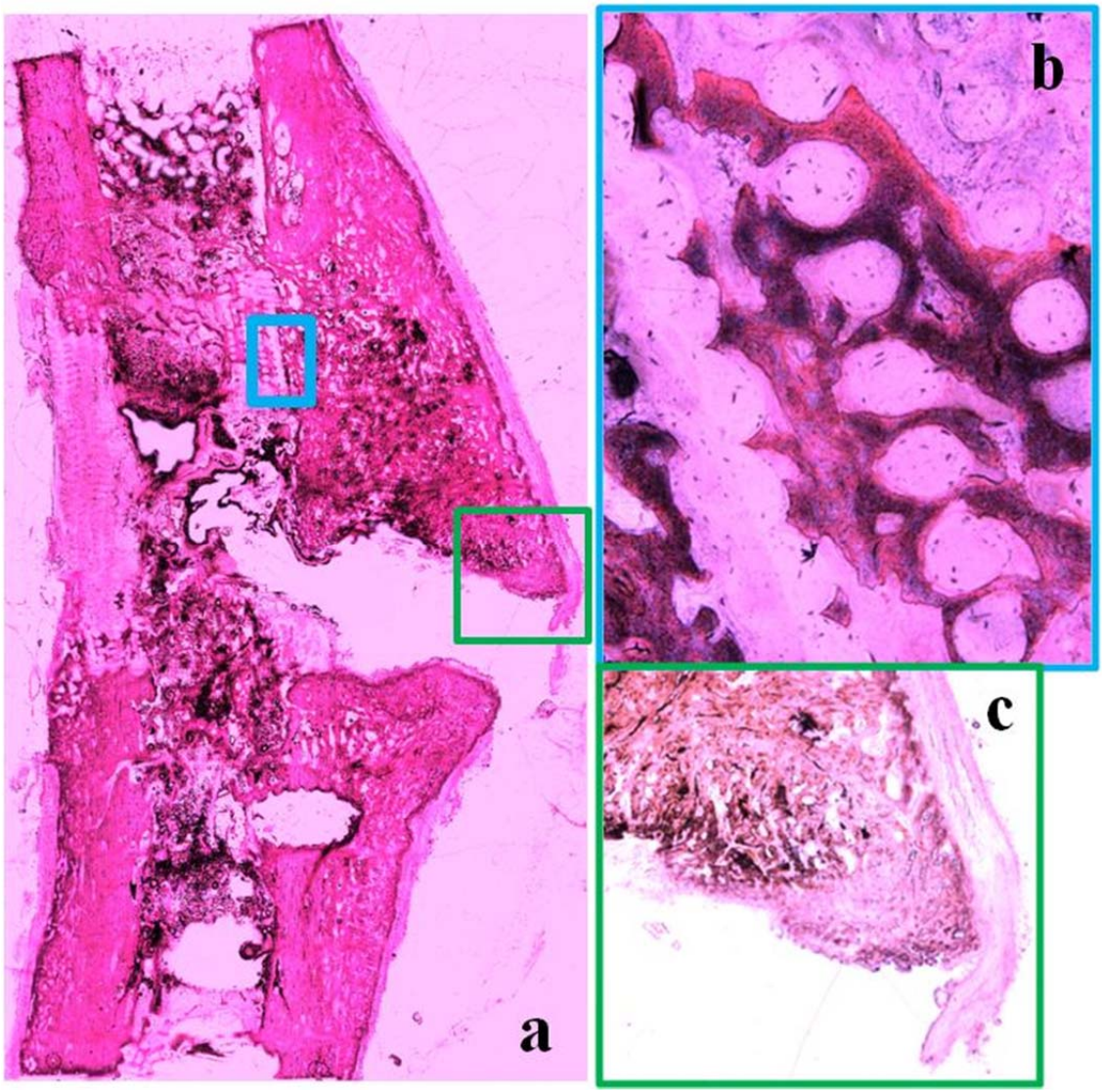

Figure 90: Hard sectioning histology image of Segmental Defect Dog 2, stained by H&E method. (a) Overview of middle of right tibia with scaffold, the locking screws marks are the two blank regions at the bottom of the image. (b) Close-up of blue rectangle region, (c) close-up of green square region, cartilage covers the external surface of the cancellous bone. The discontinuation in the right side of the bone is due to the torsional fracture from biomechanical testing.

In all of the four histological slices shown in Figure 91 through Figure 94, there were oblique gaps from upper left to the bottom right that were the spiral fractures caused by the torsional failure testing. Figure 91 and 92 are of the entire mid-diaphysis of right tibia implanted with a cadaveric allograft. The allograft is hard to distinguish due to its fusion with the tibial body. Figure 93(a) and 94(a) are of the entire mid-diaphysis of the right tibia, including the scaffold and associated callus. The scaffold region can be distinguished by their appearance from the neighboring cortical bone. The bony ingrowth into most of the voids of PCL-HA scaffold and the lumen, are shown in Figure 93(c) and 94(c). The bone covering of the scaffolds is mostly cancellous bone, which can be clearly identified from Figure 93(b) and 94(b), and cartilage, which as can be seen in the bottom parts of Figure 93(b) and 94(b). The black tissues through the entire tibia in the middle level represent the soft tissues of the bone marrow.

From the biomechanical test results in terms of failure torque and rotational energy, the failure torques of Dog 4 and Dog 5 were very close, possibly indicating a similar healing process for both allograft and unseeded scaffolds. The histological sections also show that the healing patterns on both kinds of implants were also very similar.

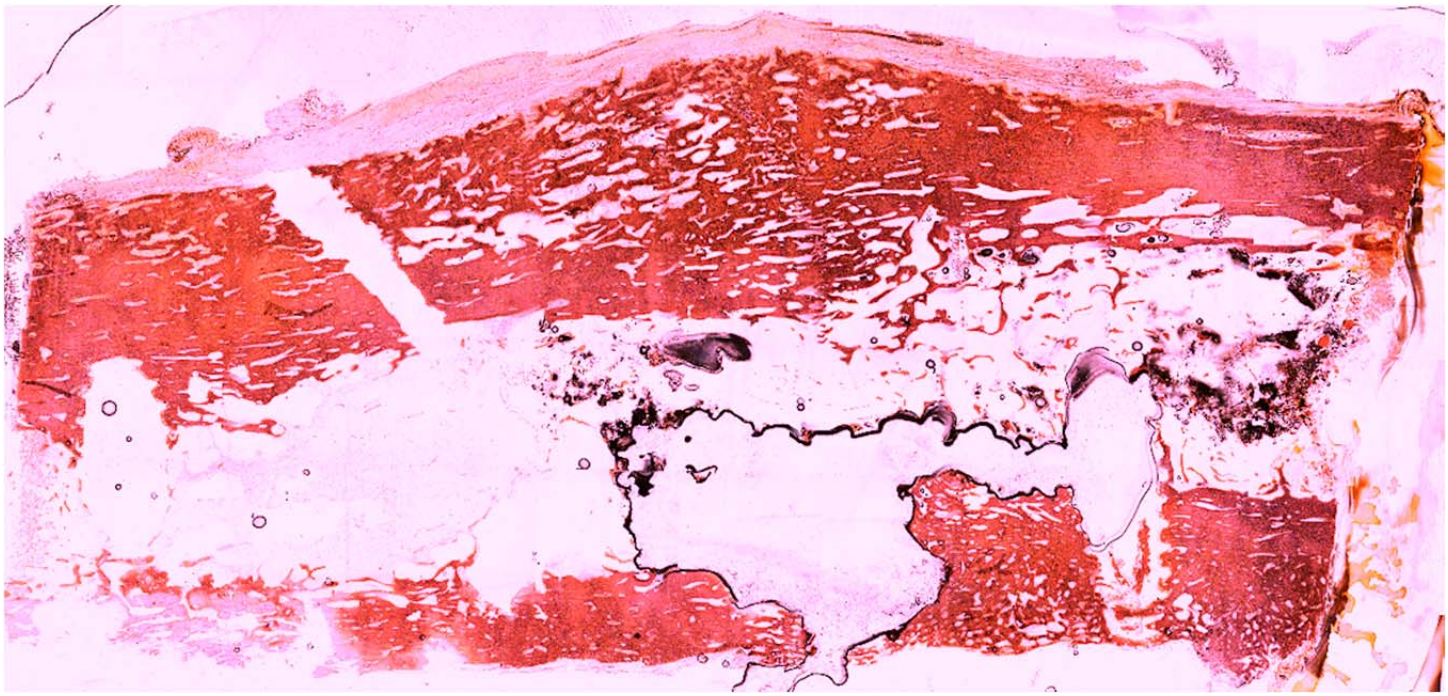

Figure 91: Hard sectioning histology image of Segmental Defect Dog 5 implanted with canine cadaveric allograft, stained by H&E method. Overview of mid-diaphysis of right tibia with canine cadaveric allograft. The oblique crack was the fracture generated by biomechanical testing.

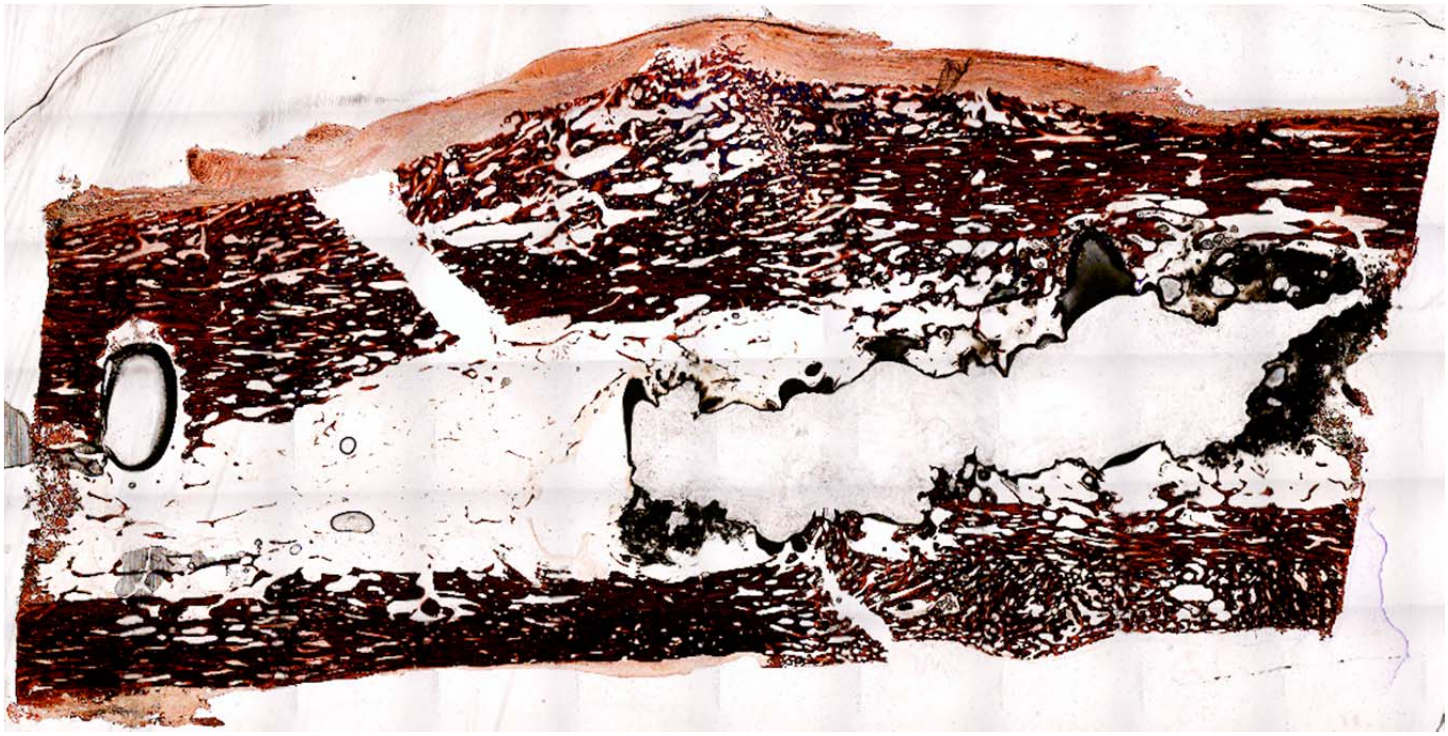

Figure 92: Hard sectioning histology image of Segmental Defect Dog 5 implanted with canine cadaveric allograft, stained by Masson's Trichrome method. Overview of mid-diaphysis of right tibia with canine cadaveric allograft. The black tissues in the middle level at right half are the bone marrow soft tissues. The oblique crack was the fracture generated by biomechanical testing.

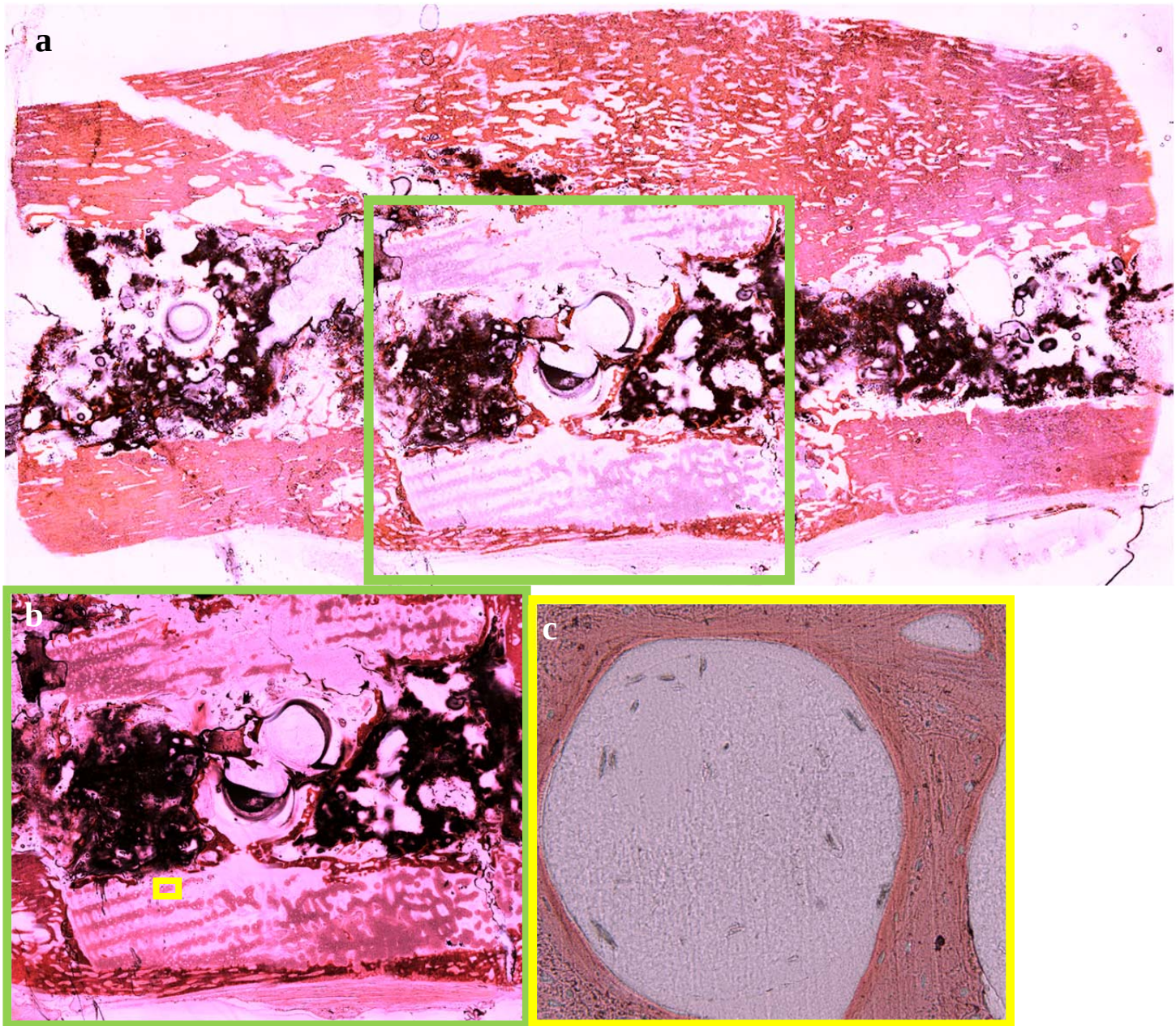

Figure 93: Hard sectioning histology image of Segmental Defect Dog 4 implanted with unseeded scaffold, stained by H&E method. (a) Overview of mid-diaphysis of right tibia with unseeded scaffold, (b) close-up of green rectangle region, (c) close-up of yellow rectangle region. The oblique crack was the fracture generated in biomechanical testing.

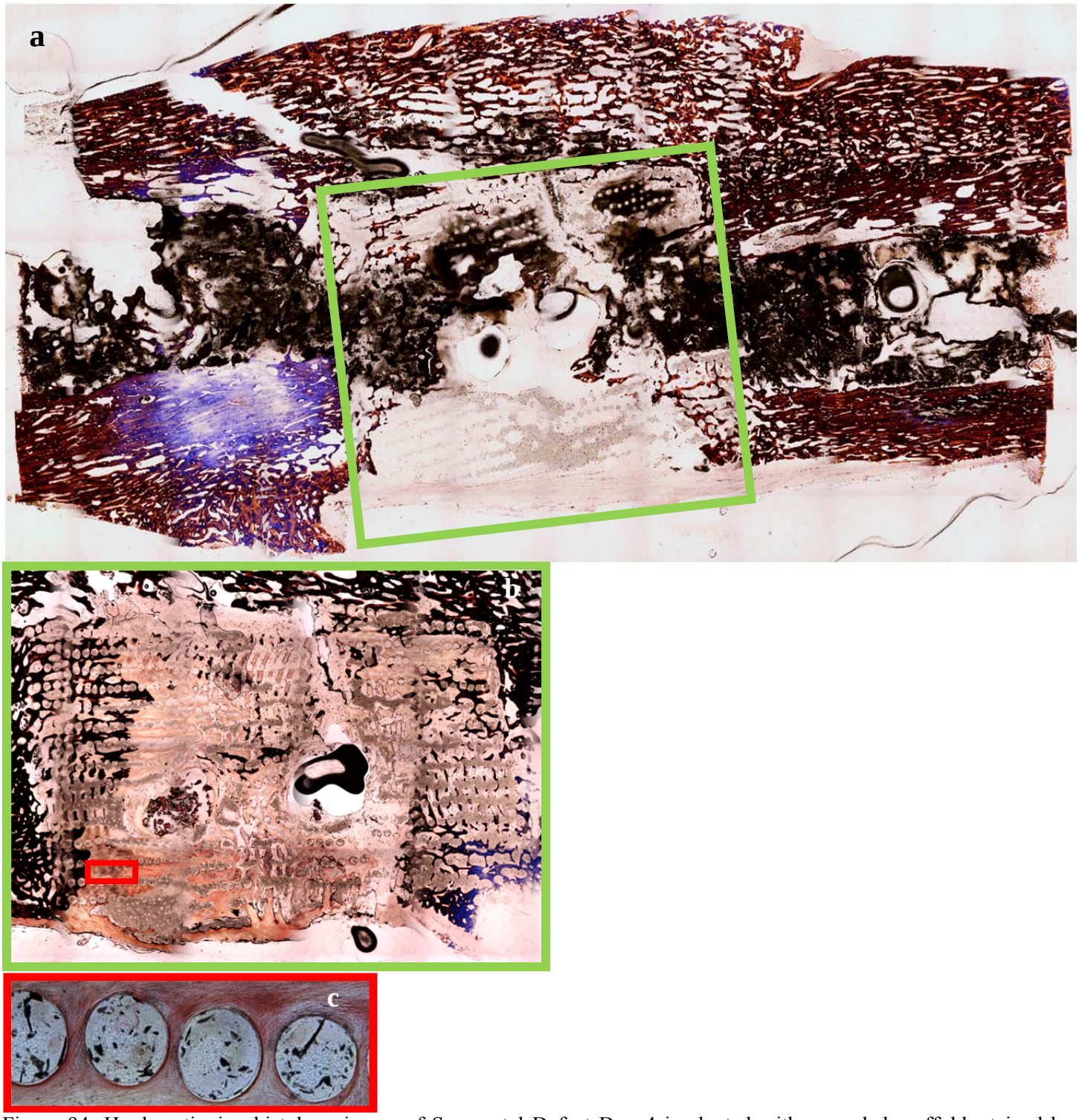

Figure 94: Hard sectioning histology image of Segmental Defect Dog 4 implanted with unseeded scaffold, stained by Masson's Trichrome method. (a) Overview of mid-diaphysis of right tibia with unseeded scaffold, (b) close-up of green rectangular region coming from another Trichrome-stained slice, (c) close-up of red rectangular region. The oblique crack was the fracture generated by biomechanical testing.

2.3: Aim 3: Human Cadaveric Testing

Human cadaveric testing was performed to assess the stability of the scaffold at time zero for Aim 2 (segmental) defects. Twelve human cadaveric tibiae specimens (6 matched pairs) were used for this study.

2.3.1 Mounting of Plate in Human Cadaveric Tibia

A medial incision was made and the soft tissue was sharply dissected down to the bone. The surrounding soft tissue and fibula were maintained to ensure that when the approximately 5 cm segmental defect was created, the native length of the tibia would be maintained. A 14-hole 4.5 mm broad, 260 mm long locking compression plate from Synthes (Paoli, PA) was used with five 5.0 mm diameter locking screws placed both superior and inferior to the scaffold. Two 4.5 mm diameter cortical screws were placed into the scaffold to secure it. Prior to placement of the cortical screws, two sutures were placed around the scaffold to hold it tightly to the plate as the screws were applied. All screws bridged both cortices. The scaffold was created using a mixture of 90% poly-caprolactone (PCL) and 10% hydroxyapatite (HA) by weight. The scaffold was created with 500 μm microchannels with 300 μm strands and did not have a cortex shell to replicate the scaffold architecture implanted in the dog. Figure 95 compares the implanted scaffold to the segment of bone removed from the tibia and its placement in the segmental defect. This mirrored the lateral approach that was used for the segmental defect surgeries in the dogs.

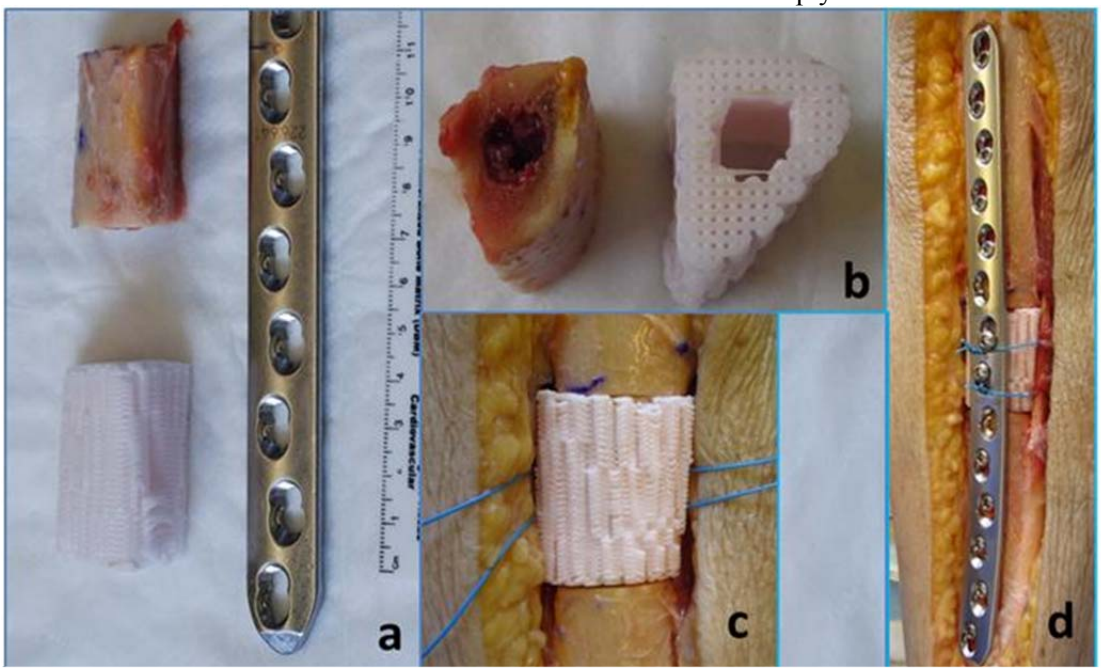

Figure 95: Human cadaveric tibial specimen showing a) excised segmental defect and scaffold to replace it, b) cross-sectional view showing human bone segment removed and scaffold, c) implanted scaffold showing tight-fit, d) locking plate, scaffold and bone construct.

2.3.2 Mechanical Testing of Human Cadaveric Tibia

The tibial plateau was first prepared by cutting off the raised portions to create a flat surface. Both the superior and inferior ends of the tibia were placed in polycarbonate square tubes. For torsional stability, two orthogonal 2.6 mm Steinmann pins were drilled through the tube and the tube-bone-pin construct was filled with PMMA. A metal plate was placed on the superior tube for axial loading via a steel ball was placed into the spherical depression in the plate and the tibia was loaded via a flat platen (Figure 96(a)). When torsion loading was to be applied, the ball was removed and the square tube, coated with grease to prevent axial loading, was placed into the square clamp (Figure 96 (b)). The square superior clamp allowed the key to slide in the axial direction to permit superior/inferior motion of the plate as the tibia was torqued to minimize any compressive force resulting from the applied torque. The distal end of the tibia was potted in a similar manner and rigidly secured into a rigid square clamp at the base of the machine.

The loading was applied using a MTS 858 Bionix (MTS Eden Prairie, MN) testing system. Axial loading was applied via a series of step loads of 50 N, 400 N, 500 N, 600 N and 700 N. At each step, the load was applied in a sinusoidal fashion for 50 cycles at a rate of 2 Hz. Data were collected at a rate of 10 Hz. Bending loads were applied to the middle of the plate also via a series of step loads of 50 N, 200 N, 250 N, 300 N and 350 N in the same manner as was done for the axial loading (Figure 44). Finally, torsional loading was applied via a series of step loads of ±3, ±6 and ±9 N-m for 20 sinusoidal cycles at a rate of 0.5 Hz. The loading protocol closely replicated the protocol used by Choi et al (4). Axial, bending and torsional stiffness values were obtained from the slope of the force versus axial displacement, bending moment versus mid-span displacement, and torque versus angular displacement curves, respectively. Following

testing with the scaffold in place, the scaffold was removed and the same series of tests repeated without the scaffold. The axial compression, bending and torsion tests were randomized. Then a cyclic torsional failure test under torque control was performed, measuring angular rotation in internal and external rotation as a function of increasing torque from 10 N-m to 45 N-m in increments of 5 N-m. Statistical analyses were performed with a 2-way ANOVA test.

The results of the biomechanical tests are provided in Table 3. There is one series of test data for Specimen 985L missing because of preliminary torsional failure in the first torsion test. The results showed no significant difference for bending or axial stiffness with non-locking vs locking fixation with the scaffold present or absent. Torsional stiffness was significantly higher ($p=0.002$) with the scaffold present for both non-locking and locking compared to the scaffold absent. In testing to failure, angular rotation was found to be significantly greater in internal rotation ($p=0.034$) for the non-locking construct than for the locking construct. External rotation was also greater for the non-locking construct, though it did not reach significance ($p=0.168$). The non-locking construct failed first for 5 of the 6 pairs and at approximately the same number of cycles for the 6th pair. The mode of failure for the non-locking construct varied between catastrophic failure and screw loosening. All locking constructs failed catastrophically, with no screw loosening prior to failure.

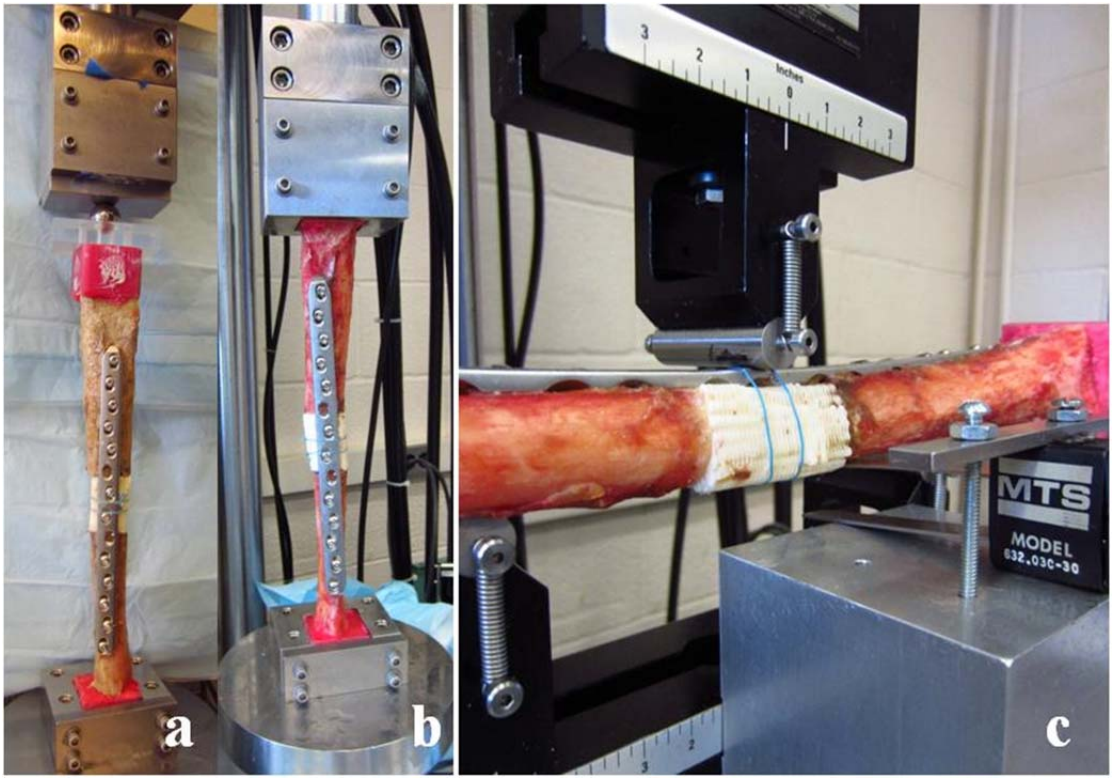

Figure 96: Mechanical testing of human cadaveric tibia with scaffold in segmental defect, (a) axial loading via ball bearing, (b) torsional loading via rectangular block, (c) three-point bending of tibia-plate-scaffold construct, bending load is applied to the middle of the locking plate.

Specimen Number		Screw Type		Axial Compression Stiffness (N*mm)	Torsional Stiffness (N*m*deg)	3-Point Bending Stiffness (N*mm)	Total Energy to Failure (N-m-deg)
979	L	Cortical	scaffold	5358	2.052	212	56396
	L	Cortical	no scaffold	2952	2.005	37	
	R	Locking	scaffold	2525	2.486	938	560
	R	Locking	no scaffold	2369	2.19	551	
980	R	Cortical	scaffold	1518	1.481	1990	30888
	R	Cortical	no scaffold	1337	1.196	1755	
	L	Locking	scaffold	1423	1.785	1495	2706
	L	Locking	no scaffold	1618	1.632	1292	
981	R	Cortical	scaffold	2954	2.194	994	14401
	R	Cortical	no scaffold	2815	2.092	1763	
	L	Locking	scaffold	1868	2.473	676	5503
	L	Locking	no scaffold	1240	2.261	827	
983	L	Cortical	scaffold	1559	2.105	345	5078
	L	Cortical	no scaffold	1597	1.794	166	
	R	Locking	scaffold	1798	1.981	969	14103
	R	Locking	no scaffold	2512	1.798	805	
984	R	Cortical	scaffold	1539	2.637	1367	2362
	R	Cortical	no scaffold	1526	2.404	1020	
	L	Locking	scaffold	1931	2.334	748	4636
	L	Locking	no scaffold	1599	2.175	902	
985	L	Cortical	scaffold				
	L	Cortical	no scaffold				
	R	Locking	scaffold	930	1.533	758	620
	R	Locking	no scaffold	854	1.532	287	

Table 3: Mechanical test results for human cadaveric tibiae with and without scaffolds present in the segmental defects. Axial compression, torsion and three-point bending loading were applied in a randomized sequence. After cyclic loading, the specimens were failed in torsion.

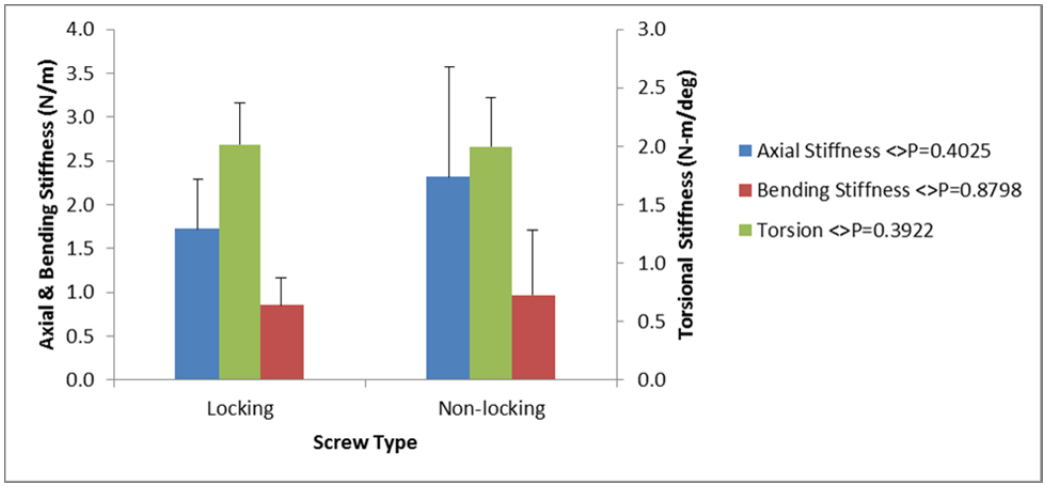

Figure 98. Axial, bending, and torsional stiffness for locking vs non-locking constructs. Error bars denote 1 standard deviation.

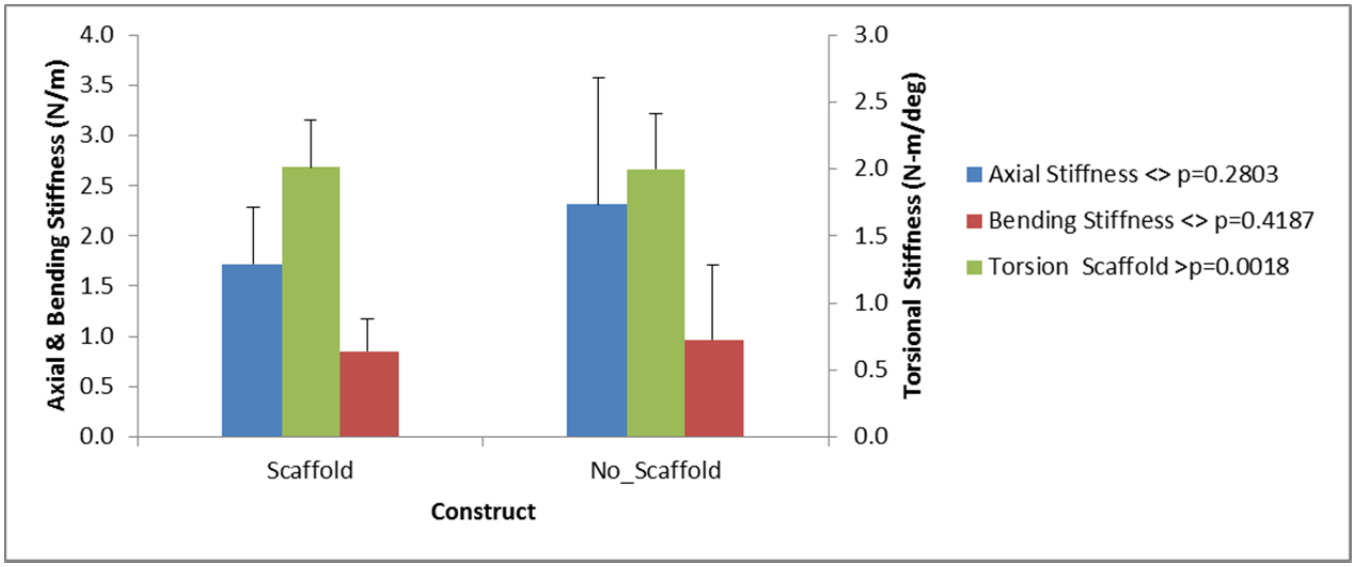

Figure 99. Axial, bending, and torsional stiffness for specimen with and without scaffold. Error bars denote 1 standard deviation.

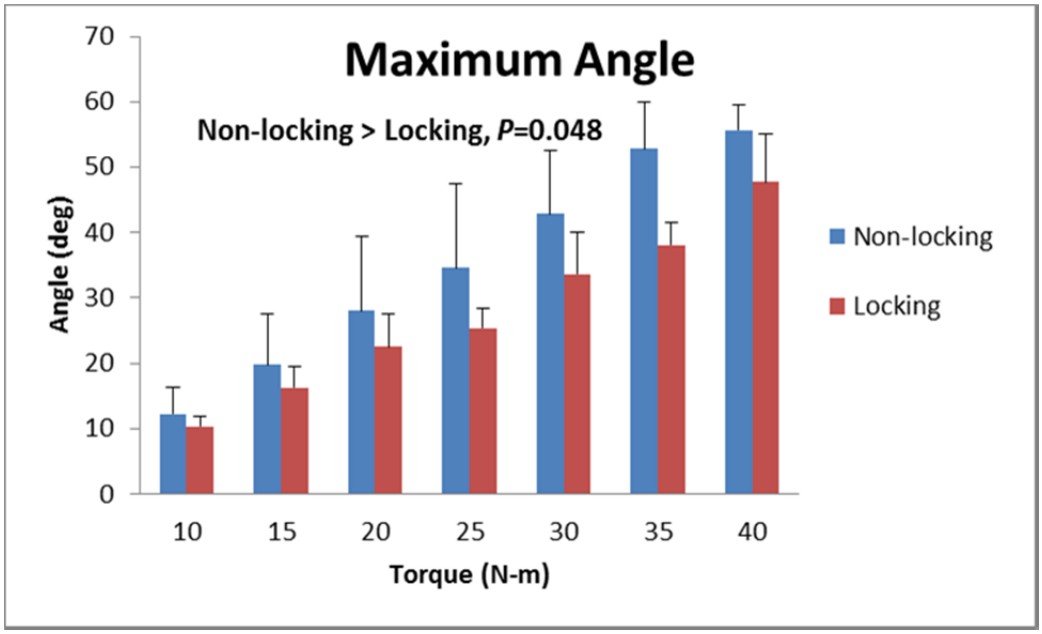

Figure 100. Maximum angular displacements as a function of torque for non-locking and locking constructs. Error bars denote 1 standard deviation.

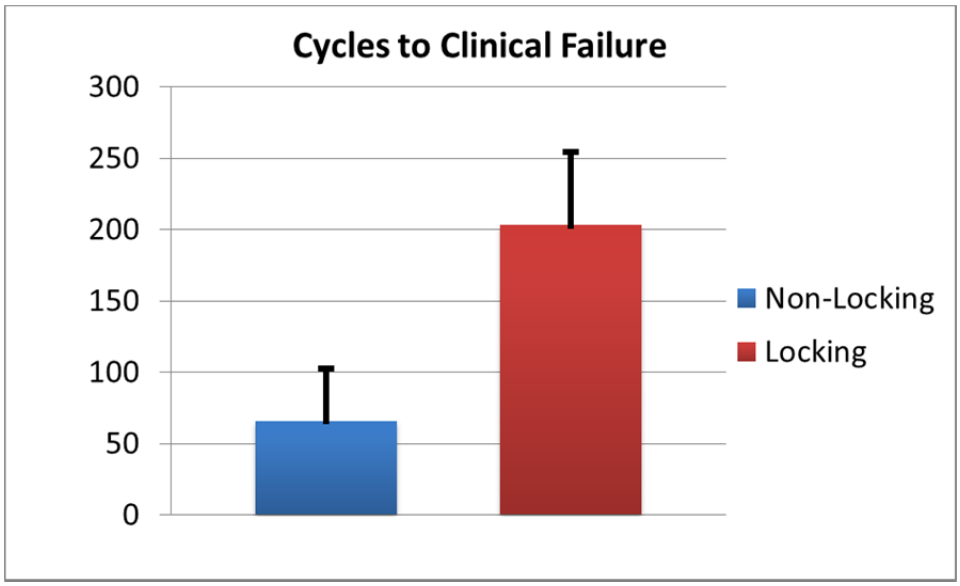

Figure 101. Cycles to clinical failure for non-locking and locking constructs. Error bars denote 1 standard deviation.

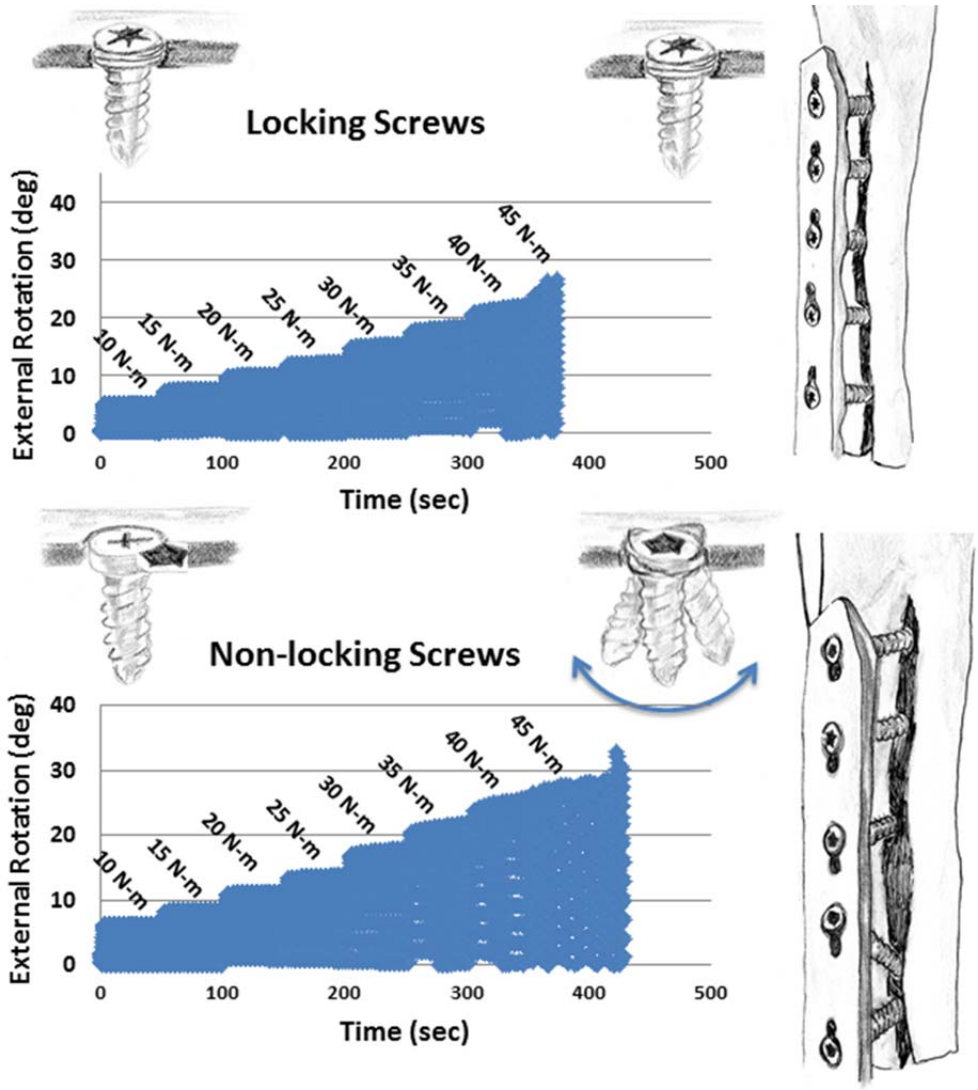

Figure 102. Depiction of locking screws and non-locking screws showing mechanism of loosening and crack formation. Note the screw loosening, toggling and back-out for non-locking screw as compared to the locking screw that resulted in

progressive widening of the crack. Plots are of representative failure tests showing tibial rotation as a function of time and applied torque for a paired specimen. Note the larger rotation at higher applied torques for the non-locking screw.

2.3.3 Mechanical Testing Summary

The presence of the scaffold was found to increase the torsional stiffness of the construct. Locking fixation resulted in a stronger construct with increased cycles to failure compared to non-locking fixation. It is envisioned that currently available locking plate-screw scaffold constructs may provide rigid enough fixation to allow early mobilization and weight bearing of patients with critical sized intercalary bone defects.

3. KEY RESEARCH ACCOMPLISHMENTS

3.1 Both the poly-caprolactone (PCL) + hydroxyapatite (HA) osteochondral and segmental defect scaffolds were found to be compatible to *in vivo* conditions and was well-tolerated by all dogs, demonstrating no immune response.

3.2 Thirty-one surgeries, three osteochondral defect (Aim 1) and twenty-eight segmental defect surgeries (Aim 2) were performed and all but two successfully completed the full 16 weeks post-surgery recovery period without incident.

3.3 Outcome measures for both osteochondral (Aim 1) and segmental defect dogs (Aim 2) demonstrated that the surgical procedures were well-tolerated by the dogs and did not impair their quality of life.

3.4 Hard sectioning histology demonstrated tissue in-growth in both the osteochondral (Aim 1) and segmental defect (Aim 2) dogs.

3.5 Scanning electron microscopy provided direct evidence that BMP-2 microspheres succeeded in attaching to the inside walls of the scaffolds.

3.6 A technique to obtain sterile bone marrow aspirate for the culturing of canine stem cells was successfully demonstrated.

3.7 Human cadaveric testing (Aim 3) demonstrated that the presence of the scaffold was found to increase the torsional stiffness of the construct. Locking fixation resulted in a stronger construct with increased cycles to failure compared to non-locking fixation.

4. REPORTABLE OUTCOMES

A manuscript based on the results of our mechanical testing of human segmental defects reported in Section 2.3 was published in the *Journal of Clinical Biomechanics*, 30 (2015) 1114-1118 and is included in the Appendix. An abstract on the osteoconduction in the tibial segment defects was presented as a poster at the Orthopaedic Research Society 2013 Annual Meeting and is included in the Appendix.

5. CONCLUSIONS

The design of the osteochondral defect implant (Aim 1) was found to be stable, with no need for additional fixation. Mechanical testing of the canine tibiae with segmental defects found that the allografts and unseeded scaffolds exhibited mechanical properties closer to the control limb than did the dogs that received scaffolds seeded with BMP-2. We have successfully demonstrated that canine stem cells can be cultured from bone marrow aspirate and will infiltrate the PCL-HA scaffold**.** The outcome measures demonstrated consistent results between measurement metrics and with

clinical observations. They are felt to form a quantitative and qualitative approach to accurately assessing the results of surgical interventions. Radiographs were consistent with clinical outcome measures and mechanical testing, but were not a strong indicator of healing. Mechanical testing of the human cadaveric analog representative of immediate post-surgery of the segmental defect (Aim 3) found that the presence of the scaffold was found to have no effect for bending or axial loading, and a slight effect in torsion. When comparing a locking construct to a non-locking construct, the non-locking construct was found to have greater compliance to internal rotation than the locking construct. The implication of this testing is that the bone/plate construct is sufficiently strong without the need for additional load support from the scaffold and that this construct is mechanically stable at time zero, even without surrounding soft tissue support. Furthermore, the locking screw construct resulted in a less compliant construct than the non-locking screw construct.

5.1 Impact

The results of this study took another step towards military application of PCL-HA scaffold technology by verifying successful implantation of the osteochondral implant (**Aim 1)** and segmental defect scaffold (**Aim 2**) in segmental canine bone defects and by confirming biomechanical and functional suitability in human cadaveric tibia defect models (**Aim 3**). **Aim 1** and **Aim 2** are significant in that they introduce a simpler, more cost-effective approach to tissue engineering that obviates the need for extensive cell culturing and laboratory support. **Aim 3** is significant in that the injured soldiers can start early rehabilitation and ambulation following reconstructive surgeries using Ready-to-Use anatomically and biomechanically conforming biogenic scaffolds.

6. REFERENCES

1. Lee CH, Cook JL, Mendelson A, Moioli EK, Yao H, Mao JJ. Regeneration of the articular surface of the rabbit synovial joint by cell homing: a proof of concept study. Lancet. 2010;376(9739):440-8.
2. Kwak SKD. Experimental and Mathematical Investigation of the Human Knee : Anatomy, Kinematics and Contact [dissertation]. \New York, NY: Columbia University; 1997.
3. Aro HT, Wahner HT, Chao EY. Healing patterns of transverse and oblique osteotomies in the canine tibia under external fixation. J Orthop Trauma. 1991;5(3):351-64.
4. Kloc PA, 2nd, Kowaleski MP, Litsky AS, Brown NO, Johnson KA. Biomechanical comparison of two alternative tibial plateau leveling osteotomy plates with the original standard in an axially loaded gap model: an in vitro study. Vet Surg. 2009;38(1):40-8.
5. Schaefer SL, Lu Y, Seeherman H, Li XJ, Lopez MJ, Markel MD. Effect of rhBMP-2 on tibial plateau fractures in a canine model. J Orthop Res. 2009;27(4):466-71.
6. Gorman SC, Kraus KH, Keating JH, Tidwell AS, Rand WM, Parkington JD, et al. In vivo axial dynamization of canine tibial fractures using the Securos external skeletal fixation system. Veterinary and comparative orthopaedics and traumatology : VCOT. 2005;18(4):199-207.
7. Tyler JM, Larinde W, Elder SH. A device for performing whole bone torsional testing in a single-axis linear motion testing machine. Veterinary and comparative orthopaedics and traumatology : VCOT. 2008;21(5):478-80.
8. Choi JK, Gardner TR, Yoon E, Morrison TA, Macaulay WB, Geller JA. The effect of fixation technique on the stiffness of comminuted Vancouver B1 periprosthetic femur fractures. J Arthroplasty. 2010;25(6 Suppl):124-8.

7. APPENDICES

7.1 Manuscript published in the Journal of Clinical Biomechanics 30 (2015) 1114-1118.

7.2 Abstract presented as a poster at the 2013 Annual Meeting of the Orthopaedic Research Society.